THE SYNTHESIS OF NOVEL Pt-BASED NANOPARTICLES

A DISSERTATION PRESENTED TO THE FACULTY OF ENGINEERING AND BUILT ENVIRONMENT

BY

GERARD LETEBA

IN FULFILMENT OF THE REQUIREMENTS FOR THE DEGREE OF MASTER OF SCIENCE IN MATERIALS ENGINEERING

UNIVERSITY OF CAPE TOWN

SUPERVISORS: PROF. CANDACE LANG

DR. MIRA TOPIC

FEBRUARY 2011

DECLARATION

I know the meaning of plagiarism and declare that all of the work in the document, save for that which is properly acknowledged, is my own.

---------- ----------

Gerard Leteba *Date*

ABSTRACT

Highly monodisperse and uniform-sized nanoparticles of platinum (Pt), vanadium (V) and vanadium oxide of different morphologies were synthesized by employing various novel chemical solution-based synthetic approaches comprising thermal decomposition (thermolysis), thermal reduction and nonhydrolytic sol-gel reactions. Synthesis of these colloidal nanocrystals involved the heat-up of chemical mixtures of metal precursors, surface active agents (surfactants) as stabilizers, solvents and reductants from room temperature to high temperature. The newly developed synthetic routes reported herein for the preparation of Pt, V and V oxide nanocrystals are highly reproducible and require less size selective processing. Amongst all the techniques developed, the most successful protocol for the controlled synthesis of Pt, V and V oxide nanocrystals is the thermolysis of the metal precursor-surfactant complex in high boiling point organic solvents under reflux at the ageing temperature of 200 – 350 ºC for 30 – 60 minutes.

A detailed microstructural investigation of the high boiling point surfactant stabilized Pt, V and V oxide nanoparticles was performed using transmission electron microscopy (TEM). The as-prepared nanoparticles adopt mostly cubic, cuboctahedral, irregular and triangular morphologies, depending on the nature of the metal precursor salts, stabilizers and reductants employed. The diameters of the particles can be tuned to various range sizes by altering the heating rate of the solution. These nanoparticles show excellent solubility in polar solvents such as chloroform, hexane and toluene and remain as stable colloidal suspensions even after repeated washing and drying.

The ultimate goal of this project was to explore alternative and various synthetic routes for the design and fabrication of V@Pt core-shell and bimetallic nanoparticles. The novel preparative techniques resulted in the synthesis of uniform VPt bimetallic nanoparticles, although synthesis of core-shell nanoparticles still remains a challenge. The development of monodisperse VPt nanoparticles paves the way for facilitating oxidation-reduction reactions (ORR) in hydrogen fuel cells.

ACKNOWLEDGEMENTS

First and foremost, my sincere gratitude goes to my supervisor, Professor Candace Lang, for her excellent guidance, encouragement and infinite support during the course of my entire studies. The freedom she gave me to explore and pursue my own research ideas is deeply appreciated. These distinct experiences have not only greatly enriched my university career, but have also established a platform for my future career.

I would also like to especially and deeply thank Prof. Richard Vanfleet for generously providing his TEM expertise.

I would like to especially and deeply thank Mr. Mohammed Jeffer from the Electron Microscope Unit at the University of Cape Town for training me and giving me the privilege of using both the low and high resolution TEM instruments.

I would like to thank Dr. Frik Koch from the University of the Western Cape for all his help on the TEM at UWC.

I would also like to thank Prof. Rob Knutsen for teaching me about safety in the laboratory.

Finally, I thank my fellow colleagues and members of the Centre for Materials Engineering, the Department of Mechanical Engineering and the Department of Chemistry for their incredible assistance at various stages of my research work.

TABLE OF CONTENTS

1 INTRODUCTION

The field of nanocatalysis, the utilization of nanoparticles to facilitate reactions, has recently emerged as an area of interest in both homogeneous and heterogeneous catalysis. Nanoparticles, the building blocks of nanocatalysts, display diverse attributes such as monodispersibility, processibility, solubility and stability as a function of size, shape, composition and surface properties[1]. In heterogeneous catalysis, reactions take place on the surface of the catalyst and it is desirable to increase the surface area of the catalyst to optimize reactant-exposed metal atoms. Nanoparticles possess a large surface-to-volume ratio relative to bulk materials and as a result they are promising candidates as more effective catalysts[2]. However, most nanocatalysts employed in heterogeneous catalysis rely extensively on expensive platinum group metals (PGMs): there is a considerable economic benefit in reducing the PGM volume. Size reduction and the deployment of mixed-metal nanoparticles are therefore crucial parameters in the design and engineering of new-generation PGM catalysts.

To reduce loadings of expensive catalyst elements such as platinum (Pt) or palladium (Pd), synthesis of nanoalloys and core-shell nanocatalysts (where highly catalytically active Pt or Pd is alloyed with relatively inexpensive and less catalytically active metals), is of interest. Nanoalloyed catalysts have been reported to function better than their monometallic counterparts due to synergistic effects in which the catalyst system displays enhanced catalyst activity and selectivity[3].

Meunier's model[4] of catalyst design, shown in Figure 1.1, demonstrates the importance of understanding the structure-activity relationships in the fabrication of nanoparticles with novel properties. The activity of these new-generation metal nanocatalysts depends sensitively on their size and shape: size reduction (to increase the surface area) and nanoparticles of different shapes (with more corners) result in improved catalytic functionality. If the design of these model system catalysts is fully understood and well-defined, then this will provide an opportunity to design and engineer a catalyst with improved selectivity, in other words, increased production of the desired product

without any by-products (wastes): this is known as “green catalysis/chemistry” [5],[6],[7]. The ability to tailor structures at the atomic level offers enhanced reaction rates and reaction selectivities which are governed by the nanocatalyst size and shape.

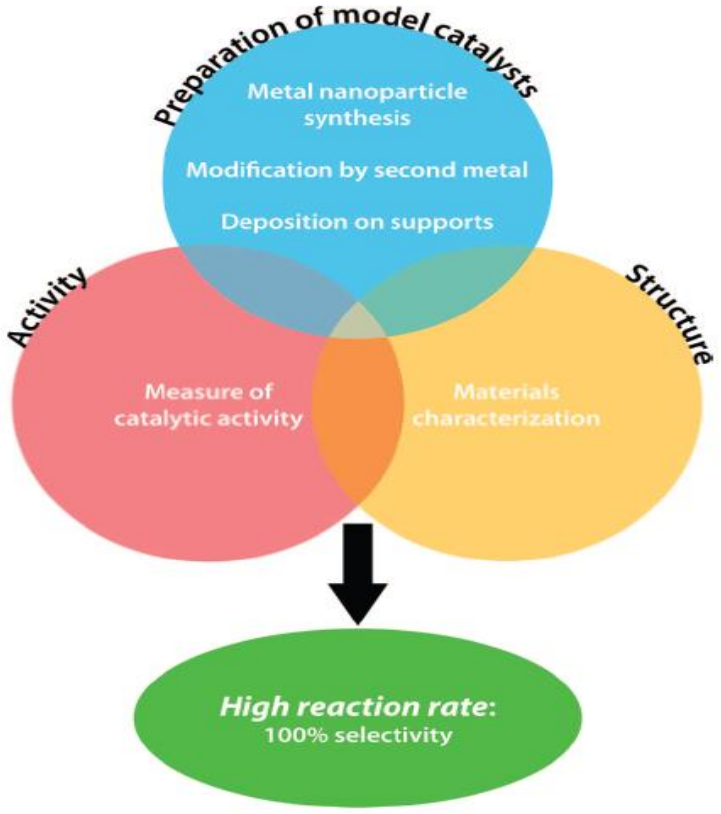

Figure 1.1: Design of metal catalysts for heterogeneous catalysis (after Meunier[4]).

The preparation of catalysts with improved catalytic activity and complete selectivity for a specific reaction requires the optimization of the catalyst surface structure (size and shape). The development of such nanocatalysts, with the structure targeted for a specific reaction, optimizes its catalytic functionality and results in near 100% or 100% selectivity towards the production of the desired product.

Figure 1.2 shows the reaction conditions (specifically temperature, pressure and reaction time in addition to the nature of the support, reactants and products) that influence the chemical and thermal stabilities of the catalysts during the course of the

catalytic reaction. Adjusting these experimental parameters affects the product selectivity. Seven molecular factors are reported to influence the selectivity of heterogeneous nanocatalyst (platinum) reactions at temperatures below 600K, as shown in Figure 1.2. These are surface structure, adsorbate-induced restructuring, adsorbate mobility, reaction intermediates, surface composition, charge transport and oxidation states[6].

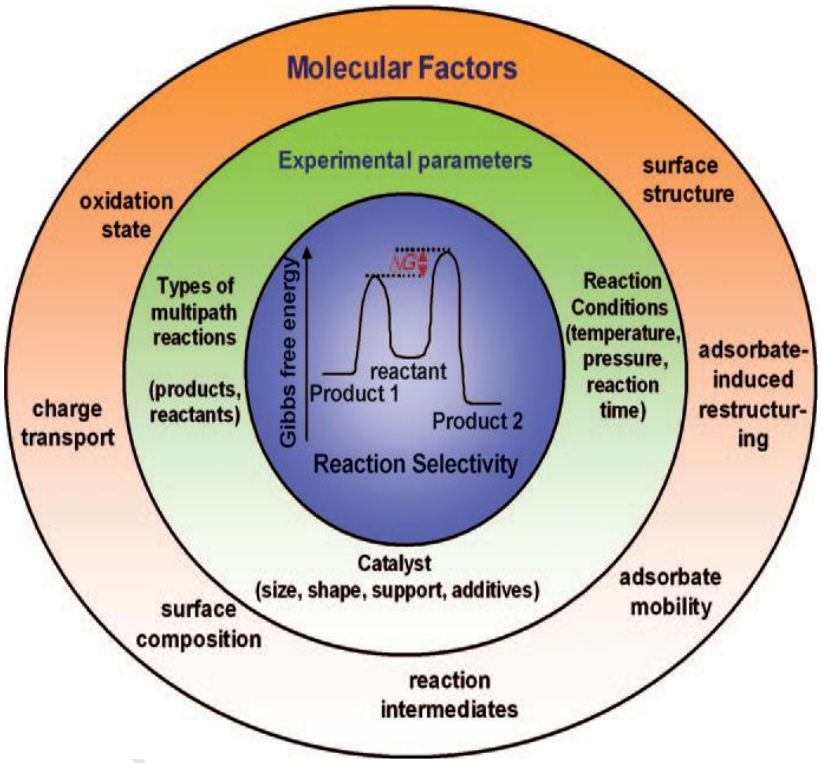

Figure 1.2: Seven molecular parameters that influence the selectivity of heterogeneous nanocatalyst reactions (after Somorjai *et al.*[6]).

The development of hydrogen fuel cells to generate electrical power from simultaneous half-reactions of hydrogen/oxygen gases has emerged recently as an area of great interest. Currently efforts are being devoted to the fabrication of high performance, robust and inexpensive catalysts for hydrogen fuel cell commercialization[1]. A schematic illustration of a proton exchange membrane hydrogen/oxygen fuel cell (PEMFC) is shown in Figure 1.3. These fuel cells are continuous-flow systems as the

reactants (hydrogen and oxygen) are continuously fed and electricity is continuously withdrawn as steady current. Water is produced as a by-product, hence minimizing air pollution and greenhouse gas concerns. PEMFCs offer economic advantages due to their high conversion efficiency, high power density, low pollution and low mass[1].

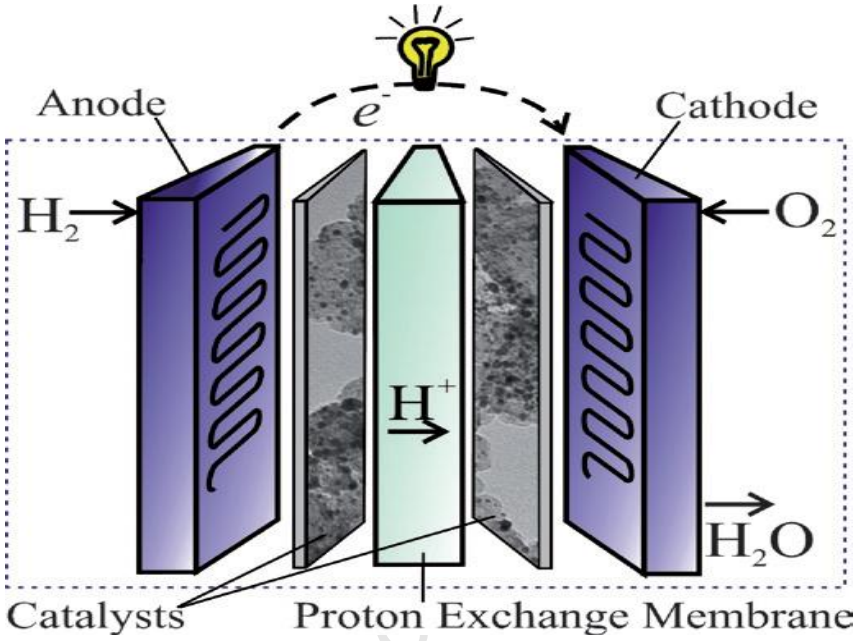

Figure 1.3: The components of a proton exchange membrane (PEM) hydrogen/oxygen fuel cell (after Zhong *et al*.[1]).

Recent computational models show the VPt alloy to have improved catalytic functionality at the nanoscale[8],[9], with particularly good performance for the oxygen-reduction reaction (ORR) and hydrogen dissociation. However, there is no experimental work to date on the surface catalytic properties of this alloy, or the preparation of VPt nanoalloys. The preparation of high surface energy nanostructured catalysts fabricated from VPt alloys with the desired surface catalytic properties for PEMFCs remains a challenge which has driven the current investigation.

Great efforts are currently devoted to the employment of chemical solution-based synthesis routes for the fabrication of novel metal nanoparticles of different morphologies from atomic level: the preformed nanoparticles of one metal element can

act as the precursor in the preparation of bimetallic and core-shell nanoalloyed catalysts, for the catalysis of oxygen-reduction reaction (ORR) and hydrogen dissociation in fuel cells. The ultimate goals of this project are therefore to:

- Design and prepare platinum (Pt), vanadium (V) and vanadium oxide nanoparticles of different morphologies with an extremely high surface area

- Develop bimetallic VPt and V@Pt core-shell nanoalloys.

2 LITERATURE REVIEW

2.1 PLATINUM

Platinum (Pt) is a silvery-white transition metal. All transition metals possess strong inter-atomic bonds and this bonding plays an important role in the determination of the crystalline structure and physical properties of these metals and their alloys. The metallic phases are influenced by the energy states of electrons in the crystal lattice[10],[11]. The physical properties of platinum are shown in Table 2.1.

Platinum belongs to a family of six members including palladium, osmium, rhodium, iridium and ruthenium. These six metallic elements, commonly found grouped together in nature and usually alloyed with each other, are classified as platinum group metals (PGMs)[12]. The PGMs are found in association with gold and silver and are therefore referred to as precious metals, being rare and desirable[12],[13],[14]. Among the platinum group metals, pure platinum is the most widely used metal, followed by palladium[13]. The PGMs exhibit similar outstanding chemical properties which include good corrosion resistance, resistance to chemical attack and a high melting point. Owing to their high melting points, the PGMs are ideal candidates for use at elevated temperatures[15],[16]. Furthermore, on heating above 1000 ºC, corrosion resistance, thermal stability, ductility and strength are retained[14]. The fcc metals of the platinum group exhibit good workability. Platinum in its pure metallic form is both ductile and malleable[13],[17].

The platinum group metals are able to catalyze chemical processes in a wide range of industrial applications. Platinum exhibits excellent resistance to oxidation and preserves its mechanical strength at both low and high temperatures[13],[15],[16]. Although platinum is relatively inert, it is easily attacked by substances such as bismuth, phosphorus, arsenic, lead, antimony, tin, and their oxides. Platinum loses its useful catalytic function once contaminated by these materials: this is referred to as “poisoning”. In addition, it

dissolves in aqua regia, which is simply a mixture of nitric and hydrochloric acids, although it is insoluble in either of these acids individually[13].

Table 2.1: Physical properties of platinum (after Ross[10]).

PROPERTY	**VALUE**
Atomic number	78
Atomic weight	195.09
Crystal structure	fcc
Colour	white
Specific gravity	21.45
Density [kg/m^3]	21 450
Melting point [ºC]	1769
Boiling point [ºC]	3800
Specific heat [10^{-1} J/g ºC]	1.34
Thermal conductivity [W/m ºC]	69.1
Coefficient of linear expansion (20 – 100ºC) [10^{-6}/ ºC]	9
Latent heat of fusion [J/g]	113
Latent heat of vaporization [J/g]	2704
Electrical resistivity [ρ] [μΩ-cm]	9.8
Electrode potential [V]	+1.2
Magnetic susceptibility [10^{-6}]	1.1
Temperature Coefficient of electrical resistance [10^{-3}/ ºC]	3.9
Young's modulus [10^9 N/m^2] [GPa]	152
Tensile strength (annealed) [N/mm^2] [MPa]	140
Hardness (annealed) [VHN]	37

Drawbacks that limit the use of platinum in various industrial applications are its scarcity, difficulty in purification and resultant high cost[10]. Regardless of these disadvantages, this precious and noble transition metal offers an excellent combination of catalytic properties and chemical stability, and is suitable for high temperature

applications. This combination of outstanding properties does not exist in metals outside the platinum group[12]. The high cost of this scarce and precious material is offset by its extended, dependable service in a wide range of industrial services[12] where the service of other nonmetallic and metallic candidate materials is almost impossible[14].

2.2 VANADIUM

Vanadium (V) in its metal form exhibits a brilliant white colour. The discovery of vanadium dates back to the early 1800s and it is one of the most plentiful and widely dispersed metals as it is found in approximately 152 different earth's crust minerals[18]. The physical properties of vanadium are shown in Table 2.2. Vanadium is fairly stable at room temperature but it has a high affinity for oxygen and nitrogen at elevated temperatures which alters the desired properties of this metal. At low temperatures, vanadium is resistant to atmospheric attack as well as to hydrochloric and sulfuric acids. Conversely, strong oxidizing acids attack vanadium at higher temperatures. In order to avoid the unwanted effects presented by atmospheric attack during hot working, vanadium must be shielded from air by heating under vacuum or in an inert gas environment[10].

Vanadium is soft, ductile and strong in its pure metallic form and thus it has good formability and exhibits excellent cold working properties[10]. It plays an important role in industrial applications. It has been used in aerospace applications due to its low density, high strength and resistance to high temperature and high stress operations. It has also been used in ceramics: vanadium salts are well known to present unique brilliant orange and blue colours in ceramic materials as well as in dyes for textiles and leather[18].

Table 2.2: Physical properties of vanadium (after Ross[10]).

PROPERTY	**VALUE**
Atomic number	23
Atomic weight	50.95
Crystal structure	bcc
Colour	Brilliant white
Specific gravity	6.11
Density [kg/m^3]	6110
Melting point [ºC]	1735
Boiling point [ºC]	3000
Specific heat [10^{-1} J/g ºC]	5.02
Thermal conductivity [W/m ºC]	31.0
Coefficient of linear expansion (20 – 100 ºC) [10^{-6}/ ºC]	8.33
Electrical resistivity [ρ] [μΩ-cm]	24.8
Electrode potential [V]	-1.5
Magnetic susceptibility [10^{-6}]	1.4
Temperature Coefficient of electrical resistance [10^{-3}/ ºC]	2.8
Young's modulus [10^9 N/m^2] [GPa]	125.5
Tensile strength (cold rolled) [N/mm^2] [MPa]	800
Hardness [VHN]	170

2.3 PLATINUM-VANADIUM ALLOYS

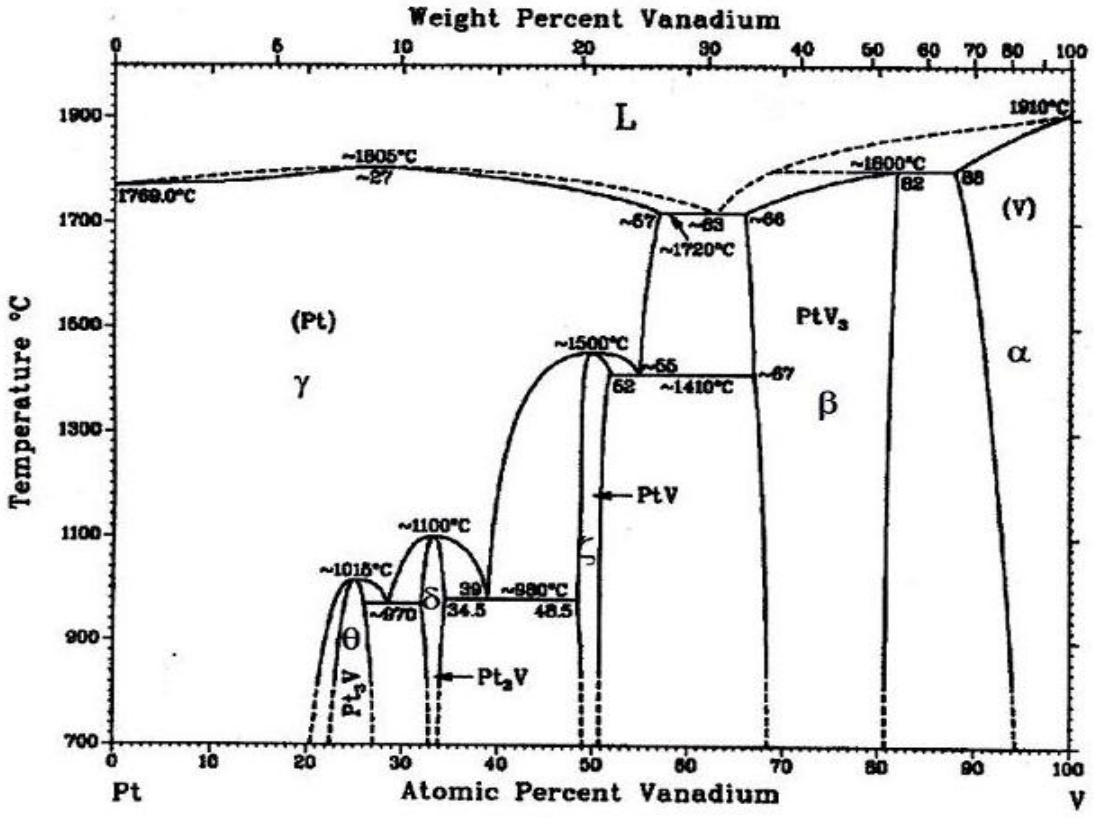

Figure 2.1: Platinum-vanadium equilibrium phase diagram (after Waterstrat[17]).

The platinum-vanadium phase diagram was established by Waterstrat[17]. It is complex and comprises a eutectic region as well as four intermediate phases and two terminal solid solutions, as shown in Figure 2.1. In this phase diagram, the maximum solubility of vanadium in platinum is approximately 57 at. % and this is exhibited at temperatures above 1500 ºC. In the platinum-base solid solution area, the liquidus goes through a flat maximum at about 1805 ºC. The four intermediate solid phases are PtV, Pt_2V, Pt_3V and PtV_3 which form at approximately 1500 ºC, 1100 ºC, 1015 ºC and 1800 ºC, respectively. The composition ranges of these phases at 900 ºC are as follows: 48.5 – 51.5 at. % V for PtV, 32.5 – 34 at. % V for Pt_2V, 22 – 23 at. % V for γ Pt_3V and 23 – 27 at. % V for θ Pt_3V. At 1800 ºC the peritectically formed compound is PtV_3 which exhibits a

composition range from 68 to 81 at. % V. The eutectic equilibrium is formed between the Pt-base solid solution and PtV_3, at 63 at. % V and ~1720 ºC ($L \rightarrow \gamma + \beta$). Three eutectoid invariant equilibria occur: between PtV_3 and PtV at 1410 ºC and at about 55 at. % V ($\gamma \rightarrow \varepsilon + \beta$); between PtV and Pt_2V at 980 ºC and 39 at. % V ($\gamma \rightarrow \sigma + \varepsilon$); and between Pt_2V and Pt_3V at 970 ºC and 28 at. % V ($\gamma \rightarrow \theta + \delta$). The maximum amount of Pt to dissolve in V is approximately 12 at. % and drops to about 5 at. % at 900 ºC[17].

Guo and Kleppa[19] calculated the standard enthalpies of formation of the four stable intermediate compounds reported in the vanadium-platinum system (PtV_3, PtV, Pt_2V and Pt_3V) as shown in Figure 2.2. The calculated standard enthalpies were compared with experimental results obtained using direct synthesis calorimetry. The pure element references vanadium and platinum are bcc and fcc phases, respectively[19].

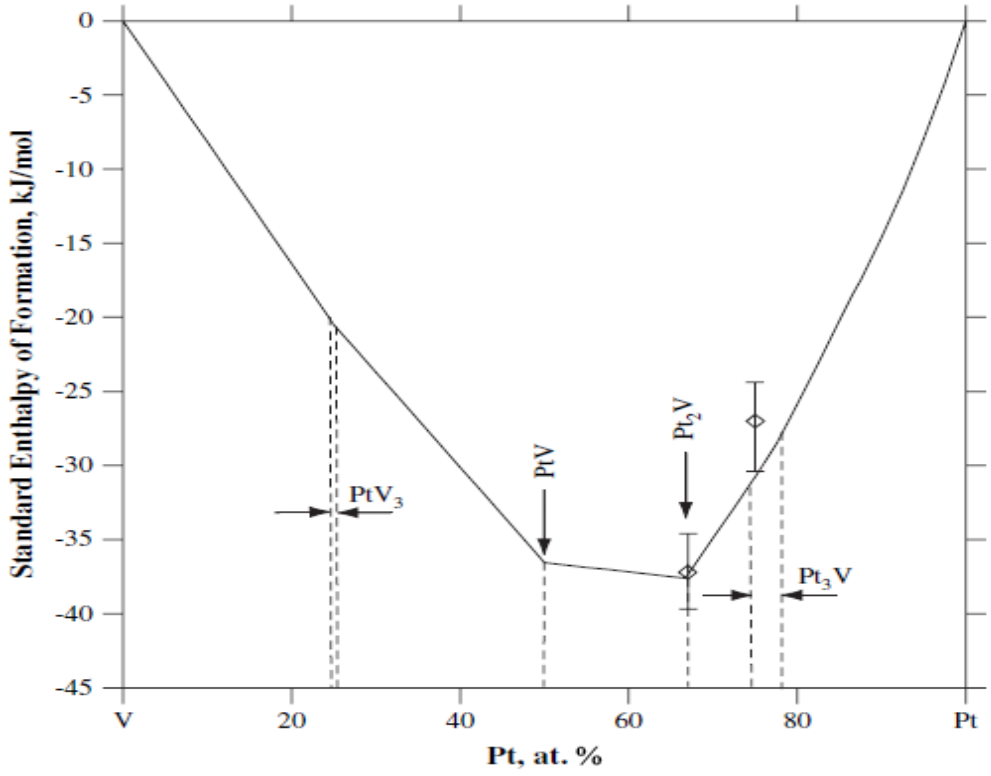

Figure 2.2: The computed standard enthalpies of formation of four stable V-Pt intermediate compounds (after Guo and Kleppa[19]).

2.4 CATALYSIS

Catalysis is a process that involves the use of a catalyst to accelerate the rate of a reaction[20]. The catalyst speeds up a chemical reaction without itself being consumed during the course of the reaction[20]-[21], and remains unaltered, hence is available for the next reaction. Thus, the catalyst is reused continuously during the reaction[20]. As long as the reacting species are available, the catalyst always participates in the chemical reaction, subject to the catalyst not being poisoned[21]. It achieves its function by forming bonds with the reactants, forming the product and detaching the product by breaking the bonds[20]. In this regard, catalysis is a process that: (1) alters the rates at which chemical bonds are formed and broken[22], (2) regulates the yields of chemical reactions, (3) enhances the quantity of desirable products while (4) decreasing the amounts of by-products. In the ideal form, this is termed “green catalysis”, where 100% or near 100% catalyst selectivity results in the production of a single desired product and thus, the chances of forming unwanted wastes are minimized[7, 23]. Industrial processes require solid catalysts which are stable, active and selective toward the production of desired commercial products. Solid catalysts should possess high surface area and suitable mechanical strength. The high surface area is an important requirement as reacting molecules will be accessed by a maximum number of active sites[24].

Good catalysts must possess the following characteristics: (1) higher activity (less catalyst employment), (2) selectivity (minimal or no production of by-products and wastes) and (3) stability (lifetime) [25]. The design and engineering of catalysts displaying these hallmarks are perceived as ideal candidates in a chemical process[23].

(i) The activity describes the increase in reaction rate of a particular reaction toward the desired product upon the use of the catalyst[25]. That is, the increase in rate of the reaction per unit surface area or per surface site[26]. The catalyst activity is appraised by its turnover frequency (TOF). TOF is the number of molecules that react per active

center per unit time, in units of reciprocal time[27]. The catalytic activity of transition metals for a given reaction process varies mainly due to the disparity in the strength of the adsorbate-surface interaction from one metal to the next[28].

(ii) Selectivity is a vital characteristic that measures the efficient use of the reactants and the possible purification requirements. That is, selectivity relates to the ratio of reaction rates related to the desired and undesired pathways during the reaction process[25]. The reactivity and selectivity of nanocatalysts can be tailored by well controlled and defined shapes of metal nanocrystals[29]. The properties that determine catalytic activity and selectivity include factors such as bulk and surface chemical composition, local microstructure and phase composition[25].

(iii) Stability (in other words prolonged lifetime or reduced catalyst cost) refers to a slow rate decrease of one or more steps in a reaction network over a period of time, where such changes could arise due to morphological changes in the catalyst or poisoning processes[25]. Stability is governed by how slowly the catalytic performance deteriorates and determines how often the catalyst should be replenished[30]. Properties of paramount importance for their use in specific catalytic processes involve porosity, shape and dimension, thermal and mechanical stability[24].

Catalysts are divided into two main categories, homogeneous catalysts and heterogeneous catalysts[26].

(a) Homogeneous Catalysis

In homogeneous catalysis, the catalysts and the reactants are dispersed in a single phase, such as a gas[26],[21] or a liquid[26],[21],[24],[31]. Homogeneous catalysts are mostly used in organic solvents at 300K – 500K and exhibit high activity with outstanding selectivity[24],[32]. In this temperature range, the selectivity and activity of homogeneous catalysts is higher than that of heterogeneous catalysts. Important drawbacks that limit

the use of homogeneous catalysts include poor recovery and inability to operate in continuous flow reactions. Additionally, it is very difficult and expensive to segregate nano-sized metal catalysts from the reaction products[,33]. Because of the different operating conditions, heterogeneous and homogeneous catalysis have emerged as two distinct disciplines and therefore have developed independently[32, 34].

(b) Heterogeneous Catalysis

In heterogeneous or contact catalysis, the catalysts and the reactants are in different phases[26],[21]. Heterogeneous catalysts typically operate at 400 – 800K in the presence of vapour phase reactants and product molecules[24],[35]. They are active solid metals[33] often deposited on very high surface area oxide supports such as silica or alumina, in order to utilize their high surface area. This achieves high turnover rates and also optimizes their thermal and chemical stability. The high surface area of the supports originates from their porous or spongelike structure[26] which provides a large interfacial area between the catalyst and the support, leading to proper binding for stabilizing the catalyst[36]. Heterogeneous catalytic reactions occur on the solid catalyst's surface atoms[26].

Alternatively, in heterogeneous catalysis, the reactants (gas or fluid) interact with the catalytic surface of very finely divided metal nanoparticles: this activates the chemical bonds in the reactants, resulting in their dissociation or rearrangement. When the nanoparticle catalyst is exposed to reactants, its catalytic surface can become restructured[22]. The surface atoms relocate during chemisorption (the bonding between the catalyst surface and the reacting species) and occupy positions which optimize their bonding to the adsorbate atoms or reacting molecules[37]. A series of important steps that occur in contact catalysis are summarized in Figure 2.1.

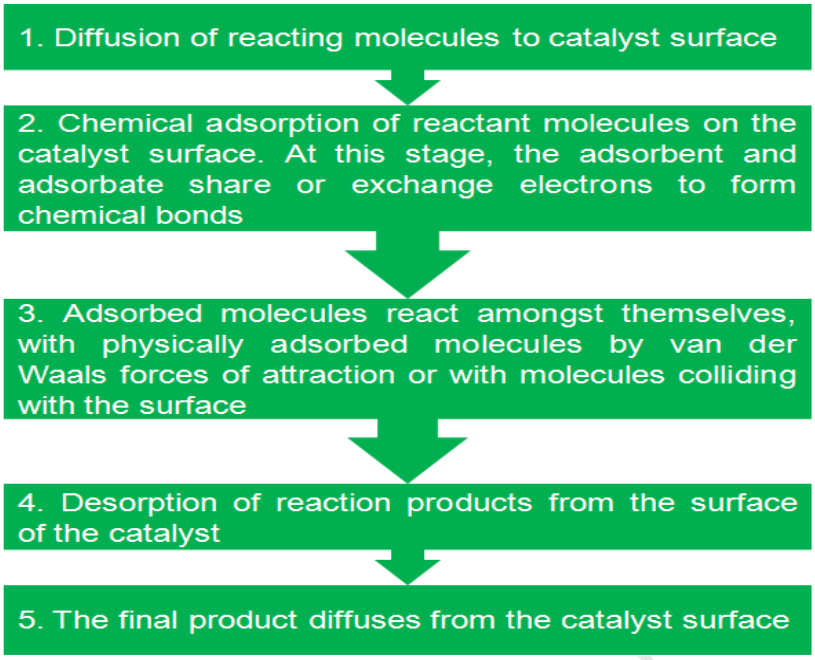

Figure 2.1: A series of steps that occur in contact catalysis (after Coughlin[38]).

Surface properties of transition and noble metals which are important in adsorption and dissociation of adsorbate bonds include the following: (a) the centre ϵ_d of the d-bands, (b) the extent of filling f_d of the d-bands, and (c) the coupling matrix element V_{ad} between the adsorbed molecule state and the metal d-states. During adsorption, the metal sp states are coupled to the adsorbed molecules and this produces a shift and broadening of the adsorbate states. This, in turn, releases adsorption energy. The development of a model of surface reactivity showed that surface alloying or overlayer formation (thin films) contributes greatly to the shift in the d-band states of transition and noble metals. The d-band center is the key parameter that determines the catalyst surface-bond to more than a few adsorbates[39]. Thus, the d-electrons determine the catalytic functionality of transition metals.

It has been reported[22] that the bonds formed between the catalyst surface atoms and the adsorbates generate heat. This heat provides energy which weakens the bonding between the metal atom and its neighbours. The metal atom moves from its original position and strengthens the chemical bond between the metal and the adsorbed

molecules. Thus, heterogeneous catalysis involves the movement of catalyst surface atoms. Without mobility of catalyst surface atoms and adsorbed molecules no catalysis occurs[22]. Furthermore, various catalytic surface irregularities which serve as more active sites for catalysis such as edges, terraces, steps, ledges, kinks and corners exhibit different reactivities[33].

The advantages of designing and engineering nanoscopic metal particles as solid heterogeneous nanocatalysts include ease of recovery and long life span (good recyclability). Thus, solid heterogeneous catalysts can be reused until their catalytic activity vanishes. These catalysts are well suited to use in continuous flow reactions[35],[34]. Apart from their ease of separation from the reaction, recovery and re-usability, heterogeneous catalysts offer several characteristic merits: stability, low cost and low toxicity[40]. Compared to homogeneous catalysts, the selectivity and activity of heterogeneous catalysts is lower in mild conditions[35]. Table 2.3 below compares the advantages and disadvantages of both heterogeneous and homogeneous catalysis.

Table 2.3: Heterogeneous catalysis versus homogeneous catalysis (after Nur[35]).

	Heterogeneous	Homogeneous
Activity	-	+++
Selectivity	+	+++
Catalysts Description	-	++
Catalyst Recycling	+++	-
Turn Over Number	+++	+
Quantity of Catalyst	+++	++

2.4.1 Supported Metal Catalysts

Heterogeneous (contact) catalysis involves the deployment of metal nanocatalysts supported on an inert surface (carrier) such as silica or alumina support material. The structural parameters and kinetic effects of these thermally stable and very high surface area oxide supports are displayed in Figure 2.3. The support or carrier material exhibits various exposed reaction sites which are very effective for breaking the chemical bonds of adsorbates and in catalyzing a specific reaction. The nature of these active sites originates from the orientation, size, shape and structure of carrier material employed[28]. Surface defects comprising edges, corners, interfaces, steps and kinks together with different crystal planes are realized. However, the activity of these bond-breaking reactive surfaces may be influenced by poisons and promoters during catalysis as they may alter the specific properties of exposed sites[25].

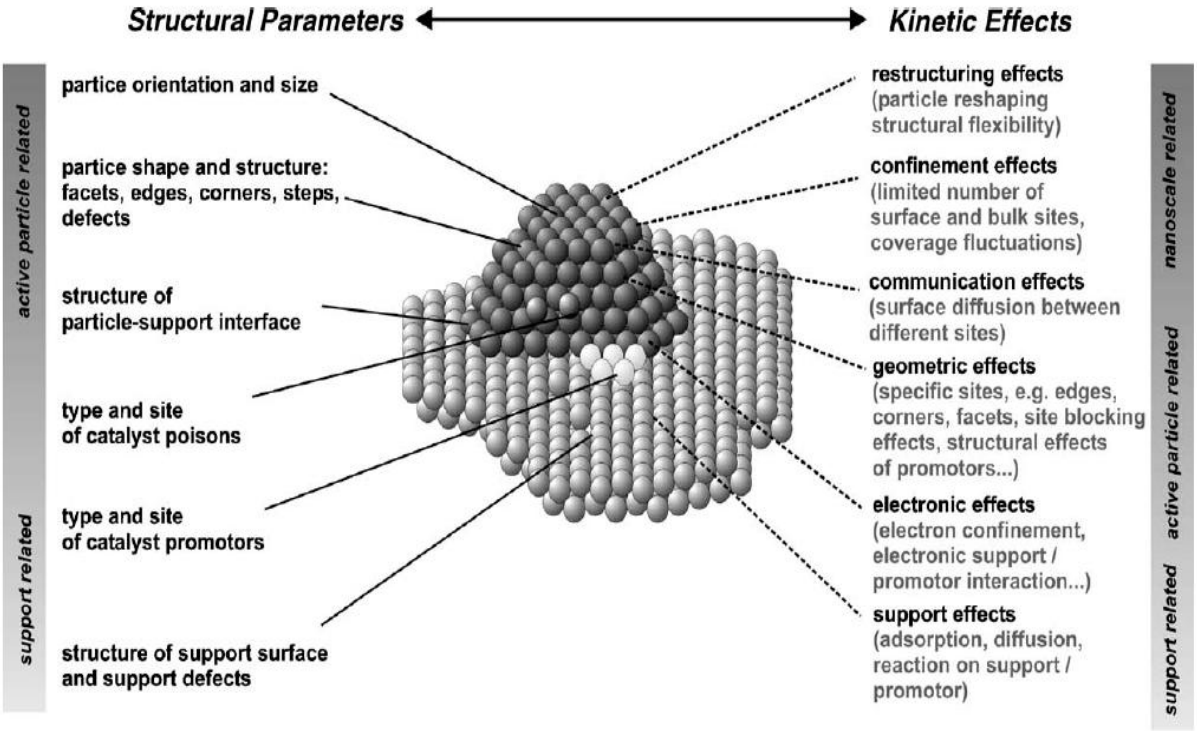

Figure 2.3: Structural parameters and kinetic effects on supported metal catalysts (after Libuda and Freund[25]).

2.4.1.1 Nanoparticle Synthesis

There are two methods that have been employed in the fabrication of nanomaterials: "top-down" and "bottom-up" approaches[41],[42].

1) The "top-down" method creates a gap between the bulk transition metals and nanocrystals through the division of bulky solid metal into microscopic portions, followed by their stabilization with surface active agents (surfactants)[41]. This approach embraces chemical methods, milling or attrition, and volatilization of a massive amount of solid material followed by condensation[42]. It is therefore difficult to prepare uniform-sized or monodispersed nanoparticles, and to control their size, by deploying the top-down method.

2) The "bottom-up" approach is the most widely successful method, used in the synthesis of nanoparticles from atomic level in wet chemical solution through the reduction of metal precursor salts. Atoms or molecular units are concentrated either in gas phase or in chemical solutions[41, 42]. The reduction of metal precursor salts in chemical solutions using reductants (reducing agents) is the most commonly employed method to produce colloidal metal nanoparticles of different sizes and morphologies.

Hydrogen gas[43-49] has been used as the reducing agent for the synthesis of colloidal metal nanocrystals and is a very slow reductant. This method requires the bubbling of hydrogen gas into a solution containing the transition metal salt and capping agents. Alcohols such as ethanol[50, 51] and methanol[52] have also been used as the reductants. The reduction of the transition metal precursor salts using alcohols occurs rapidly, forming colloidal nanoparticles. In most cases these alcohols act as both solvents and reductants, requiring refluxing of the resultant solution. The alcohols become oxidized to form carbonyl compounds whereas the transition metal precursors are reduced to zero-valent metals in the presence of stabilizing agents. Several other reductants have been reported in the literature that reduce transition metal precursor salts to colloidal

nanoparticles in chemical solutions. These include formic acid[53], ascorbic acid[54, 55], ethylene glycol[56-59], sodium citrate[60, 61] and hydrazine[62, 63]. Another reductant that has been commonly used in the preparation of colloidal transition metal nanocrystals is sodium borohydride[54].

Thermal reduction (thermolysis) has been successfully employed in the decomposition of organometallic precursor salts to synthesize metal nanoparticles. The surfactants used serve as both solvents and reductants[64]. This method involves the employment of high-boiling point solvents, and inert gases such as argon or nitrogen[64, 65]. Upon heating the reaction at elevated temperatures, the metal precursor salt decomposes into atoms or forms monomers which then form nanoparticles. The subsequent growth of these nanoparticles is dependent on the surface active agents used. The creation of nanoparticles is a two-step process: (a) in the first step (nucleation), the metal precursor salt decomposes to form atoms or reacts to generate saturated monomers at higher temperatures. (b) This generation of atoms or monomers is followed by a burst nucleation of nanocrystals. Finally, the nuclei grow by integrating other monomers present in the solution[66].

Colloidal nanoparticles can also be synthesized from metal precursor salts using capping agents as the reducing agents dissolved in higher boiling point solvents such as benzyl ether[65]. However, it requires the refluxing of the resulting solution. Surface active agents or capping agents are added in the solution prior to the decomposition or reduction of the precursor in order to manipulate nanocrystal growth and to preclude their agglomeration. The “bottom-up” method has provided room for the preparation of inorganic nanoparticles of precisely controlled shape, composition and highly monodispersed size distribution[41],[42]. Because nucleation and particle growth are regulated at the atomic level, nanostructured materials of diverse shapes with well-defined surfaces and morphologies can be made. In attaining crystal surface facet control through tuning of nucleation and growth phases in wet colloidal solutions, the critical factors to be considered are: (1) thermodynamics (such as temperature,

reduction potential) and (2) kinetics (reactant concentration, diffusion, solubility, reaction rate) as they regulate chemical reactions and hence control colloidal shape[67].

(a) Nucleation and Particle Growth

Nucleation is a process whereby atoms form aggregates. Therefore, as the nuclei grow larger crystalline particles are generated. The key driving force in the formation of nuclei of nanoparticles in wet chemical solutions is the degree of supersaturation[68]. During the synthesis of nanoparticles, the precursor salt is either decomposed (bond breaking of compounds) or reduced to zero-valence metal (reduction of metal ions) in the embryonic phase of nucleation[41],[69, 70]. During the decomposition of the metal precursor salt, the concentration of metal atoms increases gradually over time up to a point where they become supersaturated. The degree of supersaturation increases as the temperature offset increases.

The reduction of metal precursor salts breeds stable nuclei or “seeds” of zero-valent metal nuclei. Once the supersaturation point is reached, the atoms form small clusters[41],[70],[71], as shown in Figure 2.4. These small nanoclusters are thermodynamically unstable and tend to redissolve prior to reaching a critical radius. Depending on the redox potential differences between metal precursor salts and the reductants as well as the strength of the metal-metal bonds, “seeds” of < 1 nm are attainable. Futhermore, nanoparticle size is determined by the rate of nucleation and finally particle growth.

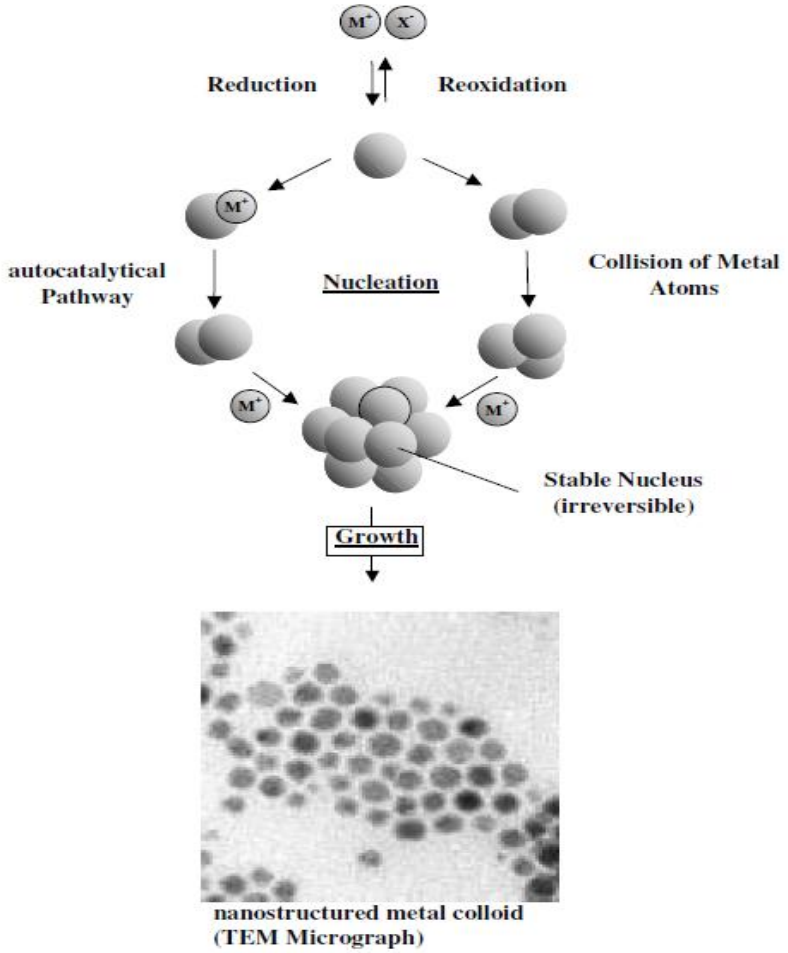

Figure 2.4: Creation of small structure metal colloids through the precursor salt reduction method (after Bonnemann and Nagabhushana[41],[70]).

Since nucleation during nanoparticle synthesis occurs when the solution becomes supersaturated, the conditions favourable for this process to occur involve dissolving the solute at higher temperatures followed by cooling to low temperatures, or the addition of reactants to make a supersaturated solution during the course of the reaction[72]. The induction of precipitation as a result of necessary supersaturation conditions originates from chemical reactions. That is, any reaction factors that affect the mixing processes (such as the rate at which reactants are added and stirring rate) are critical in particle size distribution, morphology and particle size[68]. According to the modified La Mer and Dinegar model[73] shown in Figure 2.5, synthesis of highly monodispersed metal

nanoparticles requires rapid nucleation followed by slow controlled growth of the present nuclei to develop stable nuclei. In the reaction vessel, the precursor salt concentration is raised above the nucleation threshold (or equilibrium state) upon rapid addition of reagents (reductants)[29],[73].

The creation of nanocrystals from the growing nuclei in wet chemical solutions ("bottom-up" synthesis method) originates from free or unstable atoms. Atomic concentration increases with time as the precursor salt decomposes but once the supersaturation point is reached where unstable atoms collide and grow into clusters, a critical size for stability is reached[29] and hence nucleation of a new stage occurs[71],[74]. The concentration of free atoms drops. However, with continuous decomposition of precursor salt, thus increased supply of atoms, the nuclei grow bigger, resulting in the formation of larger nanoparticles until equilibrium between surface atoms and atoms in solution is attained. As shown in Figure 2.6, upon the reduction or decomposition of the precursor, nuclei form and grow bigger to develop seed crystals which then result in the creation of different nanoparticle shapes[29], hence the evolution from seeds to nanoparticles and the morphology of the nanostructured materials.

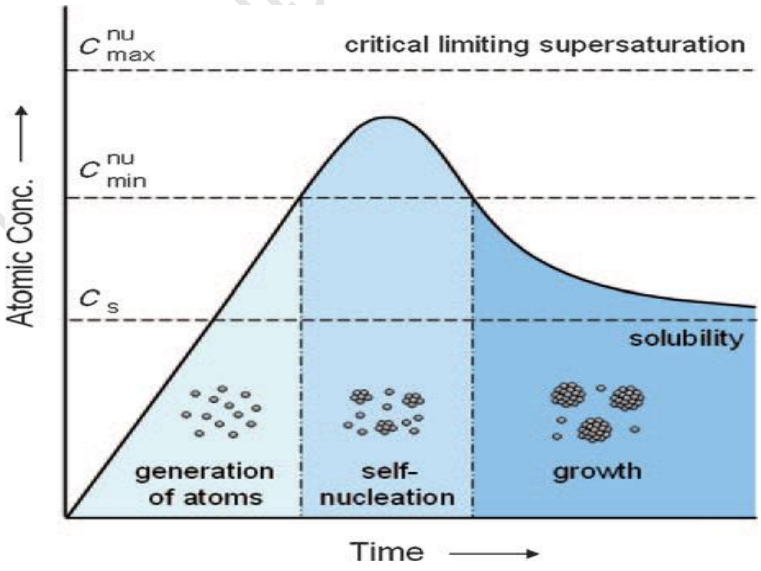

Figure 2.5: Atomic concentration versus time, indicating the creation of atoms, self-nucleation and particle growth (after Xia *et al.*[29]).

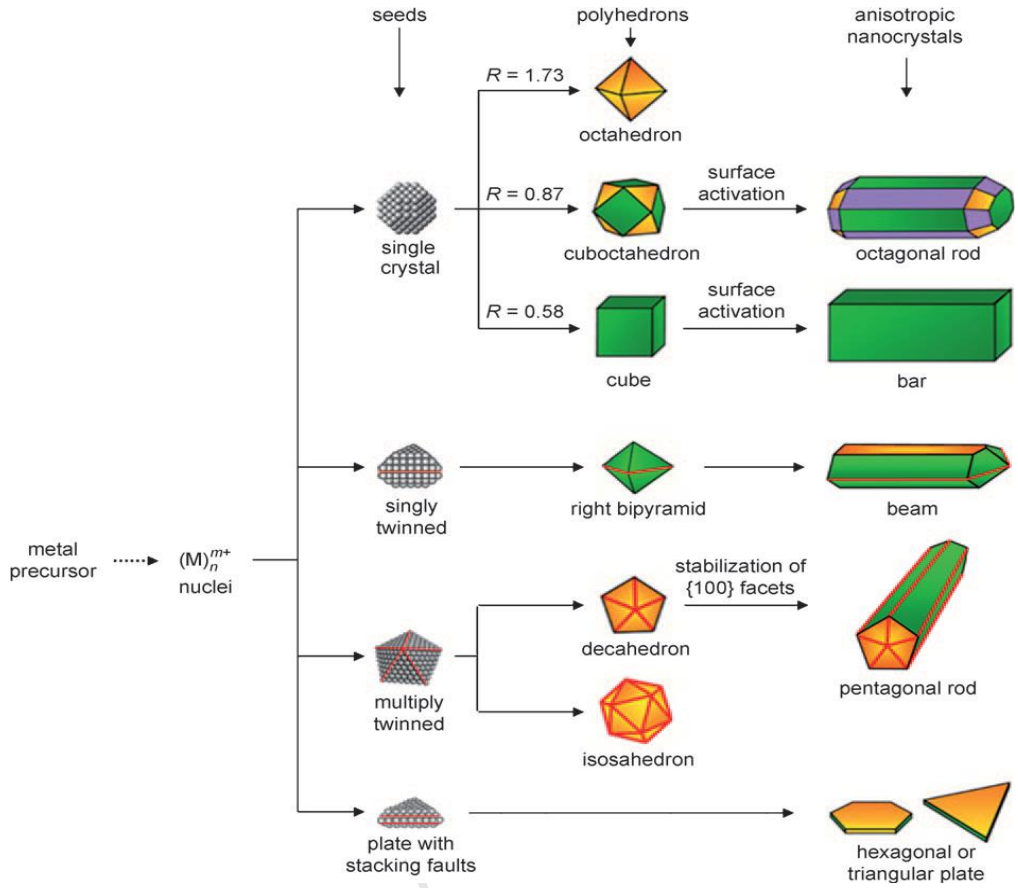

Figure 2.6: Showing fcc metal nanoparticles of tunable different shapes (after Xia *et al.*[29] and Skrabalak *et al.*[75]).

The supersaturation is relieved by a rapid but short nucleation stage. The initiation of particle growth and particle size distribution is largely influenced by the time over which nuclei form and initiate growth. That is, the slower the nanoparticle growth compared to the nucleation phase, the more uniform particle size distribution remains over time. This is referred to as focusing of the size distribution.

In order to harvest greater uniformity of nanocrystals or nanocluster properties, the initial diameter distribution of the so-called “near-monodisperse” nanocrystals should be ≤ ±15%[73, 74]. With tunable size range of 1 – 10 nm, highly monodispersed (≤ ±5%) metal nanocrystals are obtainable[73]. The growth mode of precipitated nanoparticles

depends on: (a) temperature, (b) cooling rate and (c) the concentration gradients of reactants. These parameters are the main contributors to the formation of a supersaturated solution during the reaction of reactants, hence precipitation of particles[68],[72]. Nucleation determines the shape of nanoparticles: shape regulation of finely divided nanocrystals can, therefore, be obtained via heterogeneous nucleation or homogeneous nucleation processes[67]. Thus, the nucleation process during colloidal synthesis is divided into two categories, namely heterogeneous and homogeneous nucleation.

Heterogeneous Nucleation

Heterogeneous nucleation of nanoparticles employs preformed seeds to accelerate the reduction of the metal precursor ions. The preformed seeds are added to a wet chemical reaction mixture. Thus, nanoparticle nucleation and growth occur as two segregated fabrication steps. These seeds possess preliminary shapes and the fabrication of particle shape is based on the zero-valent seeds. The reaction and reduction conditions are different from homogeneous nucleation as the activation energy for the metal ion's reduction on the preformed seeds is lower[76]. This overgrowth process employs a diversity of growth conditions such as lower temperatures, milder reductants or aqueous solutions for the regulation of shape. The research work by Murphy and co-workers[77] showed that the inclusion of preformed seeds to metal precursor salt in the presence of a weak reductant segregates the nucleation and growth steps while manipulating the size and morphology of the resultant nanocrystals.

Heterogeneous nucleation as a two-step or an overgrowth synthetic process facilitates the fabrication of bimetallic nanoalloys and core-shell nanoparticles. The regulation of shapes and sizes that are unattainable via homogeneous nucleation depends on the selection of metal precursors for overgrowth[78].

Homogeneous Nucleation

In homogeneous nucleation, seed particle formation occurs due to the reduction of metal precursor salts in solution. Consequently, nucleation and growth progress sequentially in the same solution. The creation of seed particles occurs according to the LaMer model[79] shown in Figure 2.7, where the reduction of metal ions to zero-valent metal particles evolves from the critical composition C_{crit} of atomic species. Nucleation above this critical concentration brings about rapid enervation of the reactants and successive growth occurs only on the preceding nuclei. Additionally, nucleation is suppressed if the concentration of the reactants is retained below the critical level and highly shape-monodispersed nanoparticles are formed when nucleation happens rapidly. Prolonged nucleation results in disproportionate depletion of reactants and as a result the growth rate of seed particles generated varies due to the different reaction times. The regions **I**, **II** and **III** signify prenucleation (creation of zero-valent atoms), nucleation or self-nucleation, and growth phases (seeds growing to form nanoparticles), respectively.

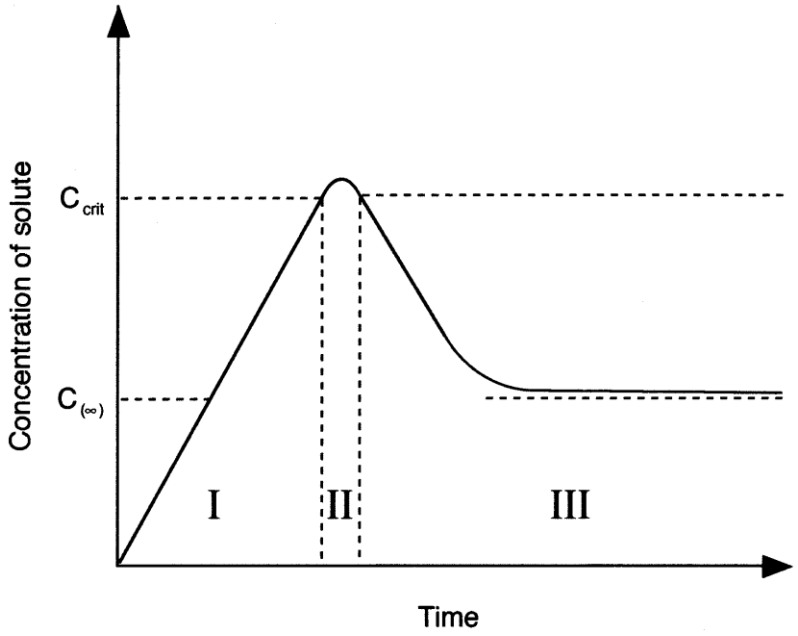

Figure 2.7: Schematic representation of LaMer model system (after Lar Mer and Dinegar[79]).

Sequential addition of metal ions to the solution speeds up fast nucleation. In contrast, fast reduction of metal ions is retarded in chemical solutions requiring temperatures of reflux. This permits the build-up of reactant species to reach the critical concentration of nucleation[76]. Even though the LaMer model system shows the phases of the creation of monodispersed particles from atomic level, it says nothing about the final particle size, their relationship and their shapes. The burst-up of reactants is achieved by modifying the reactivity of metal precursor salts through the use of capping agents or surfactants to construct metal complexes in the solution, thus coordinating the metal precursor and the surface-regulating agents or capping agents to form metal ion-capping agent complexes. These metal-polymer or metal-surfactant complexes delay the reduction reaction in spite of the highly suitable reduction conditions[53],[54]. The creation of seed particles that are either single crystals or exhibit single-crystal surfaces is a prerequisite condition for homogeneous nucleation, which occurs in the same solution, in order to regulate the shape of nanoparticles through subsequent growth.

(b) Ostwald Ripening/Coarsening

Ostwald ripening or coarsening is a mechanism whereby larger particles grow at the expense of smaller ones[71, 72],[68]. As the larger particles grow and the smaller ones decrease in size during the growth process, the smaller particles dissolve and finally become consumed by larger particles. Very small nanocrystals have extremely high energy surface which in turn influences their dissolution and redeposition on larger nanoparticles. The reduction in the mean size of smaller nanocrystals increases over time as they become consumed by the larger ones[68, 72]. Coarsening occurs faster at high temperatures because of increased kinetics of exchange at the crystal surface[71], as shown in Figure 2.8. That is, as entropy in the system increases, the crystal experiences more defects. Consequently, nanocrystal size distribution is not homogeneous and becomes broader; hence the uniformity of particle size distribution is lost[72]. Ostwald ripening impedes the formation of small monodispersed nanoparticles and displays a remarkable effect on particle size and particle size distribution,

morphological appearance as well as the properties of the product[68, 72].

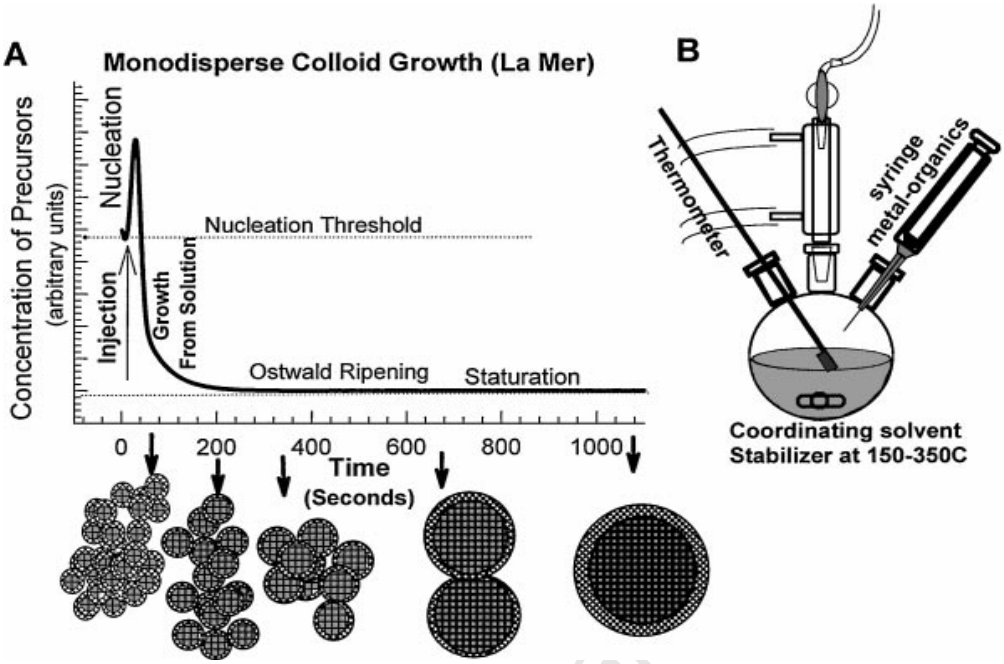

Figure 2.8: (**A**) Illustration of stages of nucleation and crystal growth over time and (**B**) a typical three-neck flask setup for nanoparticle synthesis (after Murray and Kagan[73]).

2.4.1.2 Growth Arrest and Nanocrystal Stabilization

Nanocrystals are microscopic particles and are therefore thermodynamically unstable. In order to inhibit aggregation and settling of nanocrystals, surface-active stabilizing or capping agents are introduced into the chemical solution prior to the decomposition and reduction of the metal precursor salt. These stabilizing agents allow the creation of sterically stable nanocrystals, and also preclude their aggregation and oxidation[41]. The distribution of nanocrystals is favoured by an excellent interaction between the surfactants and the solvent, providing energy to offset the van der Waals and magnetic attractions amongst individual nanocrystals[72]. Surface active agents are referred to as stabilizing molecules once they are attached to the surface of nanosized materials as monomers via covalent, dative or ionic bonding[73]. Surfactants are usually amphiphilic

organic compounds as they contain hydrophilic (water likes) heads and hydrophobic (water hates) groups which render them soluble in both organic solvents and water[29],[71].

Capping agents tend to reassemble themselves into ordered groups or micelles[6]. However, the most commonly employed solvent during nanoparticle synthesis is water because it is readily available, inexpensive and environmentally friendly. There are two different modes of stabilizing nanoparticles, namely electrostatic stabilization and steric stabilization[33],[41],[72]. In electrostatic stabilization, particles are forced apart to inhibit their aggregation as electrostatic repulsion forces are stronger than van der Waals forces which induce agglomeration. Steric stabilization involves the exploitation of sterically bulky organic surface-active agents which physically isolate particles, such as polymers, block polymers, bulky phosphines (P), amines (N) and thioether donors (S) [33], [41],[72] and long carbon chained fatty acids.

In organic preparation methods, hydrophobic ligand molecules protect the nanocrystal surface and hinder aggregation in such a way that the tail of a long carbon chain repels other nanocrystals from converging and agglomerating. The hydrophilic group (head) of the ligand molecule binds chemically to the surface of the particle. Due to chemisorption, adsorption, electrostatic or hydrophobic interactions, surfactants surround nanoparticles by forming an interfacial barrier. The result is minimum inter-particle separation in nanoparticle, reduces average particle size[73].

At low temperatures, surface-active agents bind strongly to the surface of nanoparticles by passivating (forming a capping or coating layer) and hindering their agglomeration as well as allowing their solubility in organic solvents. Thus, during nanoparticle growth surface-active agents adsorb reversibly to particle surfaces and mediate their nucleation and growth. In contrast, at higher temperatures this strong binding is lost. Instead capping agents are adsorbed on the surface and provide room for nanoparticle growth. However, at too high temperatures the growth of nanocrystals is difficult to control and it

is impossible to regulate the size and size distribution of nanocrystals. During the preparation of core-shell nanocrystals, surface-active agents can be eliminated where the shell is created from a highly catalytically active metal and is anticipated to play a great role during catalysis[71].

Surfactants also offer better control over the size, shape and quality of nanoparticles during their preparation[41]. The interaction of surfactancts and metal surface in chemical solution deviates the order of free energies for divergent crystal surface facets, hence their relative mechanisms of growth rates[29]. The deployment of surface stabilizing agents not only harvests uniform particle dispersion in colloidal solution, but also offers better shape-control, stimulating reduction onto specific crystal faces whilst suppressing precursor reduction onto other faces. The on-and-off exchange of surfactants on the surface allows the growth of nanocrystals. Thus, the selection of a suitable temperature range offers good control over the growth of nanocrystals. The growth of nanoparticles into different and well-defined shapes is restricted on the crystal planes where the surfactant or capping agent binding is strong and facilitated on the crystal planes where the binding is feeble[76]. In addition, nanocrystal size depends strongly on the ratio of surfactants to that of reagent concentration. The lower the reagent-to-capping agent concentrations, the larger the nuclei formed and hence the larger the nanoparticle size. That is, if the concentration of the capping agent-to-reagents is higher, very small nanoparticles are synthesized[72].

2.4.1.3 Nanoparticle Separation and Purification

Separation and purification of nanoparticles synthesized in wet chemical solutions is of paramount importance in order to harvest the required nanoparticles. These procedures exclude the impurities and excess surfactants, leaving unwanted preparative by-products or wastes in the solution while allowing the collection of the desirable and impurity-free nanocrystals. However, agglomerated nanoparticles are stable and tend to settle during or after their preparation. This agglomeration arises due to the repulsive

forces provided by the surfactants to offset the characteristic van der Waals attraction between nanoparticles. The energy to hinder agglomeration offered by the surfactants relies strongly on the energy of mixing between the surfactants and the solvent.

The dispersion of nanoparticles is destabilized due to the employment of nonsolvents that are miscible with the preliminary dispersing solvent. This results in agglomeration and settling of nanoparticles. Depending on how well-bound the surfactants are to the surface of zero-valent metal particles, the resultant nanoparticles can be redispersed in a diversity of solvents such as alkanes (toluene, hexane), aromatics (benzene), long-chained alcohols, chlorinated solvents (chloroform) and other organic bases (amines, pyridines, furans, phosphines). Desirable nanoparticles together with their respective intimate surface-active agents are attained through repeated flocculation and redispersion in fresh solvents[80].

Nanoparticles can be separated according to their size fractions[81] through the precipitation process, whereby the solvent is mixed with a nonsolvent to promote sluggish flocculation[82]. The largest nanoparticles often aggregate and precipitate before the smaller ones as a result of the highest van der Waals forces of attraction. Thus, the smaller particles are left behind with the by-products in the solution[83, 84]. With moderate flocculation, centrifuging the colloidal solution has been an alternative process. Nanoparticles are separated by first precipitating the larger ones whereas the smaller particles are left suspended in the supernatant (solvent or liquid). Centrifuging or adding extra nonsolvent to the decanted supernatant results in the precipitation of smaller-size distribution of nanocrystals. This precipitation procedure offers room for the isolation of decontaminated nanoparticles of different sizes[85, 86].

2.4.2 The Effect of Size Reduction

The use of noble metals (nonreactive metals) as catalysts requires the largest possible percentage of atoms at the surface in order to make them available to the reactants.

The creation of extremely small spherical metal particles presents a high surface to volume (S/V) ratio[72],[87] as shown in Figure 2.9. The S/V ratio is a fundamental parameter that plays an important role in the field of heterogeneous catalysis. The surface atoms and atoms located on the surface irregularities such as steps, ledges, edges, kinks and corners have lower coordination numbers (number of direct neighbours)[71],[88] than the bulk. The surface irregularities and the dangling bonds situated at these sites, lead to the creation of highly reactive catalyst species[89], serving as active sites in the chemical reactions for bond breaking[89]. These atoms are less strongly bound and are therefore much more flexible than those in the bulk[71]. Size and surface characteristics are thus the main factors governing the properties of materials at the nanoscale regime[80]. Nanometer-size transition metal particles containing tens-to-thousands of surface atoms[90] possess a surface that performs a key role in their basic properties[91].

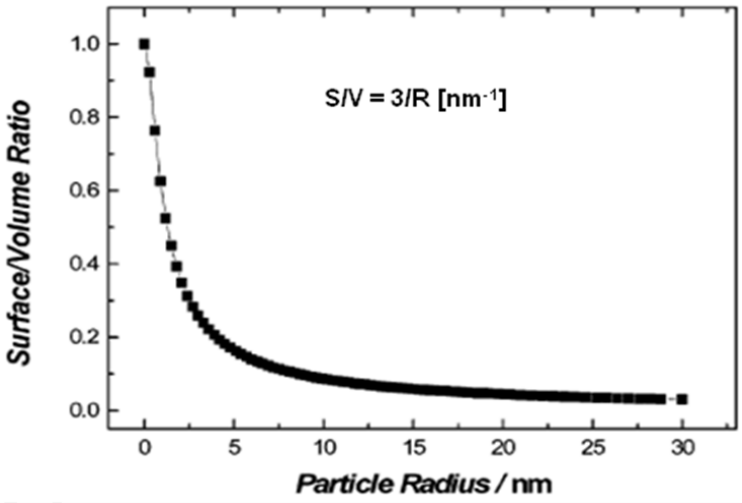

Figure 2.9: Surface-to-volume ratio as a function of particle radius (after Burda *et al.*[72]).

The S/V ratio[72] is inversely proportional to radius (R) for particles of spherical shape; however, complete-shell clusters are constructed by hexagonal and cubic closed-packed atoms[72]. It is therefore assumed that particles are shaped around a single atom by combining several dense-packed shells. Figure 2.10 shows the number of atoms in a cluster and the fraction of atoms in the surface of full-shell metal clusters[29].

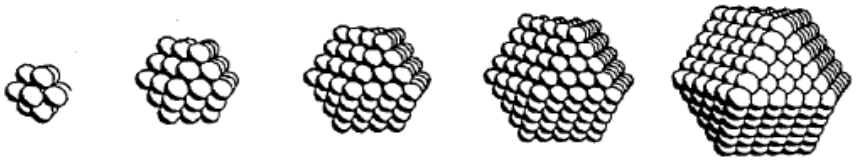

Full-shell "magic number" clusters					
Number of shells	1	2	3	4	5
Number of atoms in cluster	13	55	147	309	561
Percentage of surface atoms	92	76	63	52	45

Figure 2.10: Full-shell "magic number" formation, illustrating how the number of atoms in a cluster and the percentage of these atoms on the surface are related (after Xia *et al.*[29]).

Narayanan and El-sayed reported[92] in their studies that transition metal nanoparticles are well suited for use in catalysis because they have higher catalytic efficiency per gram than their larger counterparts. As a result of their novel structure, electronic states and highly exposed surface area with tens-to-thousands of atoms, transition metal nanocrystals are anticipated to stimulate and promote chemical reactions[93]. Additionally, the surface tension of transition metal nanoparticles is anticipated to be high, generating very active surface atoms[92]. The resulting instability can lead to changes in size and shape during catalysis[94].

Recently, the work by El-Sayed and Narayanan[94, 95] indicates that the surface atoms become physically unstable whilst retaining their chemical activity. Most of the industrial catalysts are ultrafine, high-surface-area metal nanoparticles having dimensions of 1 – 20 nm[96]. They are often distributed on supports with high-surface-area[96, 97] which offer suitable binding and interface for the catalyst stabilization[91]. Work by Chen and co-workers showed that catalytic activity does not only depend on the ratio of surface area to volume, but also on the arrangement of surface atoms[98], hence the surface structure in the nanoscopic size regime[99].

2.4.2.1 Electronic Effects

The electrical conductivity of bulk metallic materials is based on their band structure and the mobility of electrons[72]. The electrons in a metallic material are highly delocalized over a considerable space and the separation between the valence and conduction bands fades away, thus providing the metal with its conducting properties[20, 100]. Decreasing the size of bulk metallic materials to nanometer size regime with several hundred atoms, there is a dramatic decrease in the density of states in the valence band, resulting in a change of electronic properties. Alivisatos predicted that very small metal nanoparticles in the diameter range 1 – 10 nm, intermediate between atoms and bulk metal sizes, present electronic structures and the electronic band structure of nanoparticles[101] with discontinuous energy levels relative to bulk materials[102].

Clusters of metallic systems develop into semiconductors, semiconducting materials show metallic properties and behave as metallic materials, nonmagnetic elements develop into magnetic materials, the colour of particles changes, noble metals begin to be reactive, and brittle materials become malleable in the nanometer regime. These properties are due to the unusual, novel structure of these clusters[103], which exhibit different electronic structures, as well as different energy-level separations[20].

Very small particles (< 1 nm) are very ineffective during catalysis owing to insufficient valence electrons to contact both the carrier and adsorbates. Due to the size reduction of metal particles, the valence bands shift or the valance band structure is changed as the bond energy of electrons in the d-band is altered. The binding energies shift towards higher values and this transition promotes electron deficiency in metal particles. As a consequence of these energy shifts, the mode of substrate chemisorption (the bonding between the catalyst surface and the reacting molecules) is influenced[89].

When the size of metallic material is reduced and its electronic movement is restrained, the energy gap between the valence and conduction bands becomes comparable with

or larger than the thermal energy, $E_T = kT$[100, 104], and as a consequence the metal assumes semiconductor behaviour; a further decrease in metal size results in an increase in the band gap, which result in insulator behaviour. In this size domain where there is the metal-to-insulator transition, unusual and novel properties are anticipated[20].

Poole reports that the size-induced metal-insulator transition is observed when the metal particle is reduced to the size of about 20 nm and the size-dependent quantization effects materialize, as shown in Figure 2.11. The novel physical properties at this nanoscale regime are, however, dependent on the size of the particle, interparticle distance, the nature of the protecting shell (capping agent) and the shape of very small metal particles[105].

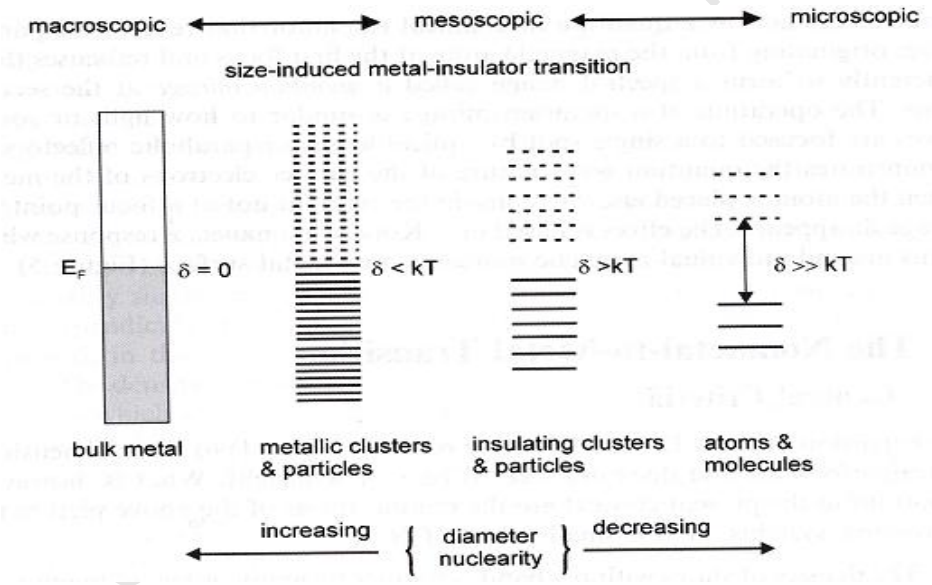

Figure 2.11: The band gap evolution and the density of states as the number of surface atoms increase (after Poole[20]).

This metal-to-insulator transition can be correlated with the results obtained by Schmid[106] in Figure 2.12. In other words, the change from bulk metal to cluster and to molecular behaviour results in complete loss of electrical conductivity as a result of increase in band gap (the distance between the valence and conduction bands)[103].

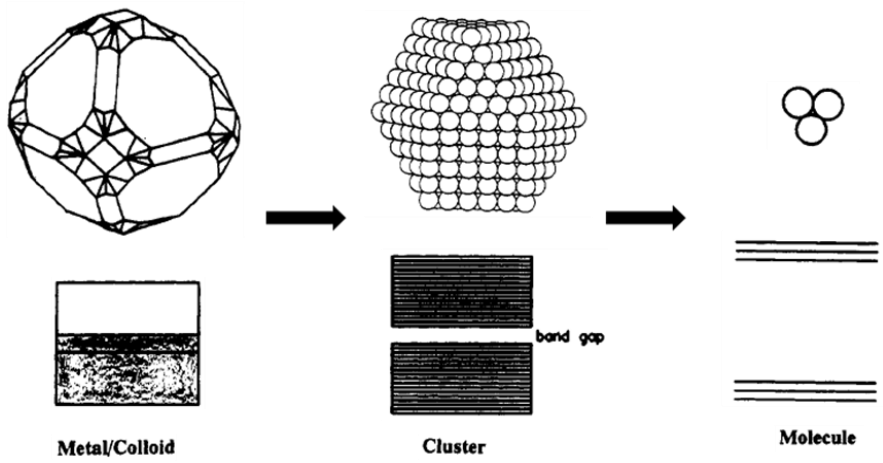

Figure 2.12: Schematic showing the electronic states in (a) metal particle with bulk properties and its typical band structure, (b) large cluster of cubic close-packed atoms with a small band gap, and (c) simple triatomic cluster with entirely separated bonding and antibonding molecular orbitals (after Poole[20], Schmid[106]).

2.4.2.2 The Melting Point of Ultrafine Metal Nanoparticles

Most atoms in bulk crystalline materials are stable and have the highest possible coordination number. Their neighbours contribute the binding energy which results in stable atoms[71]. Because nanoparticles possess surface atoms that have fewer neighbours that are coordinatively saturated, they have higher surface energy associated with them. Owing to the large surface energy contribution, the surface of nanoparticles melts easily, thus lowering the melting temperature of nanoscopic materials and affecting several other properties of the particle[71, 72].

The key understanding of the melting point stems from the fact that liquid phase always has lower surface energy in contrast to the solid phase. In the liquid phases, which exhibit dynamic behaviour, surface atoms move to reduce their surface energy. In the solid state, strong bonding results in stepped surfaces with high-energy edge and corner atoms. These surface atoms often melt first at high enough temperatures. Therefore, the more finely divided the metal particles are, the more they contribute to the overall energy of the system owing to their higher surface energy[72].

Simulation predictions[107] show that Pt nanocrystals preserve their original shapes and structures at low temperatures. However, the temperature of shape deformation is governed by their shapes, and the associated crystallographic planes on their surface. Upon the exposure to elevated temperatures, the shape of these nanounits deform to "near-spherical" prior to overall surface melting[107], as shown in Figure 2.13.

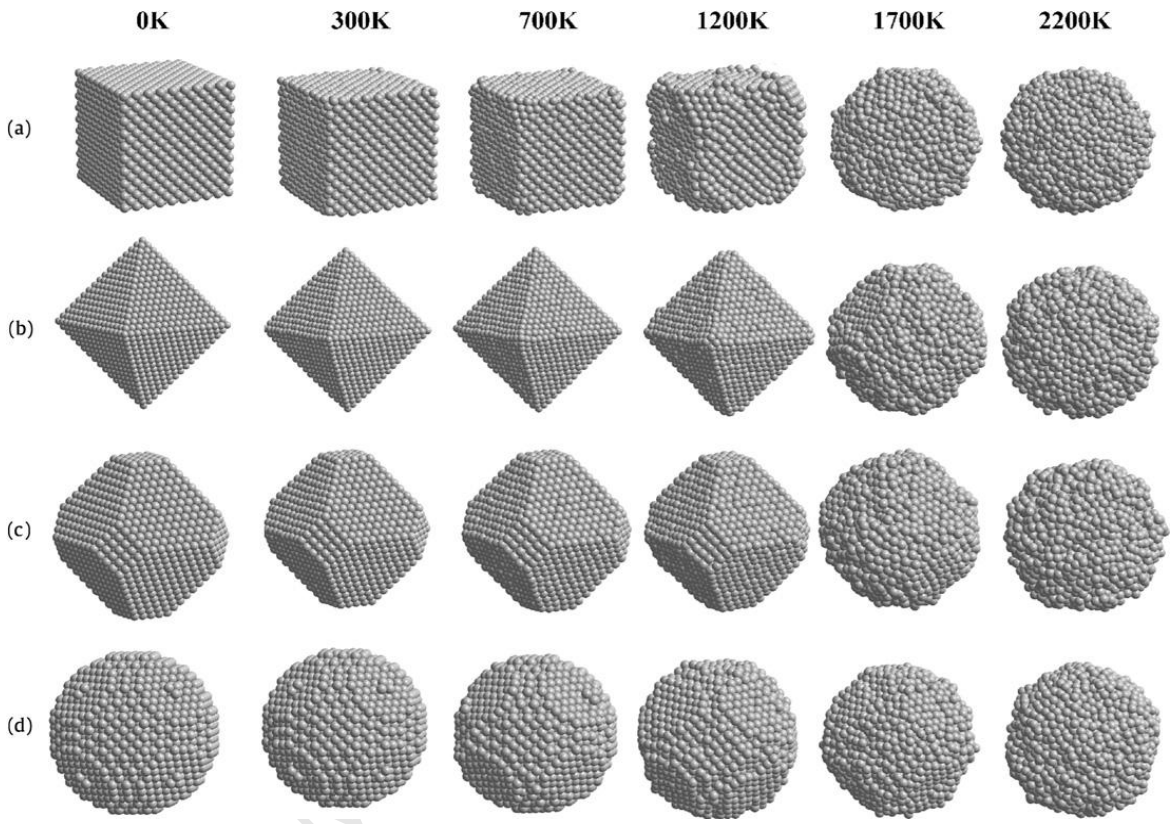

Figure 2.13: Atomic arrangement at 0K and shape deformation of (a) cubic, (b) octahedron, (c) truncated octahedron and (d) spherical Pt nanocrystals as a result of increased temperature (after Wen *et al.*[107]).

Knowledge of the size change of nanocrystals as a function of temperature aids the understanding of their thermal stability. This mode of size change with temperature is interconnected with the growth mechanism[108]. Research work by Burton[109] showed that as the metal particle size is reduced to microscopic scale its melting point decreases and with further size reduction to about 10 Å, its melting point may be half that of the parent material.

2.4.3 The Effect of Shape on Catalytic Properties

The shape of nanoparticles is of utmost importance in both heterogeneous and homogeneous catalysis since different shapes exhibit different surface facets[71][72]. These different crystalline planes have different densities of atoms located at different corners, steps, kinks and edges[71],[110]and are therefore anticipated to function as active sites for chemical transformations[111]. The catalytic performance of nanoparticles is thus anticipated to be different to the bulk in catalysing the same reaction[71].

Tailoring of shapes with high Miller surface indices {hkl} shown in Table 2.4 creates a platform and holds the key to enhanced catalytic activity. These high-index facets display a large fraction of dangling bonds and atomic steps[88]. The fcc metal surfaces are characteristically composed of {111} and {100} facets. These common and stable low-index planes contain the lowest density of corner and edge active sites. As a result, the surface energy of the shapes enclosed by low-index facets is expected to be low[112]. As shown in Figure 2.14, three basal planes (111), (100) and (110) locate at verteces in which (111) and (100) planes are characterized by closely packed surface atoms whilst the surface of (110) plane is rough with step atoms[113]. High-index planes, e.g., Pt (210), are reported to show enhanced chemical and thermal stability under both oxidising and reducing conditions as well as at high temperatures[114].

Table 2.4: Projections and geometrical parameters of polyhedral shapes enclosed by divergent high Miller surface indices (after Xiong *et al.*[88]).

Polyhedral Shape	Tetrahexahedron	Trapezohedron	Trisoctahedron
Miller Index	$\{hk0\}$	$\{hkk\}$	$\{hhl\}$
Projection Direction	[001]	[001]	[110]
Projection	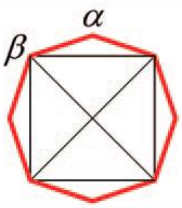	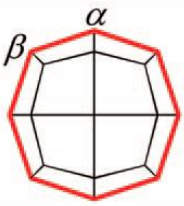	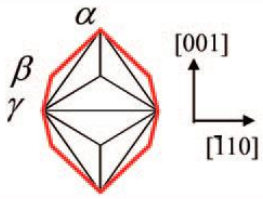
Character Angle / degree	$\alpha = 2\arctan(h/k)$ $\beta = 270 - \alpha$	$\alpha = 2\arctan(h/k)$ $\beta = 270 - \alpha$	$\alpha = 180 - 2\arctan[(1+\frac{l}{h})/\sqrt{2}]$ $\beta = 270 - \alpha/2 - \gamma/2$ $\gamma = 180 - 2\arctan(\frac{l}{\sqrt{2}h})$

The order of increase of different crystallographic planes' surface energies is

$$\gamma\{111\} < \gamma\{100\} \ll \gamma\{110\} \ll \gamma\{hkl\}$$

where, at most one of h, k and l is equivalent to two or greater. The {hkl} signifies high-index planes with high surface energies[115]. The high-index facets exhibit enhanced catalytic activity and selectivity. Figure 2.14 indicates coordination of different crystal facets whereas Figure 2.15 shows the correlation between nanoparticle shape and crystal surface facets. Due to tailored shape differences of fabricated novel nanostructured catalysts, these catalysts are anticipated to display different catalytic activities during catalysis.

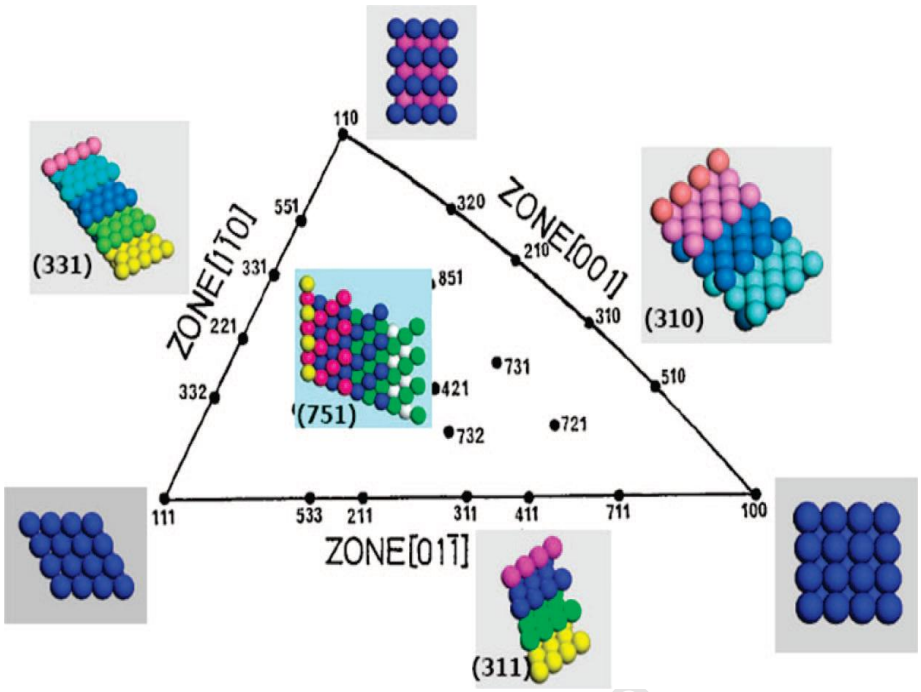

Figure 2.14: A unit stereographic triangle of fcc single-crystal and different models of surface atomic arrangement (after Tian *et al.*[113]).

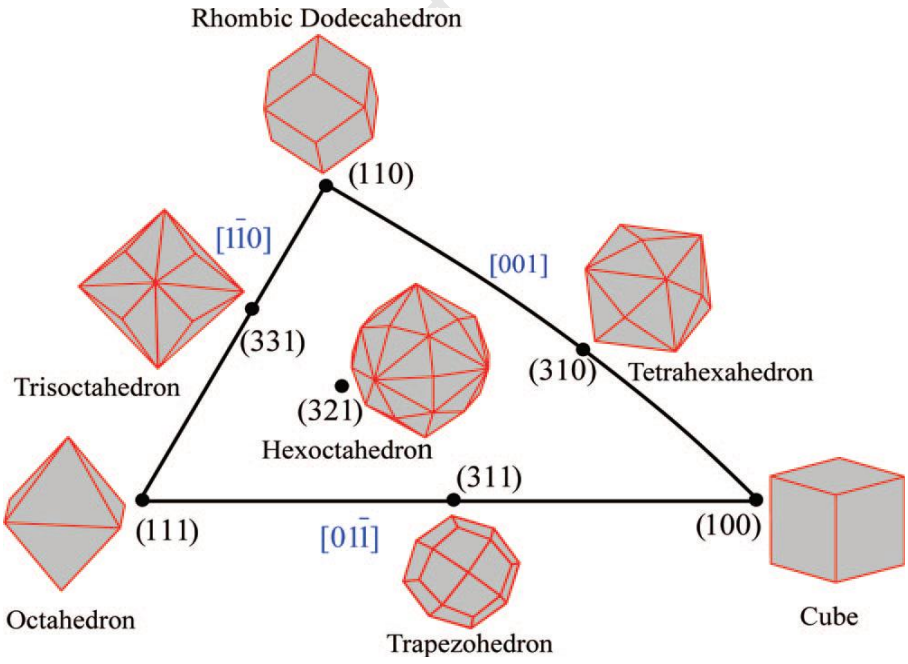

Figure 2.15: A unit stereographic triangle of polyhedral nanoparticles enclosed by different Miller indices (after Tian *et al.*[113]).

El-sayed and Narayanan[94] studied the catalytic functionality of nanocatalysts of different shapes, namely tetrahedral, spherical and cubic, as shown in Figure 2.16. Their work showed that tetrahedral metal nanoparticles are enclosed by {111} planes and display both sharp corners and edges, whereas cubic nanoparticles are {100} enclosed, with less sharp corners and edges in contrast to tetrahedral shapes. The spherical nanoparticles are encircled by several {111} and {100} facets with corners and edges at the interface of the facets. In contrast, high-index surfaces display high catalytic performance and stability more than low-index surfaces[94]. Table 2.5 shows different reproducible and controllable shapes of metal nanoparticles.

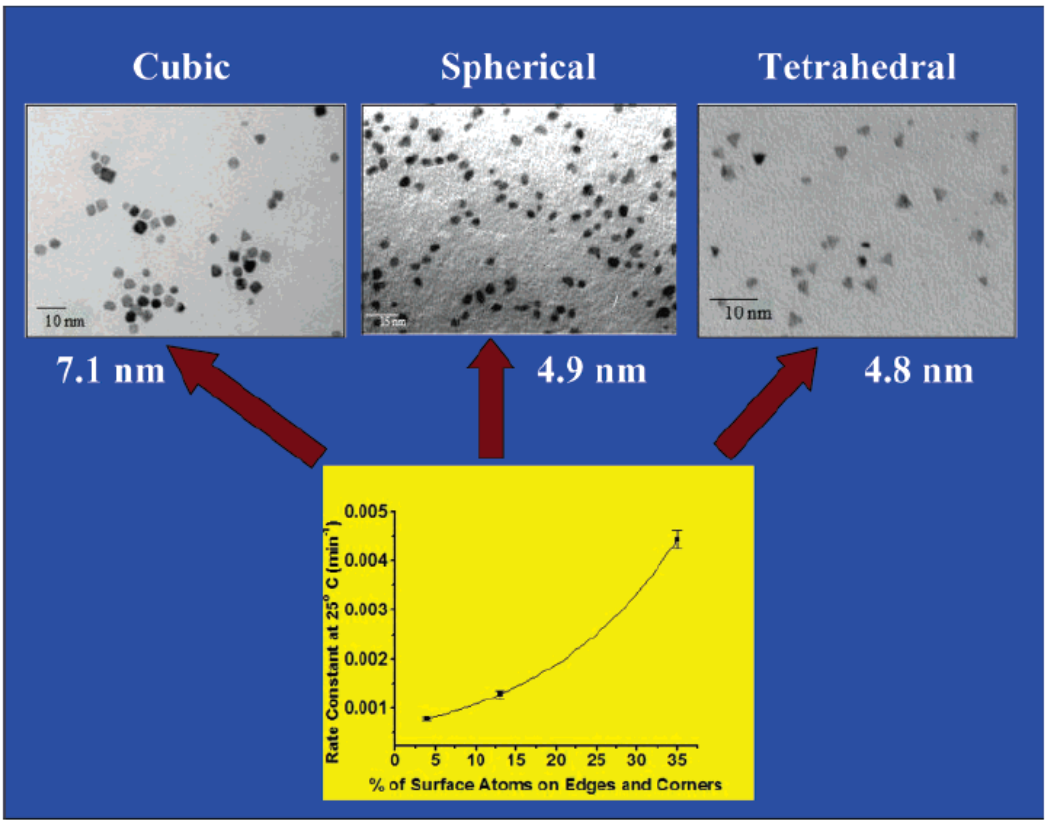

Figure 2.16: Correlation of the fraction of surface atoms positioned on the edges and corners with the catalytic activity of the nanocrystals of different shapes (after El-sayed and Narayanan[94]).

Table 2.5: A summary of reproducible different shapes of metal nanocrystals that have been achieved (after Xia *et al.*[29]).

Structures	Shapes	Schematic drawings	Metals
single-crystal	perfect/truncated cube[a]	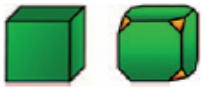	Pd, Ag, Au, Pt, Cu, Rh, Bi, Fe
	perfect/truncated octahedron[a]		Pd, Ag, Au, Pt
	perfect/truncated tetrahedron[a]		Ag, Au, Pt, Rh
	rectangular bar		Pd, Ag, Pt
	octagonal rod		Pd, Au, Fe, Co, Ni
	rectangular or octagonal wire	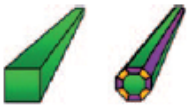	Pb, In, Sn, Sb, Fe, Co
singly twinned	right bipyramid		Pd, Ag
	beam		Ag
multiply twinned	decahedron[a]		Pd, Ag, Au
	icosahedron[a]		Pd, Au
	five-fold twinned pentagonal rod		Pd, Ag, Au, Cu
	five-fold twinned pentagonal wire	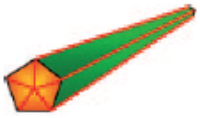	Ag, Au, Cu
	triangular/hexagonal plate		Pd, Ag, Au, Cu, Pb, Bi, Co, Ni
	disc		Sn, Co

2.4.4 Bimetallic Nanoalloys

Nanoalloys are nanoparticles composed of two or more different elements as a result of alloying of metal components. These intermetallic compounds and binary nanoalloys improve specific catalytic properties due to synergistic effects whereby the presence of a second type of metal atom in the system enhances the catalytic activity and selectivity of a single-metal catalyst. A great diversity of compositions, structures and properties of bimetallic alloys has provided room for the employment of new-generation metal nanoalloys in catalysis. Alloyed nanoparticles possess new chemical and physical properties which are unknown from those of the pure elemental nanocrystals[33].

By tuning the composition and structure of the particle surface, optimal catalytic activity and selectivity may be achieved in bimetallic nanocatalysts. In bimetallic nanoparticles, atomic arrangement is distinct from the bulk metals and may adopt a completely different type of structure due to unusual distribution of individual metal elements compared to the bulk counterparts. These structures may include particle-in-particle, particle-on-particle, aggregated nanocrystals, core-shell nanoclusters, nanoallys, segregated particles and super core-shell nanoalloys, depending on the fabrication routes[33], as shown in Figure 2.17.

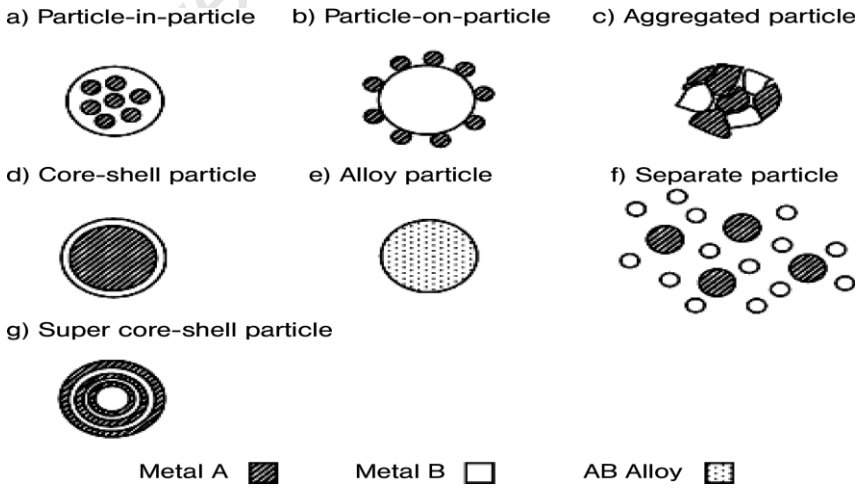

Figure 2.17: Schematic illustration of possible morphologies of bimetallic nanocrystals (after He *et al.*[115]).

2.4.5 Supported Nanocatalysts in Heterogeneous Catalysis

2.4.5.1 Types of Carriers (Supports)

Heterogeneous (contact) catalysis involves the employment of metal nanocatalysts supported onto high surface area, inert carriers (or supports)[116]. Transition metal nanocrystals are supported onto the carrier by the adsorption process. First, metal nanocrystals are synthesized from atomic level by forming a colloidal suspension of particles and impregnating them on the support. Thereafter, the supported metal nanocrystals are purified by washing the solid several times to remove the impurities. Carriers onto which nanocrystals can be impregnated include silica[117, 118], alumina[119, 120] and carbon[121-126].

Among these supports, carbon carriers have been mostly used to support metal nanoparticles for fuel cell reactions. Carbon supports include carbon nanotubes[126], carbon nanofibers[122], carbon black[123], activated carbon[124] and Vulcan XC-72[121],[125, 126]. In order to obtain high active surface area, porosity and pore size distribution; activated carbon carriers have to be prepared and modified. This pre-treatment and conditioning improves the adsorption of metal nanocatalysts onto the support during impregnation and distribution in the colloidal solution[127]. Multiwall carbon nanotubes (MWCNTs) as the carriers for heterogeneous transition metal nanocatalysts have been used because of their high porosity with a high surface area contained in pores and high electrical conductivity[127].

2.4.4.1 The Effect of the Carrier (Support)

Carriers have a profound effect on the catalytic functionality of nanocatalysts either by modifying the charge and metal particle size[128, 129], changing particle shape[130] or by forming specific dynamic centers at the metal-support deposited area[131]. Additionally, the support may participate during the course of a reaction network as it aids in

stabilizing active metal catalysts. Direct ionic or covalent bonding with the support of the metal atoms is anticipated and the density of these bonded atoms is enriched due to the size reduction of metal particles. Consequently, the performance of such highly unsaturated atoms is enhanced with finely divided particle size. Surface diffusion of the adsorbed reactants couples the adsorption processes on the support material and the reaction network on active metal nanocatalysts. In the case of weak adsorption of reacting species to the support, molecules can recoil and get dispersed in the direction of the active nanosized metal particles from the support[25].

2.4.6 Nanocrystal Superlattices

Nanocrystal superlattices or crystals of nanocrystals (ordered assemblies of crystalline nanoparticles) were first reported by Bentzon and co-workers[132]. These superlattices are also known as colloidal crystals[73, 133]. Self-assembly into close-packed and ordered superlattices (well-defined structures) requires the preparation of nanoparticles in the presence of capping agents to regulate their size, morphology and size distribution to reach a minimum free-energy state[134, 135]. Nanocrystals synthesized from various metals, metal alloys and metal oxides in colloidal solution, resulting in the formation of 2-D and 3-D ordered structures have been reported in the literature[136].

One of the successful methods that has been deployed in the preparation of highly monodisperse self-assembled nanocrystals is high-temperature solution-based synthesis. This method involves the use of high boiling point solvents in the boiling range of 100 – 300 ºC, as shown in Figure 2.18.

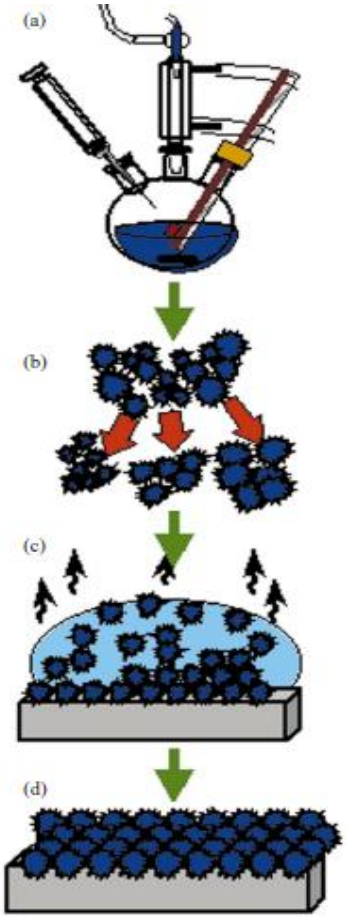

Figure 2.18: High-temperature solution-based synthesis (a) preparation of nanocrystals, (b) size-selective precipitation of narrowed nanocrystal size distribution, (c) deposition of nanocrystals from solvents to self-assemble, and (d) colloidal crystals (after Murray *et al*.[133]).

This process involves the addition of a non-solvent that is miscible with the first solvent and promotes more particle-particle than particle-solvent interactions. The non-solvent selected must not have any favourable interaction with the surface active agent, in order to minimize the barrier to aggregation while permitting the destabilization of nanoparticles. Consequently, this destabilization of particles results in their flocculation based on their size range[133, 137, 138]. The larger nanocrystals often precipitate first due to the greater forces of van der Waals attractions[136]. In addition to van der Waal forces of attractions, other contributions such as entropy, dipole-dipole and steric forces have

also been reported to encourage interparticle interactions during the evaporation process[139, 140].

A variety of uniform nanocrystal metals and semiconductors has been synthesized through the use of this method. These nanoparticles are highly soluble in nonpolar organic solvents and can be size-selectively flocculated and precipitated in size ~ 1 – 15 nm in diameter with a standard deviation of < 5%[133]. Highly monodisperse nanocrystals can also self-assemble into colloidal crystals when the carrier solvent is evaporated slowly, that is by increasing the concentration of nanocrystals in colloidal solution[73, 140-144]. The formation of a superlattice structure depends on the uniformity of nanocrystal size and the rate of carrier solvent evaporation[73]. These colloidal nanocrystals are then segregated, purified and finally resuspended in solvents to self-assemble into ordered structures. The solvents used during the redispersion of nanocrystal superlattices are chosen based on their polarities and boiling points. The solvent polarity is selected to permit milder nanocrystal interactions during the solvent evaporation, resulting in more concentrated nanocrystal dispersion whereas the boiling point of the solvent is selected to give nanocrystals sufficient time to reach equilibrium lattice prior to the solvent evaporation on the growing colloidal crystals[133].

3 EXPERIMENTAL METHODS

This chapter describes the various solution-based synthesis routes employed in the preparation and optimization of monodisperse platinum, vanadium and vanadium oxide nanoparticles. Nanoparticles of different sizes and shapes were synthesized using different platinum and vanadium precursor salts in the presence of different solvents, surface-active agents (surfactants) and reducing agents. The solvents are used to dissolve other chemicals, as prior to nanoparticle synthesis the reaction media must be homogeneous. The reductants serve as electron donors in redox reactions by forcing other ions to gain electrons so that the reductants become oxidized. The surfactants are used to regulate nanoparticle growth and adsorb reversibly to nanoparticle surfaces while providing a coating shell that mediates particle growth, stabilizes the particles at a particular size and prevents their oxidation after synthesis.

3.1 PREPARATION OF UNSUPPORTED Pt NANOPARTICLES

3.1.1 Polyvinylpyrrolidone (PVP) capped-Pt Nanoparticles

(a) Hydrogen Reduction Method

The polyvinylpyrrolidone (PVP) protected Pt nanoparticles were fabricated using the hydrogen (H_2) reduction method described by Ahmadi *et al.*[44] and Yu *et al.*[48]. A 0.01 M stock solution of the K_2PtCl_6 precursor salt was first prepared. A 2 ml aliquot of 0.01 M K_2PtCl_6 was dissolved in 200 ml of deionized water added in a 500 ml 3-neck volumetric flask equipped with a gas trap, followed by the addition of 0.25 g of PVP (MW ≈ 360 000). The solution was mixed thoroughly with no adjustment of the pH of the solution.

Thereafter, argon (Ar) gas was bubbled through the solution for 20 – 30 minutes to eliminate oxygen in the solution prior to synthesis, and then hydrogen (H_2) gas was

bubbled through the solution at high flow rate for approximately 5 minutes to saturate the solution. This led to the reduction of Pt ions in the solution. The flask was then sealed, wrapped in aluminium foil to avoid exposing the solution to the light, and stored in the dark for 12 – 18 hours. The solution changed from colourless to light/dark brown upon the completion of the reaction, indicating the decomposition of the Pt precursor salt.

(b) Ethanol (EtOH) Reduction Method

PVP protected-Pt nanoparticles were synthesized by the reduction of Pt ions with EtOH using the method described by Mahmoud *et al.*[145]. For the preparation of Pt nanoparticles: 0.01 M stock solution of the K_2PtCl_4 precursor salt was first prepared. A mass of 0.070 g of PVP (MW ≈ 55 000) was weighed and dissolved in 33 ml of deionized water in a flat bottom flask, and 4 drops of 1 M HCl were added. The solution was mixed thoroughly and heated to boiling. A 3 ml aliquot of 0.01 M K_2PtCl_4 was added and the resulting solution boiled for 2 minutes, thereafter 14 ml of EtOH was rapidly injected into the solution to reduce the Pt ions. The solution changed from colourless to dark brown upon the completion of the reaction, indicating the decomposition of the Pt precursor and the formation of Pt nanoparticles. The solution was allowed to cool gradually to room temperature.

For the preparation of a different morphology of nanoparticles: a mass of 0.140 g of PVP (MW ≈ 55 000), 9 drops of 1 M HCl and 9.6 ml of K_2PtCl_6 were dissolved in 100 ml of deionised water in a flat bottomed flask. The resulting solution was heated to boiling. A 40 ml aliquot of Pt nanoparticle solution, synthesized as described above, was added. The solution was allowed to boil. Thereafter, 36 ml of EtOH was injected. The resulting solution was refluxed for 3 hours using Quickfit Allihn condenser and allowed to cool gradually to room temperature. The colloidal solution was dark black upon the completion of the reaction.

(c) Glycerol (Gly) Reduction Method

0.076g of PVP (MW ≈ 55 000) and 2 ml of 0.01 M $(NH_4)_2PtCl_4$ were dissolved in 10 ml of gly and heated at 200 ºC. The solution turned from yellow to dark brown gradually. It was heated for a further 5 minutes, cooled to room temperature and the particles precipitated by the addition of acetone and hexane, washed several times with EtOH and finally resuspended in 5 ml of toluene.

3.1.2 Tetrabutylammonium bromide (TBABr) Capped-Pt Nanoparticles

(a) L-ascorbic Acid (AA) Reduction

(i) The TBABr capped Pt nanoparticles were synthesized using the L-ascorbic acid reduction protocol described by Lee *et al.*[54] with a few modifications. A 0.01 M stock solution of the K_2PtCl_6 precursor salt was first prepared. A 5 ml aliquot of 0.01 M K_2PtCl_6 was dissolved in 100 ml of 0.01 M aqueous solution of surface-active agent TBABr. After heating at 90 ºC, the solution became pale yellow and was held at temperature for 5 minutes, followed by the addition of 20 ml of 0.01 M AA. The equation of AA reduction of metal-surface active agent TBABr complex is represented below.

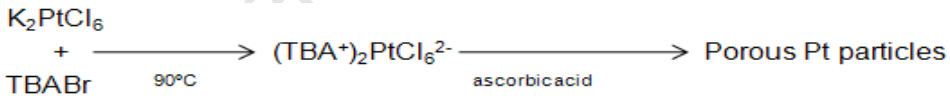

After the addition of AA, the solution became pale yellow. Thereafter, it turned dark brown slowly, indicating the formation of colloidal Pt nanoparticles. The Pt products were precipitated by centrifuging the solution at 3000 rpm for 30 minutes using Allegra™ 2IR Centrifuge to eliminate excess TBABr. The supernatant was then separated and centrifuged at 10000 rpm for 30 minutes. The precipitates were collected and re-dispersed in 2 ml of deionized water by sonicating the resultant solution for 10 minutes.

(ii) To synthesize Pt@Pt particles: 3 ml aliquot of prepared 0.01 M K_2PtCl_4 was dissolved in 50 ml of 0.01 M aqueous solution of surface-active agent TBABr. The resulting solution boiled at 90 ºC for a few minutes and 20 ml of 0.01 M AA was added. The colour of the solution changed from pale yellow to dark brown indicating the formation of porous Pt nanoparticles.

For the preparation of porous Pt@Pt nanoparticles, 10 ml of 0.01 M K_2PtCl_6 was added to 50 ml of 0.01 M TBABr. 70 ml of porous Pt particles, synthesized as described above, was added followed by the addition of 40 ml of 0.01 M AA. The solution was refluxed at 90 ºC for 3 hours using Quickfit Allihn condenser and allowed to cool gradually to room temperature.

3.1.3 Oleylamine (OAm) Capped-Pt Nanoparticles

(a) Formic Acid (FA) Reduction Method

(i) For the synthesis of Pt nanoparticles: 2 ml of 0.01 M K_2PtCl_4, was dissolved in 10 ml of OAm, as the surfactant, and the resulting solution was brought to boiling for 2 minutes and 8 ml of FA was added dropwise. The pale yellow solution changed to dark brown, indicating the formation of nanoparticles. The solution was allowed to cool to room temperature. The particles were precipitated by the addition of 20 ml of methanol (MeOH), separated, washed three times with MeOH and redispersed in 4 ml of toluene.

(ii) 2 ml of 0.01 M K_2PtCl_6 and 15 ml of OAm, as a surface-active agent, were dissolved and heated at 200 ºC under argon protection for 20 minutes. Thereafter, 8 ml of FA was added. Once the solution turned from pale yellow to dark brown, it was removed from the heat source and allowed to cool down to room temperature. The particles were flocculated and precipitated by the addition of 50 ml of MeOH. The precipitation-redispersion process was performed 4 times to remove excess capping agent and the particles were finally resuspended in 5 ml of toluene.

(iii) 2 ml of 0.01 M H_2PtCl_6 was dissolved in 10 ml of OAm. The precursor-surfactant

solution was heated at 100 ºC for 3 minutes under argon protection. 8 ml of FA was added and the temperature was increased to 150 ºC. The solution changed from pale yellow to dark brown. It held at these conditions for 5 minutes, removed from the heat source and allowed to cool down to room temperature. The particles were precipitated by the addition of 60 ml of MeOH. The precipitation-redispersion process was carried out three times to purify the particles and then redispersed in 4 ml of hexane.

(iv) 2.1 ml of 0.01 M $(NH_4)_2PtCl_4$ was dissolved in 24 ml of OAm, as the surfactant. The resultant solution was sonicated for 30 minutes to extract the Pt precursor salt from water to the amine surfactant and heated at 100 ºC under argon gas protection for 10 minutes. Thereafter, 6ml of FA was added drop-wise and temperature increased to 150 ºC. After the solution turned from pale orange to pale brown, it was held at this temperature for 20 minutes and allowed to cool down to room temperature. The particles were flocculated and precipitated by the addition of 50ml of EtOH, washed three times and re-suspended in 3 ml of toluene by slight sonication.

(b) Tetrabutylammonium Borohydride (TBAB) Reduction Method

2 ml of 0.08 M H_2PtCl_6 was first dried using an air-dryer and 36 ml of OAm was added. The resulting solution was sonicated for 20 minutes to obtain a clear pale yellow colour and 20 ml of BE was added. The resultant solution was then heated at 100 ºC for 10 minutes and was rapidly heated at 300 ºC, followed by the addition of 0.08g of TBAB. The reaction medium was held at temperature for 15 minutes, removed from the heat source and allowed to cool down to room temperature. The particles were precipitated by the addition of 100 ml of absolute EtOH. The precipitation-redispersion process was repeated 4 times using copious quantities of EtOH. The particles were dried and finally resuspended in 10 ml of toluene by mild sonication.

(c) Sodium Borohydride ($NaBH_4$) Reduction Method

2 ml of 0.01 M H_2PtCl_6 was dried using an air-dryer before 15 ml of OAm and 20 ml of toluene were added. The solution was stirred vigorously at room temperature until it became pale yellow. The resultant solution was then heated at 105 ºC, near the boiling point of toluene, for 10 minutes and 0.08g of $NaBH_4$ was added whilst stirring the solution vigorously. Once the reaction medium turned brown, it was removed from the heat source and quenched by the addition of 20 ml of EtOH. The precipitation-redispersion process was repeated 4 times using copious amounts of water/EtOH solution. The particles were finally resuspended in 5 ml of toluene.

3.2 PREPARATION OF UNSUPPORTED V METAL AND V OXIDE NANOPARTICLES

3.2.1 Oleylamine (OAm) capped-V Metal Nanoparticles

(a) Thermal Decomposition (Thermolysis) Method

(i) In this synthesis method of V nanoparticles, 0.084g of VCl_3 was dissolved in 15 ml of OE and 20 ml of OAm, sonicated for 20 minutes and heated at 220 ºC until a deep green homogeneous solution was obtained. The solution was then rapidly heated at 300 ºC for 10 – 15 minutes, removed from the heat source and the black products precipitated by the addition of 100 ml of EtOH, washed three times and redispersed in 5 ml of toluene.

(ii) In the preparation of V metal nanoparticles: 0.504g of VCl_3 was dissolved in 20 ml of BE and 15 ml of OAm. The solution was sonicated for 20 minutes and heated at 220 ºC until it turned deep green, indicating the complete solution of VCl_3. The solution was then rapidly heated at 330 ºC for 10 minutes and removed from the heat source. The black products were precipitated by the addition of excess EtOH, washed three times and resuspended in 10 ml of toluene.

3.2.2 Oleyl alcohol (OA) and Dioctylamine (DOA) capped-V Metal Nanoparticles

(a) Thermal Decomposition (Thermolysis) Method

(i) In the synthesis of V metal nanocrystals, 0.24g of VCl_3 was dissolved in 40 ml of OA and 30 ml of DOA. The resulting solution was sonicated for 30 minutes and heated at 220 ºC for 15 minutes to obtain a deep green colour, and rapidly heated at 300 ºC for 1 hour. The colloidal solution then cooled down to room temperature and the particles were precipitated by the addition of excess EtOH, washed several times and finally resuspended in 50 ml of toluene.

3.2.3 Oleylamine (OAm) capped-V Oxide Nanoparticles

(a) Thermal decomposition (Thermolysis) Method

(i) The OAm-capped V oxide nanoparticles were synthesized using a thermal decomposition synthesis route described by Nguyen *et al.*[146]: 0.14g of V_2O_5 was dissolved in 20 ml of 0.015 M H_2O_2 solution and the resultant solution was sonicated for 30 minutes under ambient conditions to obtain a homogeneous deep orange colour.

1.1g of tetraoctylammonium bromide (TOABr) was completely dissolved in 40 ml of toluene by sonication for 15 minutes and added to the as-prepared above solution to form two phases. Thereafter, the two-phase mixture was vigorously stirred for 20 – 30 minutes at room temperature to mix the deep orange solution into the toluene. The upper deep orange toluene solution (40 ml) was separated and dried at room temperature for 5 days. 5 ml of OAm dissolved in absolute EtOH was added, the solution was stirred for 1 h at 70 ºC and transferred to a 60 ml Teflon-lined stainless steel autoclave, and heated at 180 ºC for 5 h.

The reaction system was then removed from the heat source; cooled to room temperature using tap water and the particles were collected from the bottom of the

vessel and resuspended by the addition of excess toluene. The particles were then washed three times with EtOH and finally redispersed in 10 ml of toluene by mild sonication. This approach is summarized in the schematic diagram shown in Figure 3.1 (**a**):

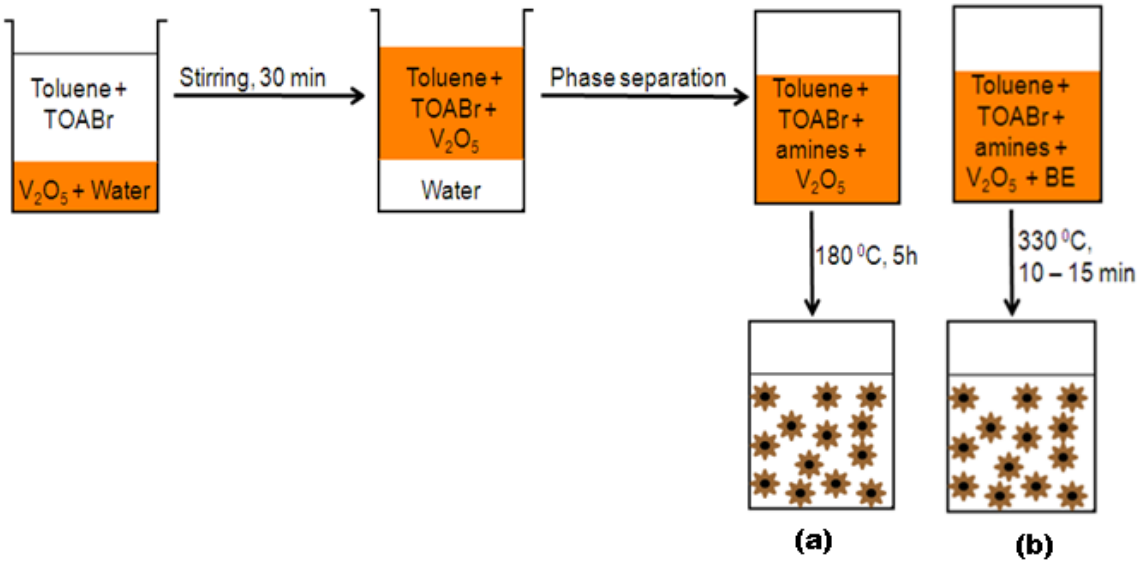

Figure 3.1: Transfer of V_2O_5 from the water into the toluene phase and the synthesis of V oxide nanoparticles by solvothermal treatment (**a**) (after Nguyen *et al.*[146]) and (**b**) with some modifications used in the present work.

(ii) The same synthetic method was employed, as described above, with some modifications. After the upper deep orange toluene solution (40 ml) was separated, 15 ml of BE and 30 ml of OAm were added: sonicated for 10 minutes to obtain a homogeneous solution and heated at 330 ºC for 10 – 15 minutes in the extraction fume hood.

BE is a high-boiling point solvent and OAm was used as the surfactant. The reaction system was then removed from the heat source, cooled to room temperature, the particles precipitated by the addition of excess EtOH, separated by discarding the supernantant, washed three times and finally resuspended in 6 ml of toluene. This approach is summarized in Figure 3.1 (**b**).

(iii) For the preparation of vanadium oxide nanocrystals: 0.134g of V_2O_5 was dissolved in 20 ml of BE and 0.5 ml of 0.5 M H_2O_2 in 6ml of EtOH. The solution was sonicated for 15 min to obtain a deep red colour. Thereafter, 7.5 ml of OLEA and 15 ml of OAm were added and the solution was stirred at 180 ºC to remove any traces of EtOH and water. The solution was heated at 300 ºC for 60 minutes, then cooled to room temperature by removing from the heat source. Particles were precipitated by the addition of excess EtOH, washed three times and finally resuspended in 10 ml of toluene.

Table 3.1 summarizes the different preparation approaches used in the synthesis of nanocrystals of Pt, V and V oxide using different precursor salts, surfactants, reductants, solvents and additives.

Table 3.1: Preparation of monodisperse Pt, V and V oxide nanocrystals in aqueous solutions.

Precursors	Surfactant(s)[a]	Reductant(s)[b]	Solvent(s)[c]	Additive[d]	Method[e]
K_2PtCl_6	PVP	H_2	H_2O	HCl	R
K_2PtCl_4	PVP	EtOH	H_2O		R
$(NH4)_2PtCl_4$	PVP	Gly	Gly		R
K_2PtCl_6	TBABr	AA	H_2O		R
K_2PtCl_4	OAm	FA	OAm		R
K_2PtCl_6	OAm	FA	OAm		R
H_2PtCl_6	OAm	FA	OAm		R
$(NH4)_2PtCl_4$	OAm	FA	OAm		R
H_2PtCl_6	OAm	TBAB	OAm		R
H_2PtCl_6	OAm	TBAB	OAm + BE		R
H_2PtCl_6	OAm	$NaBH_4$	OAm		R
VCl_3	OAm		OAm + OE		TR
	OAm		OAm + BE		TR
	OA + DOA		OAm + DOA		TR
V_2O_5	OAm		EtOH		TR
	OAm		BE		TR
	OLEA + OAm		OLEA		TR

[a] PVP=poly(N-vinyl-2-pyrrolidone); CTAB = hexadecyltrimethyammonium bromide; OAm = oleylamine; TOAB = tetraoctylammonium bromide; OLEA = oleic acid; TBABr = tetrabutylammonium bromide; TOA = trioctylamine; OA = oleyl alcohol; DOA = dioctylamine; TBA = tri-n-butylamine; TTAB = tetradecyltrimethylammonium bromide;

[b] EtOH = ethanol; Gly = glycerol; AA = ascorbic acid; FA = formic acid; TBAB = tetrabutylammonium borohydride; $NaBH_4$ = sodium borohydride;

[c] OAm = oleylamine; BE = benzyl ether; OE = octyl ether

[d] HCl = Hydrochloric acid;

[e] R = Reduction; TR = thermal reduction

3.3 PREPARATION OF UNSUPPORTED VPt NANOPARTICLES

3.3.1 Tetrahexylammonium bromide (THAB) and Tetradecyltrimethylammonium bromide (TTAB) Capped-VPt Nanoparticles

For the preparation of VPt nanoparticles: 10 ml aliquot of prepared 0.01 M VCl_3 was dissolved in 100 ml of 0.01 M aqueous solution of surface-active agent THAB and 50 ml of 0.01 M TTAB. The solution was heated to boiling, followed by the addition of 80 ml of gly and refluxed for 20 hours using Quickfit Allihn condenser at 110 ºC. Thereafter, in 50 ml of the as-prepared V nanoparticles, 10 ml of 0.01 M AA and 2 ml of 0.01 M K_2PtCl_4 were added. The resultant solution was refluxed for 4 hours.

3.3.2 Hexadecyltrimethyammonium bromide (CTAB) Capped-VPt Nanoparticles

For the preparation of VPt nanoparticles: 10 ml of 0.01 M VCl_3 and 5 ml of 0.01 M K_2PtCl_4, 1g of CTAB were added in 20 ml of deionized water in a two necked round-bottomed volumetric flask. The resulting solution was sonicated for 30 minutes to ensure proper mixing of the chemicals. The solution was then heated to boiling at 110 ºC, followed by the addition of 2 ml of FA and refluxed for 60 minutes. Colloidal VPt nanoparticles were separated by centrifuging the solution at 6000 rpm using an Allegra^{TM} 2IR Centrifuge for 40 minutes to remove excess CTAB and some impurities. The supernatant was separated and centrifuged at 10000 rpm for 20 minutes. The precipitated products were washed three times in water and redispersed in 4 ml of deionized water.

3.3.3 Stearic Acid (SA) and Trioctylamine (TOA) Capped-VPt Nanoparticles

For the synthesis of VPt metal nanoparticles: 2 ml of 8% H_2PtCl_6 was first dried, then 0.202g of VCl_3. 2.02g of SA and 24 ml of TOA were added as both surfactants, and 15 ml of BE was then as the solvent. The resulting solution was sonicated for 15 minutes,

heated at 180 ºC under vigorous stirring for 15 minutes and rapidly heated to 300 ºC for one hour.

3.3.4 Oleylamine (OAm) and Tri-n-butylamine (TBA) Capped-VPt Nanoparticles

For the preparation of VPt nanoparticles: 0.172g of VCl_3 was dissolved in 30 ml of OAm, 30 ml of TBA and 10 ml of BE. The solution was sonicated for 10 minutes, heated at 180 ºC while stirring and rapidly heated at 280 ºC for one hour.

In a separate flask 2 ml of 8% H_2PtCl_6 was first dried, dissolved in 20 ml of OAm and 15 ml of TBA by sonication for 10 minutes and added into the as-prepared V metal nanoparticles. The solution was heated for another 2 minutes and 0.04g of TBAB was added as the reductant. The resulting solution was then kept at 150 ºC for 30 minutes.

3.3.5 Oleylamine (OAm) and Dioctylamine (DOA) Capped-VPt Nanoparticles

(a) For the synthesis of VPt metal nanoparticles: 2 ml of 8% H_2PtCl_6 was first dried, 0.24g of VCl_3 was then added. 30 ml of DOA and 40 ml of OA were used as both solvents and surfactants. The resulting solution was sonicated for 15 minutes, heated at 180 ºC under vigorous stirring for 15 minutes and rapidly heated at 300 ºC for one hour.

(b) In this synthesis method: 0.26g of VCl_3 was dissolved in 34 ml of DOA and 40 ml of OA, sonicated for 20 minutes and heated at 300 ºC until a deep green homogeneous solution was obtained. The solution was then rapidly heated at 300 ºC for one hour, removed from the heat source and the black products precipitated by the addition of 100 ml of EtOH, washed three times and redispersed in 20 ml of toluene.

3 ml of 8% H_2PtCl_6 dried was dissolved in 54 ml of OA and 10 ml of BE. 20 ml of the as-prepared V nanoparticles in toluene were added and the resulting solution heated at 100 ºC for 5 minutes. Thereafter, 0.24g of TBAB dissolved in BE was added and the solution heated at this temperature for 20 minutes.

3.4 TRANSMISSION ELECTRON MICROSCOPY

Samples for TEM characterization were prepared by placing a drop of colloidal nanocrystals, resuspended in a solvent, on a carbon-supported copper grid and allowing the solvent to evaporate either under ambient conditions for at least 2 hours or by using a drying lamp. The LEO 912 TEM and TECNAI F20 TEM were used to image the nanocrystals at 120 kV and 200 kV, respectively. The chemical composition of nanoparticles was investigated using energy-dispersive X-ray spectroscopy (EDX). The sizes of the particles were calculated by measuring their diameter, from randomly selected areas of TEM images, using ImageJ software[147].

4 RESULTS

Various chemical synthesis techniques have been used in the synthesis of Pt, V and V oxide nanocrystals. These are based on chemical solution-phases and include reduction, nonhydrolytic sol-gel and thermal decomposition (thermolysis) processes. Appropriate choice of reaction systems (such as the precursor salts, solvents, surfactants, additives and reducing agents) results in the formation of well-defined nanocrystals of different morphologies. Particles with narrow size distribution and high dispersity have been synthesized through the use of these protocols.

The precursor salts were selected on the basis of their solubility in different solvents (water or organic liquids), surfactants and additives. The reaction temperature, reaction time, cooling rate and the concentration of the monomers are also critical reaction parameters that determine the growth mode of the particles.

4.1 SYNTHESIS OF PLATINUM NANOPARTICLES

4.1.1 Poly(N-vinyl-2-pyrrolidone) (PVP)-Capped Pt Nanoparticles

(a) Ethanol (EtOH) as the Reductant

(i) K_2PtCl_6 precursor salt was reduced to Pt^0 (zero valent Pt) metal with EtOH in the presence of PVP as the protective agent, following the technique described by Ahmadi *et al.*[48] and Yu *et al.*[145]. These PVP-coated nanoparticles were first characterised using UV–visibility spectroscopy (UV-vis). The platinum precursor (K_2PtCl_6) solution was pale yellow and exhibited a peak at 260 nm in its UV–vis spectrum, as shown in Figure 4.1. This is due to the ligand-to-metal charge transfer transition of the $[PtCl_6]^{2-}$ ions. Upon the synthesis of platinum nanocrystals, the colour of the solution changed from pale yellow to dark brown. The peak at 260 nm disappeared completely indicating the decomposition of the platinum precursor, hence the reduction of $PtCl_6^{2-}$ ions and the

formation of colloidal zero-valent Pt particles.

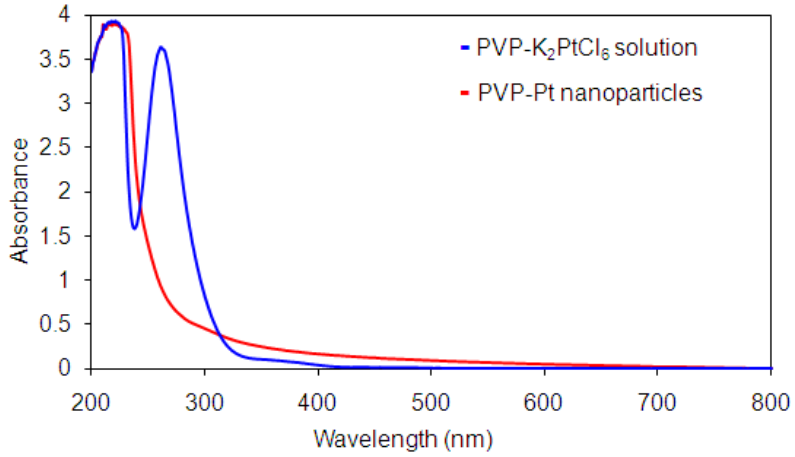

Figure 4.1: UV–vis absorption of PVP-K_2PtCl_6 solution and PVP-protected Pt nanoparticles.

Since UV-vis cannot be used to determine the size and morphology of the particles, the critical technique used to determine the size and shapes of the particles was TEM. Figure 4.2 **A** shows the as-prepared nanoparticles which appear to be tetrahedral. Figure 4.2 **B** shows the particle size distribution. The mean particle diameters (and standard deviation) of 150 particles in arbitrarily chosen areas were calculated using Image J[147], giving a mean size of 3.05 nm with a standard deviation of 1.10 nm[44, 48].

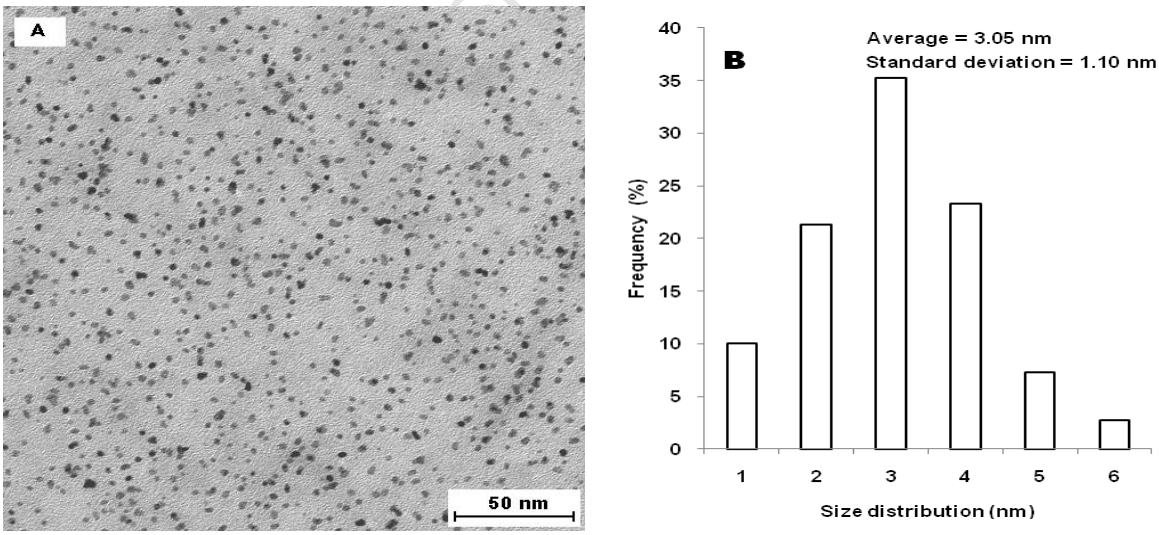

Figure 4.2: (**A**) Bright-field TEM image of tetrahedral Pt nanoparticles and (**B**) particle size distribution histogram.

(ii) Reducing K_2PtCl_6 precursor salt around the preformed seeds of tetrahedral nanoparticles shown in Figure 4.2 **A** resulted in "multiarmed" nanocrystals as shown in Figure 4.3 **A**. Figure 4.3 **B** shows the particle size distribution. The sizes of 150 particles in randomly chosen areas were calculated, giving a mean size of 6.99 nm with a standard deviation of 1.41 nm.

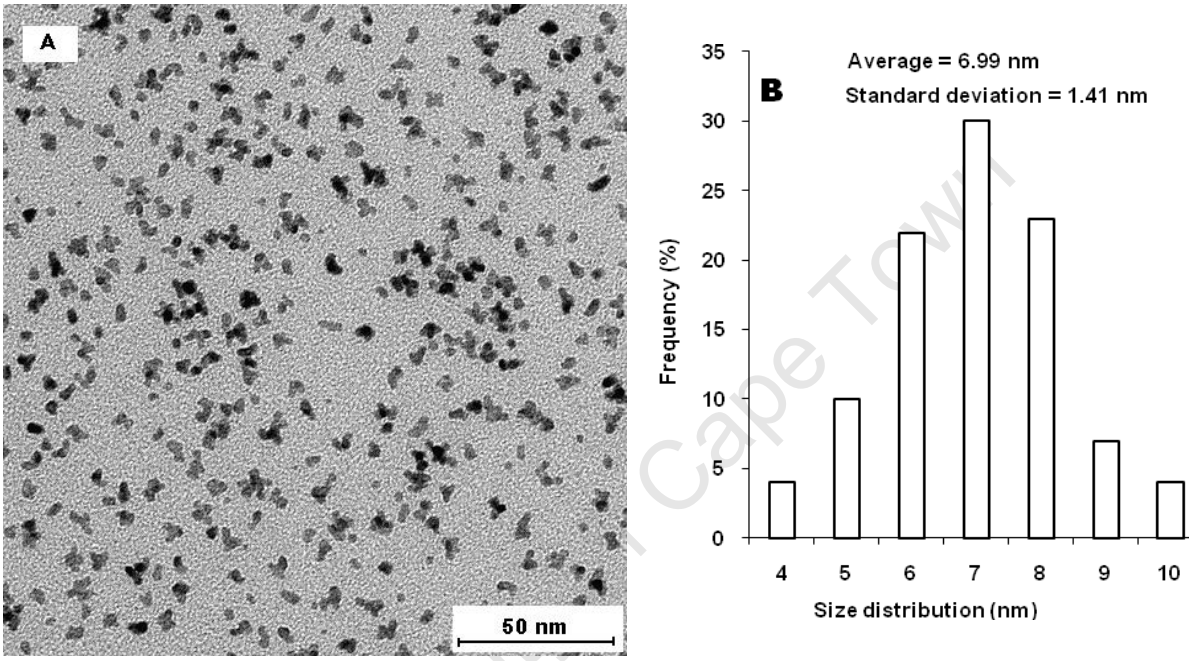

Figure 4.3: Bright-field TEM image (**A**) and particle size distribution histogram (**B**) of multiarmed nanocrystals Pt particles.

(b) Glycerol (Gly) as both the Solvent and Reductant

In this sol-gel synthetic approach, Pt nanoparticles were prepared by the reduction of K_2PtCl_6 with glycerol in the presence of PVP as the capping agent. Gly served as both the reacting solvent and reductant, yielding particles of spherical and worm-like shapes with good size distribution as shown in Figures 4.4 **A** and **B**.

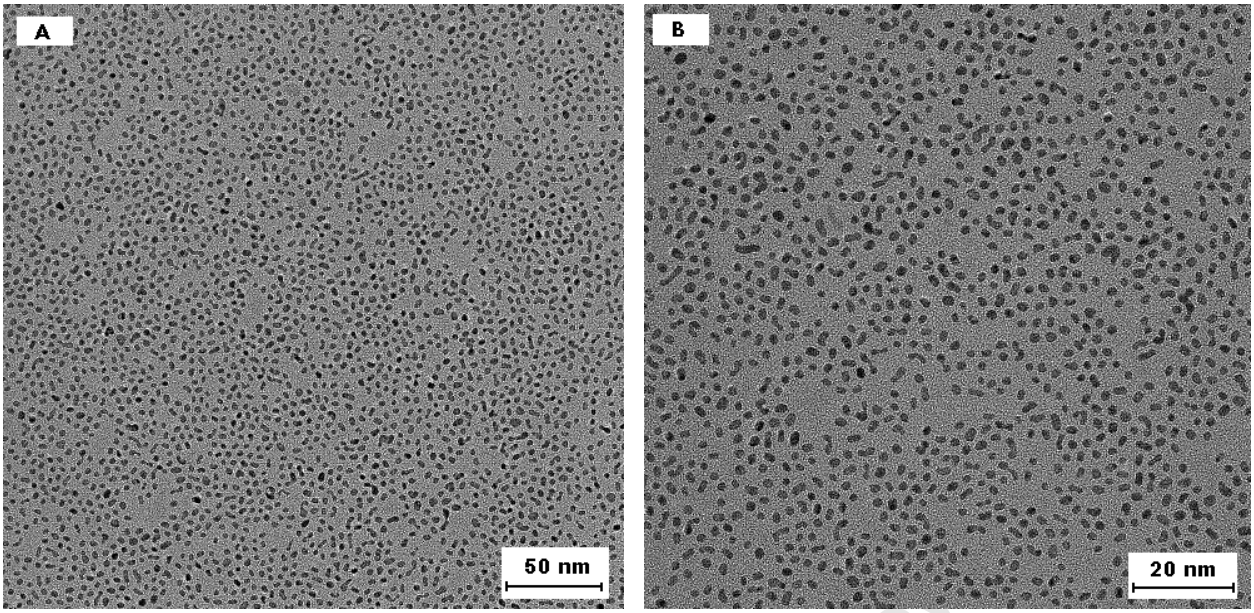

Figure 4.4: Bright-field TEM images (**A**) and (**B**) of spherical and worm-like Pt nanoparticles.

4.1.2 Tetrabutylammonium bromide (TBABr) Capped-Pt Nanoparticles

(a) Ascorbic acid (AA) as the Reductant

(i) In a published synthesis technique[54] with some modifications, K_2PtCl_6 and surfactant CTAB were used with AA as the reductant, resulting in porous Pt particles. This reduction method produced monodisperse nanoparticles as shown in Figure 4.5 **A** with a broad size distribution, as shown in Figure 4.5 **B**, yielding a mean of 29.36 nm with a standard deviation of 8.47 nm. Images of these porous Pt nanoparticles are shown in Figures 4.5 **C**, 4.5 **D** and 4.5 **E**. Figure 4.5 **F** is a high resolution TEM (HR-TEM) image showing atomic lattice fringes and the orientation of planes of Pt nanoparticles. Figure 4.5 **G** is a HR-TEM image of a single nanoparticle showing the same orientation of lattice fringes. Convergent beam electron diffraction (CBED) of this particle shows that the lattice planes have the same orientation. Energy-dispersive X-ray spectroscopy (EDX) was used to confirm the chemical composition of the Pt nanoparticles, as shown in Figure 4.6. In the EDX spectrum, excluding carbon and copper from the carbon-

supported Cu grid, the peaks for Pt, O and Br are noticeable. The oxygen peak suggests possible oxidation of nanoparticles upon synthesis, whereas the bromine peak originates from the surface-active agent employed (TBABr).

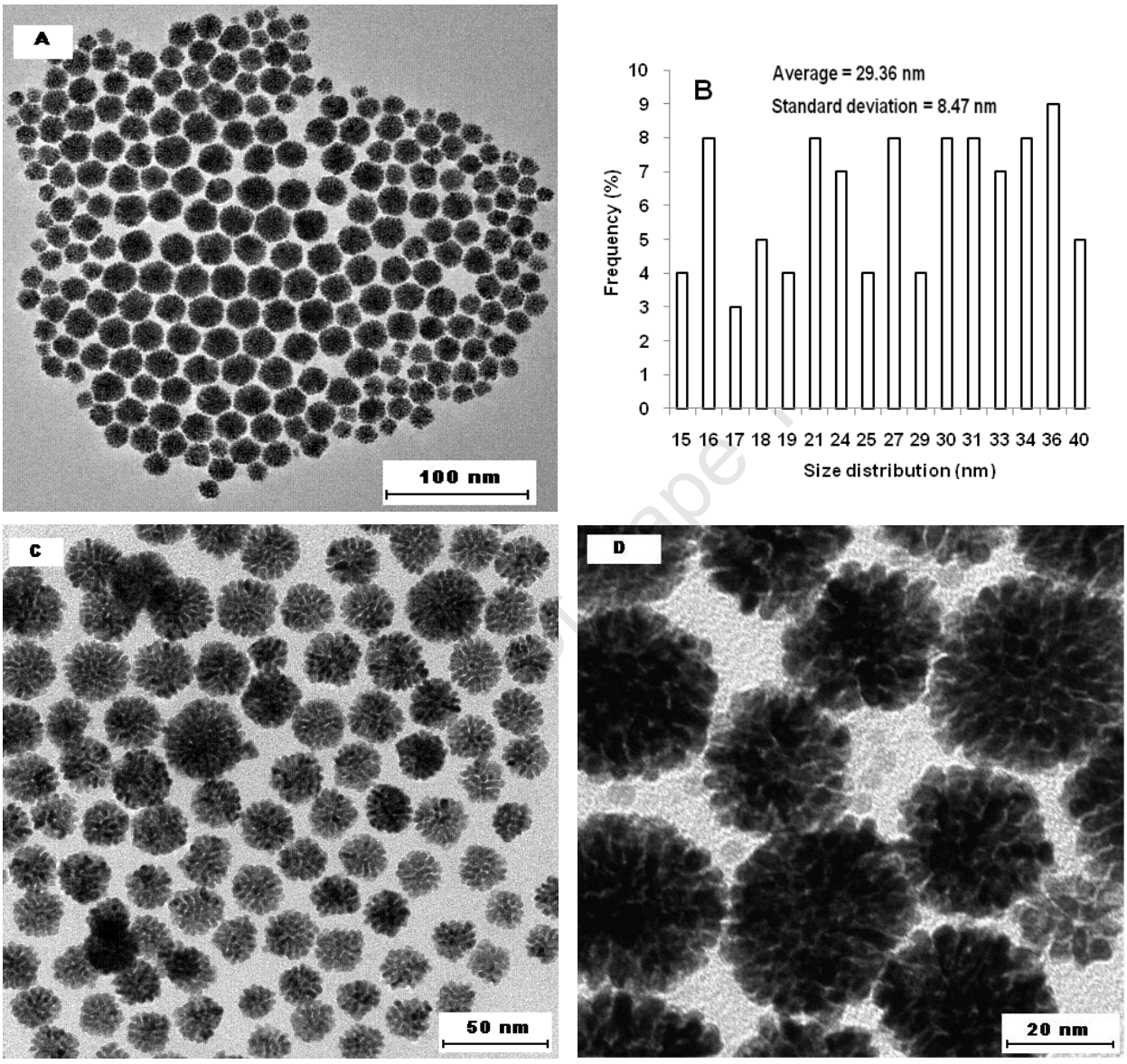

Figure 4.5: TEM images of porous Pt nanoparticles (**A**, **C**-**D**) and particle size distribution histogram (**B**).

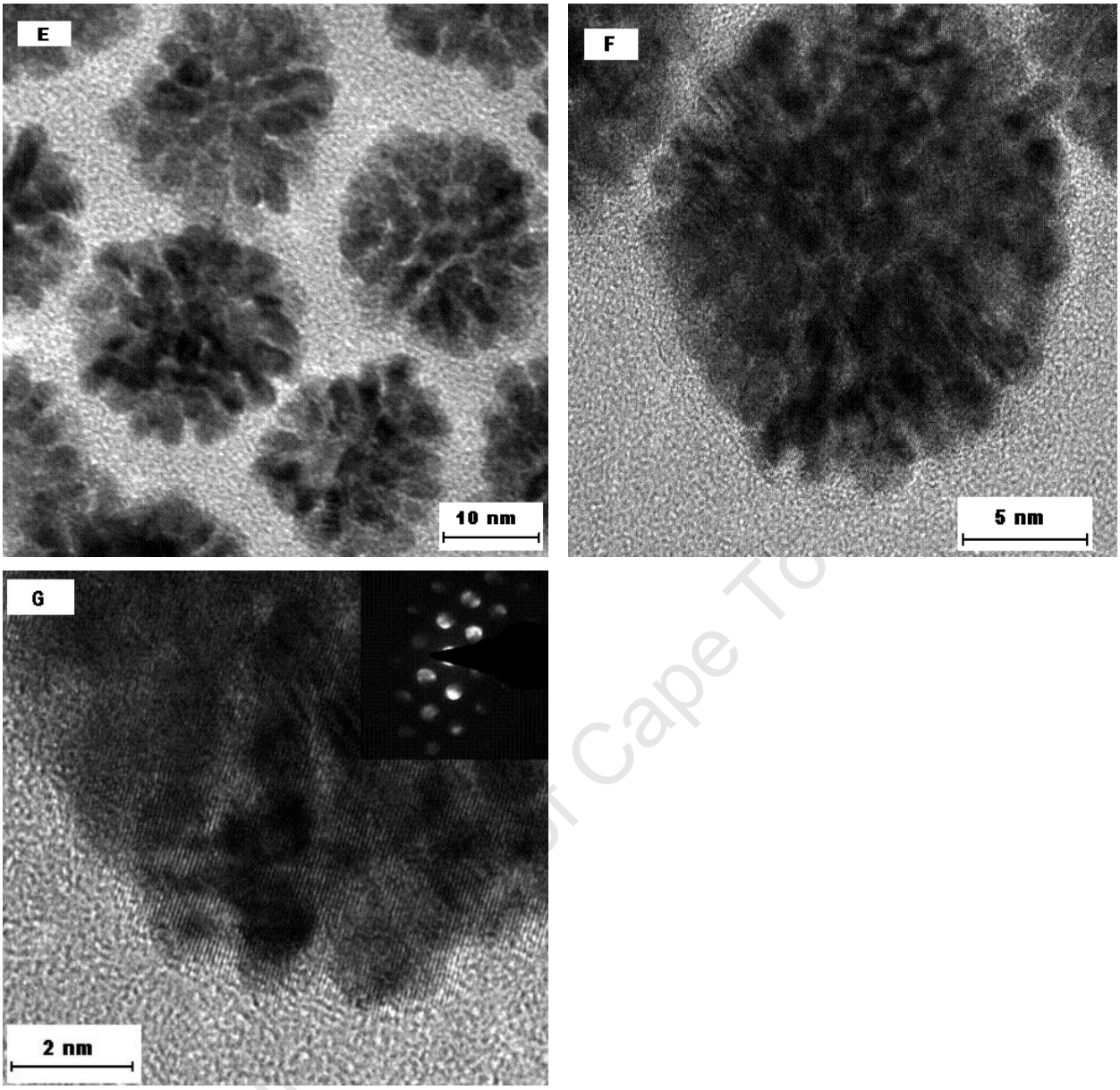

Figure 4.5: HR-TEM images of porous Pt nanoparticles (**E**-**F**) and a typical convergent beam electron diffraction (CBED) of a single particle (**G**).

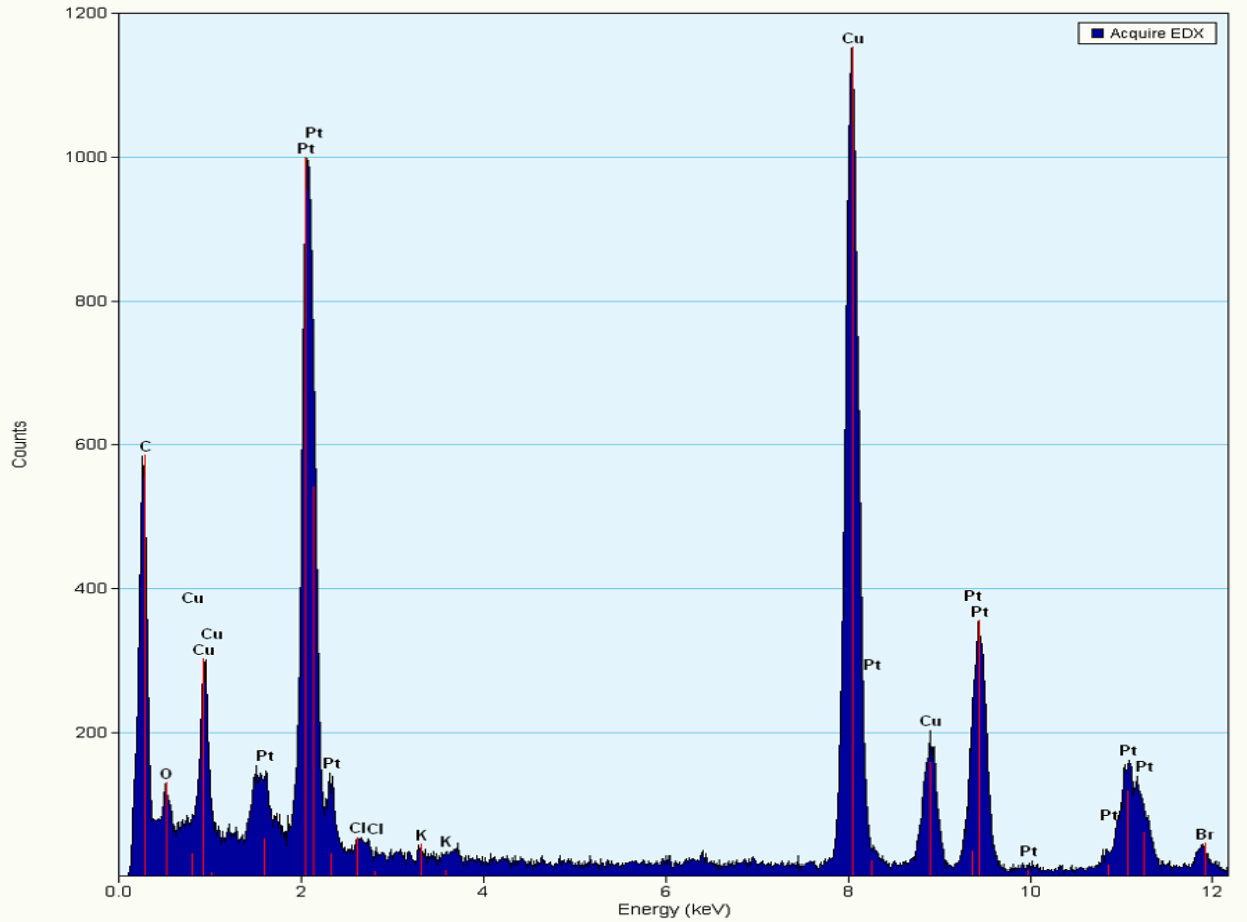

Figure 4.6: EDX spectrum of porous Pt nanocrystals.

(ii) In an attempt to synthesize Pt/Pt core-shell nanoparticles: K_2PtCl_4 was used to prepare porous Pt nanoparticles in the presence of CTAB as the coating agent and AA as the reductant. These particles were employed as seeds to form Pt@Pt core-shell nanoparticles by reducing K_2PtCl_6 precursor salt around the preformed porous particles using AA as the reductant. Figures 4.7 **A** and **B** show spherical nanoparticles with a dark core. The outer shells are brighter and exhibit more porosity. These Pt/Pt core-shell nanospheres have an extremely high surface area.

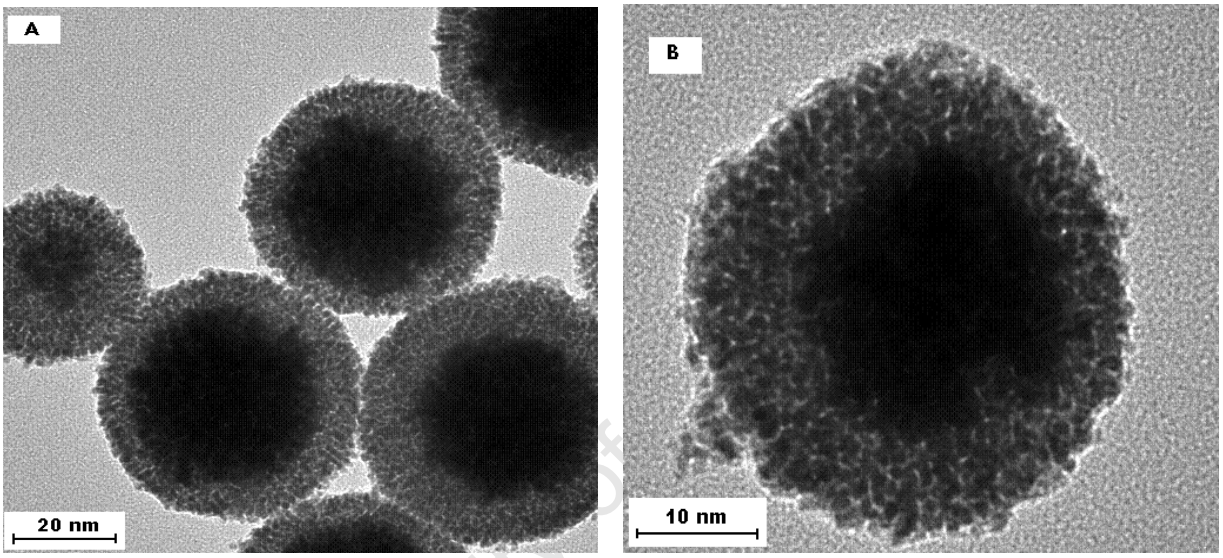

Figure 4.7: Bright-field TEM images (**A**) and (**B**) of Pt_{core}-Pt_{shell} nanoparticles.

4.1.3 Oleylamine (OAm) Capped-Pt Nanoparticles

(a) Formic Acid (FA) as the Reductant

(i) Pt nanoparticles were synthesized using a new preparative route involving the reduction of precursor salt, K_2PtCl_4, by FA in the presence of OAm as the surface-active agent. This nanosynthesis route produced nanoparticles exhibiting well-defined cubic, irregular and elongated morphologies with a narrow size distribution, as shown in Figure 4.8 **A**. The particle size distribution histogram is shown in Figure 4.8 **B** and the mean diameter of the particles is 4.10 nm with a standard deviation of 0.78 nm. Figure 4.8 **C**

and **D** show HR-TEM images (bright field and dark field, respectively) of these monodisperse nanoparticles, exhibiting good crystallinity.

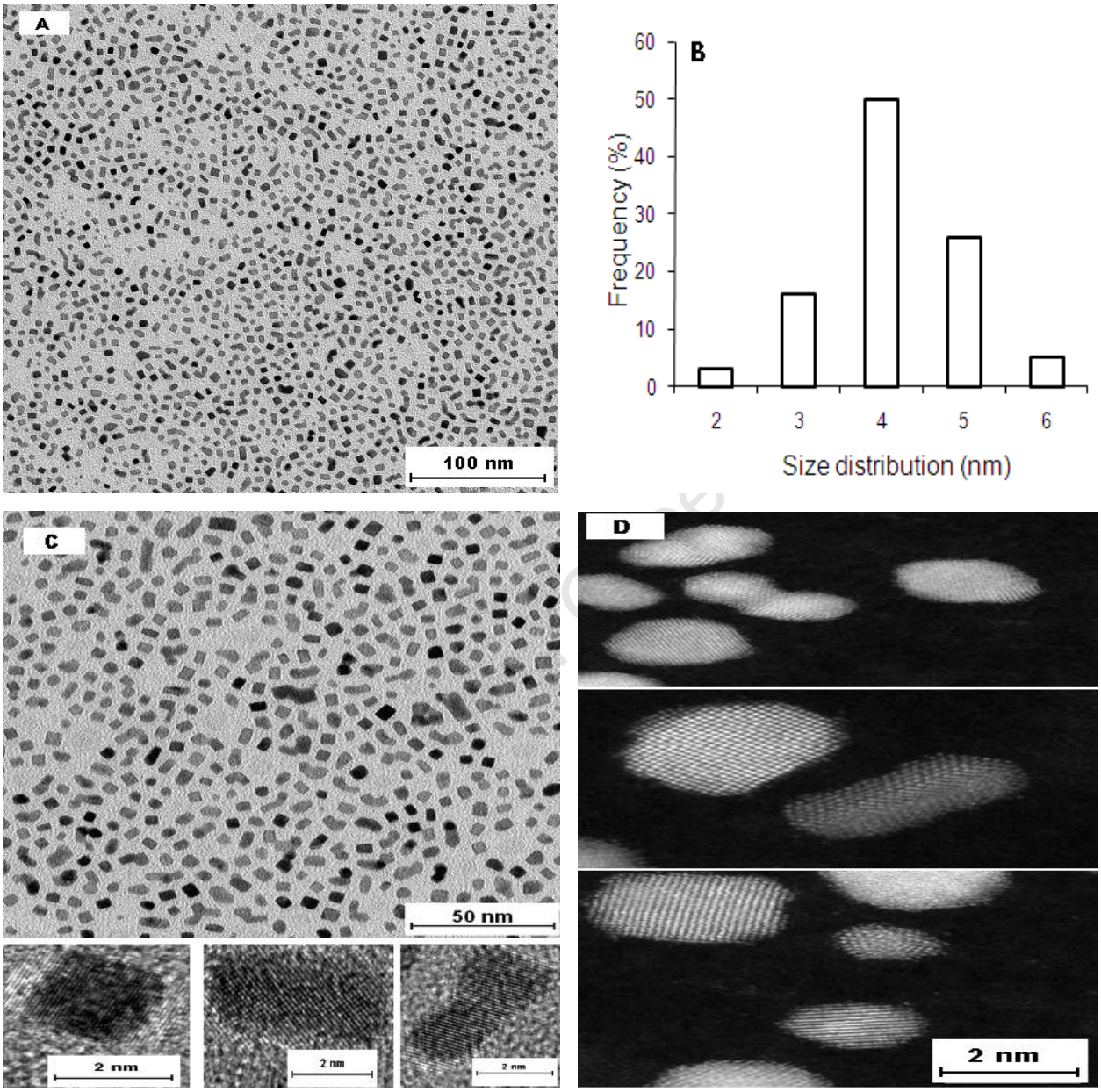

Figure 4.8: Bright-field TEM image (**A**), particle size distribution histogram (**B**), HR-TEM images (**C**) and dark-field HR-TEM image (**D**) of cubic, irregular and rod-like Pt nanoparticles.

(ii) A change in precursor salt to K_2PtCl_6, reduced and decomposed to form zero valent Pt metal as in (i) above, yielded particles of controlled growth with uniform size, size distribution and shape. This synthesis protocol produced particle monomers of cuboctahedral and cubic shapes with good crystallinity. The morphologies of Pt nanocrystals are shown in Figure 4.9 **A** and the particle size distribution histogram is shown in Figure 4.9 **B,** giving an average diameter of 6.25 nm with a standard deviation of 1.47 nm. Figure 4.9 **C** is a dark field TEM image of the particles. Figure 4.9 **D** shows a HR-TEM image of these morphologies.

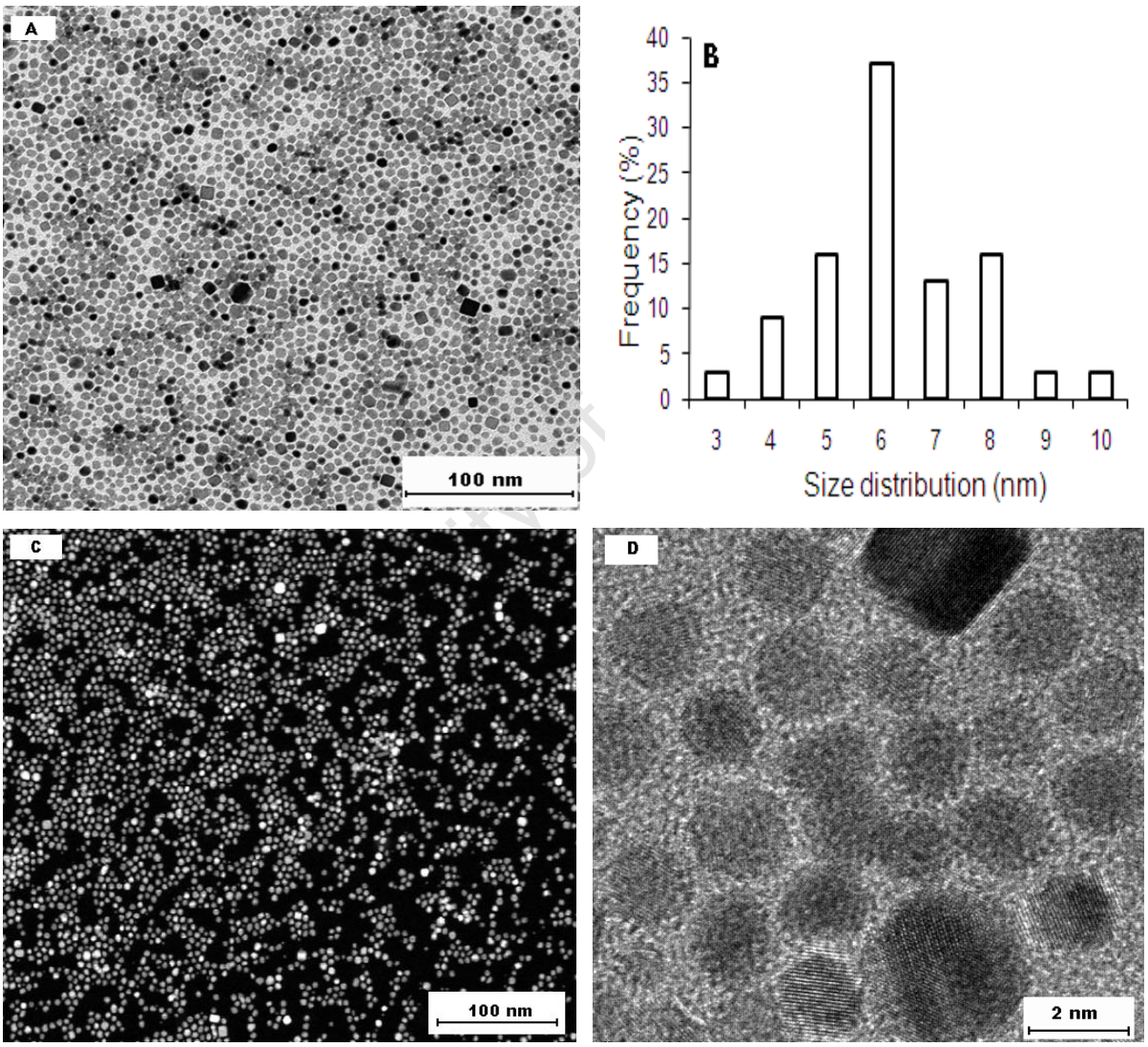

Figure 4.9: Bright-field TEM image of cuboctahedral and cubic Pt nanoparticles (**A**), particle size distribution histogram (**B**), dark-field TEM image (**C**) and HR-TEM image (**D**).

(iii) Zero-valent Pt particles were synthesized by reducing H_2PtCl_6, with FA and OAm as before [(i) and (ii)]. The morphologies of monodisperse Pt nanocrystal assemblies are shown in Figures 4.10 **A** and **B**. Figure 4.10 **C** shows HR-TEM image of the nanocrystals, the orientation of lattice fringes and the electron diffraction pattern of this selected area. This reductant method produced very small particles of cubic, cuboctahedral and irregular shapes with a broad size distribution, requiring size selection process. The diffraction pattern of fcc Pt shows good crystallinity.

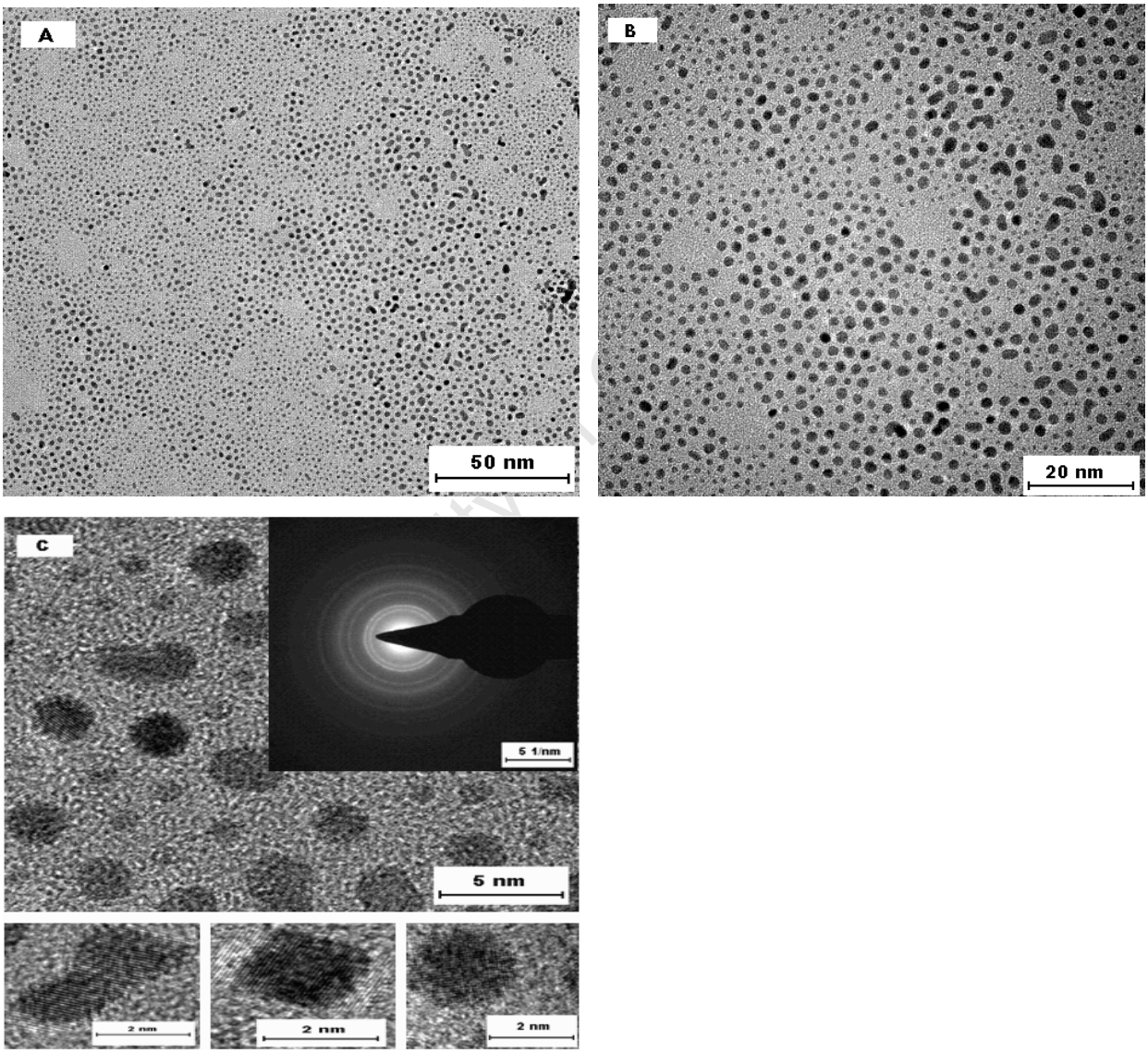

Figure 4.10: Bright-field TEM images (**A**) and (**B**), and HR-TEM image (**C**) of irregular, cubic and cuboctahedral Pt nanoparticles.

(b) Tetrabutylammonium Borohydride (TBAB) as the Reductant

(i) The formation of colloidal zero-valent Pt particles by reducing H_2PtCl_6 precursor salt with TBAB in the presence of OAm as the surface-active reagent, and BE as the solvent, yielded particles of controlled growth with a nearly uniform size distribution and shape requiring no size-selective processing. The morphology of Pt nanoparticles is shown in Figure 4.11 **A** and **B** with an electron diffraction pattern showing typical fcc Pt diffraction rings.Figure **C** shows an HR-TEM image of the particles, exhibiting good crystallinity. This synthesis route gives particles of well-defined cuboctahedral shape. These particles were observed to form nearly complete hexagonal close-packing. The average particle size is 4.41 nm, with a standard deviation of 0.85 nm as shown in Figure 4.11 **D**.

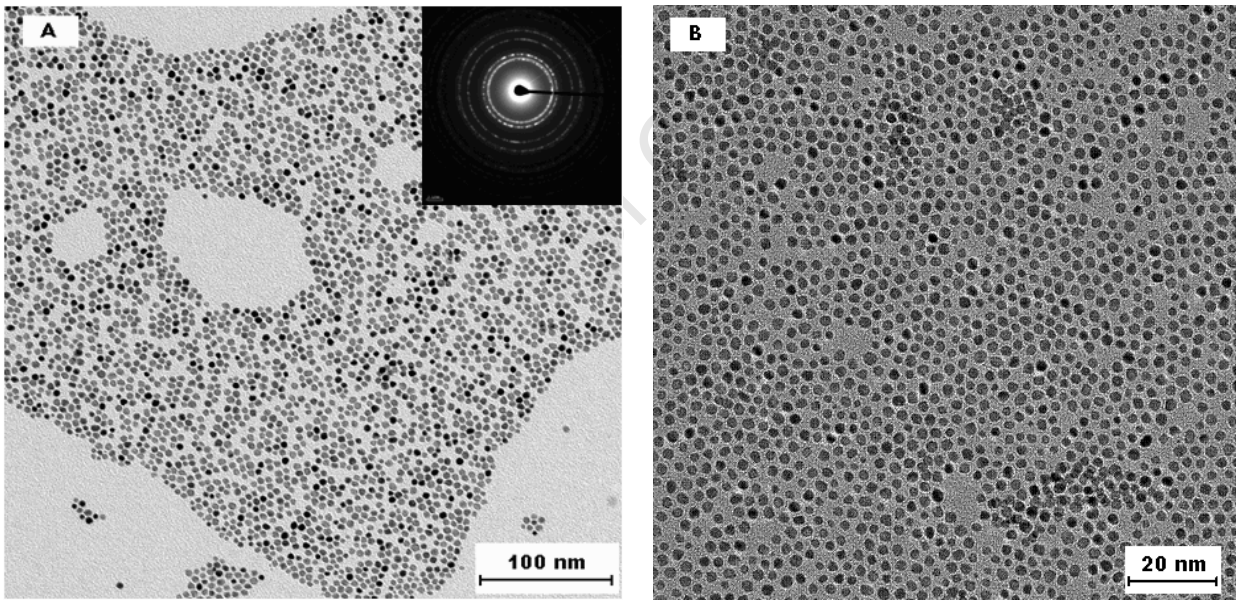

Figure 4.11: Bright-field TEM images (**A**) and (**B**) of cubic, cuboctahedral and irregular Pt nanoparticles.

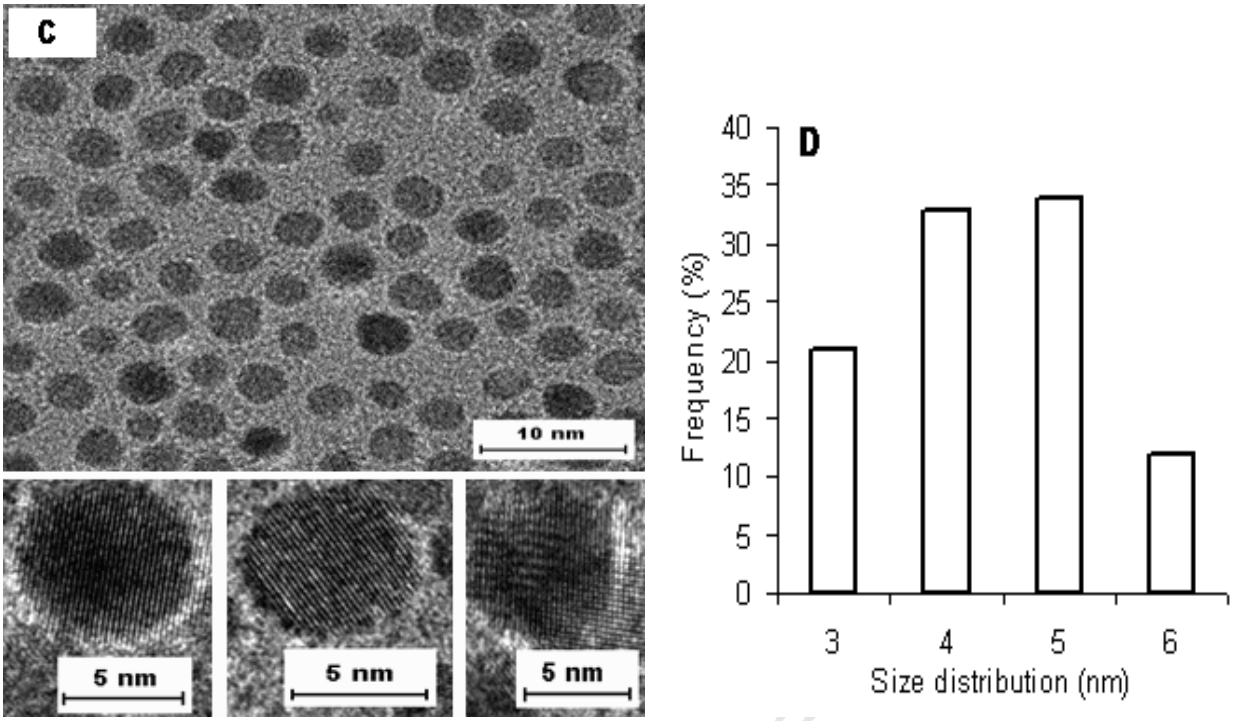

Figure 4.11: HR-TEM images (**C**) and (**D**) particle size distribution histogram cuboctahedral Pt nanoparticles.

(ii) The synthesis of Pt metal from H_2PtCl_6 precursor salt using OAm and TBAB as the surfactant and reductant, respectively, produced nanoparticles that have a narrow size distribution and good dispersity. The reduction process is performed under argon protection to prevent the OAm from evaporating. TEM images are shown in Figures 4.12 **A**, **B** and **C** (dark field). It was determined that this synthesis method yielded nanoparticles of triangular and irregular shapes. Figure 4.12 **D** is a particle size distribution histogram, yielding a mean of 4.63 nm with a standard deviation of 1.49 nm.

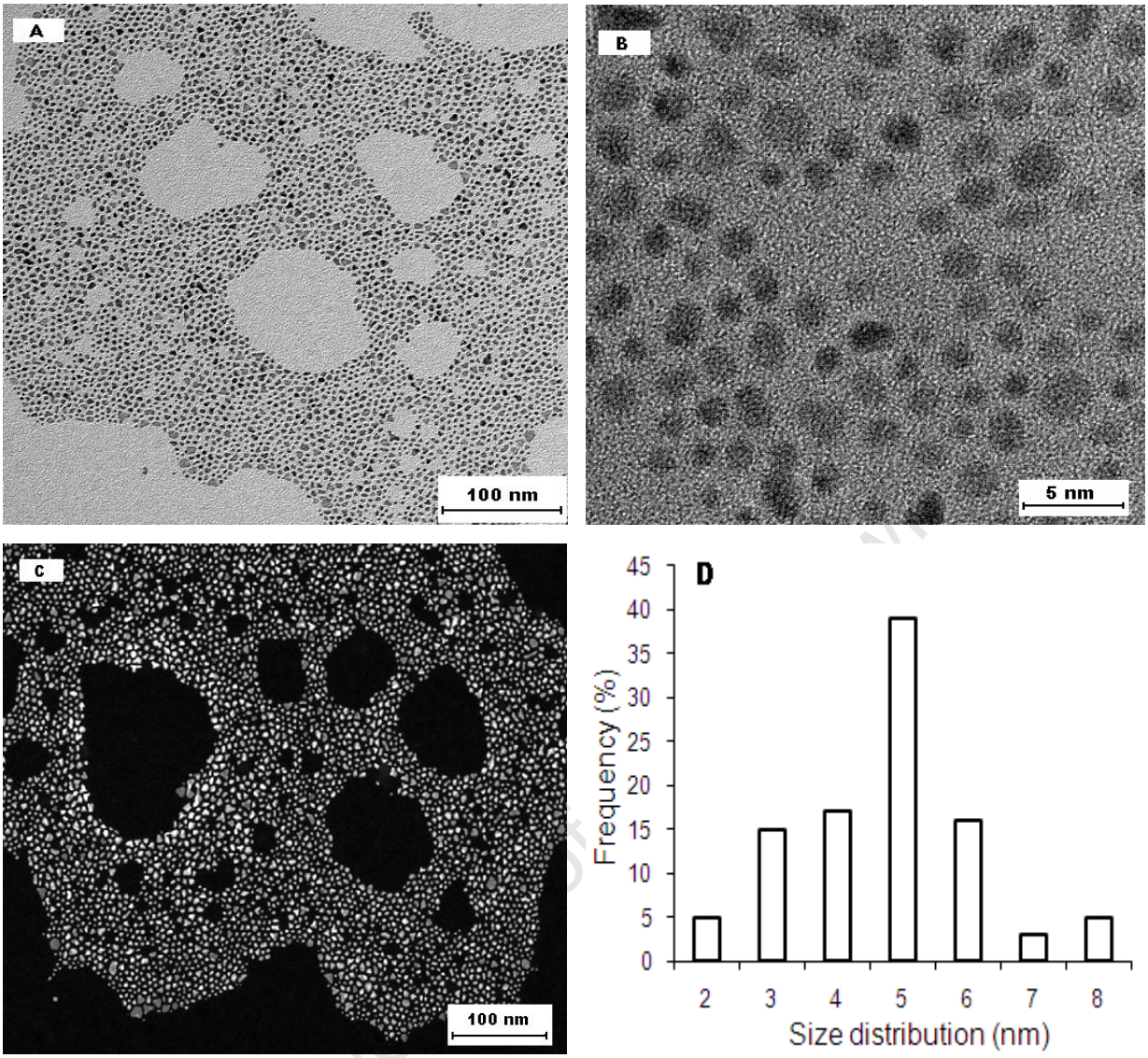

Figure 4.12: Bright-field TEM images (**A**) and (**B**), (**C**) a dark-field TEM image of triangular and irregular Pt nanoparticles, and particle size distribution histogram (**D**).

(c) Sodium Borohydride ($NaBH_4$) as the Reductant

(i) The reduction and the decomposition of K_2PtCl_4 precursor salt to form Pt^0 metal with $NaBH_4$ in the presence of OAm as the surface-stabilizing reagent yielded Pt nanoparticles with uniform size and good distribution, as shown in Figures 4.13 **A** and 4.13 **B**. This synthesis protocol produced particle monomers of irregular shapes with good crystallinity. Figure 4.13 **C** shows the particle size distribution histogram; the mean

diameter of the particles is 4.07 nm with a standard deviation of 0.90 nm. Figure 4.13 **D** is a dark-field TEM image.

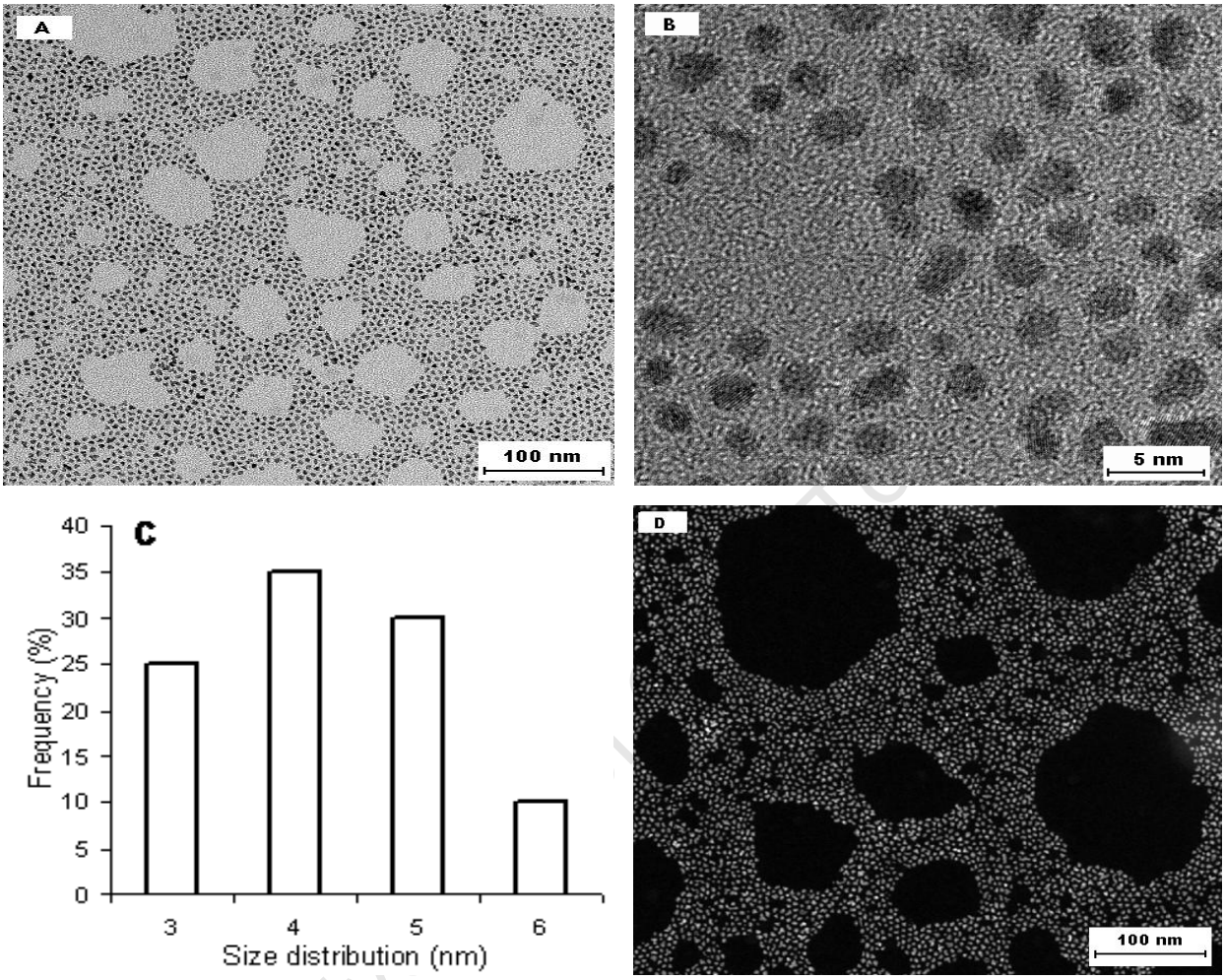

Figure 4.13: Bright-field TEM image (**A**), HR-TEM image (**B**), (**D**) dark-field TEM image and particle size distribution histogram (**C**) of irregularly shaped Pt nanoparticles.

(ii) OAm capped Pt nanocrystals were prepared using H_2PtCl_6 as the starting material and $NaBH_4$ as the reducing agent, in an inert environment. This reduction protocol resulted in the formation of particles of different morphologies with a good distribution. A TEM image of these different Pt morphologies is shown in Figure 4.14 **A**. Figure 4.14 **B** shows HR-TEM image of these monodisperse nanoparticles, exhibiting good crystallinity. These particles adopt irregular and triangular shapes as seen in Figure 4.14 **C**, dark-field TEM image. The size of the particles were calculated from a pool of

100 nanoparticles in randomly chosen areas, giving a mean of 5.10 nm with standard deviation of 0.92 nm as shown in Figure 4.14 **D**.

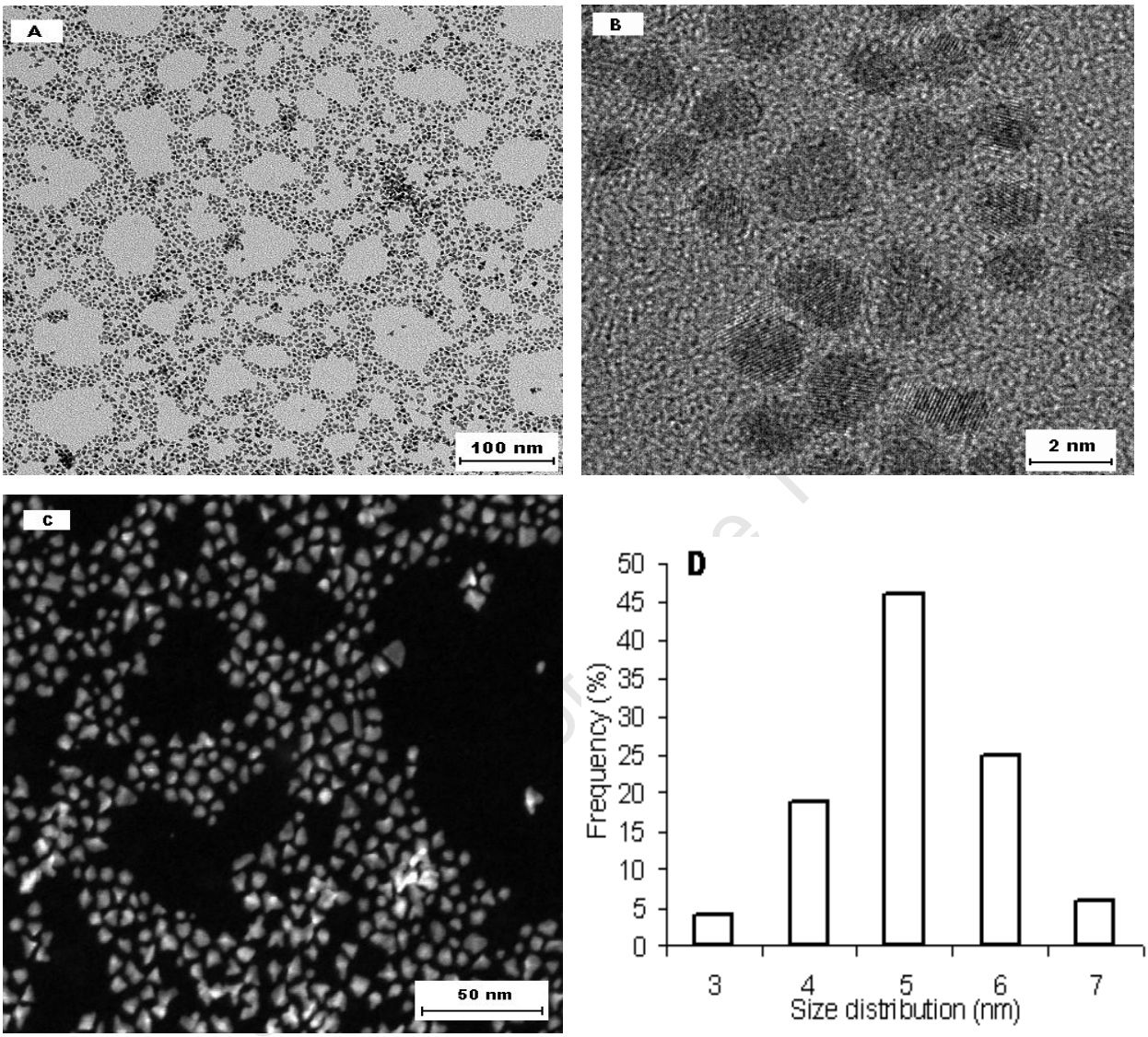

Figure 4.14: Bright-field TEM image (**A**), HR-TEM image (**B**), a dark-field TEM image of Pt nanoparticles (**C**) and particle size distribution histogram (**D**).

(iii) Zero-valent Pt particles were synthesized by reducing H_2PtCl_6 with excess $NaBH_4$ and OAm was used as the surfactant and toluene as the solvent. This reduction method yielded very small particles with a very narrow size distribution, showing good dispersion and crystallinity. Images of cubic, cuboctahedral and irregular Pt nanoparticles are shown in Figure 4.15 **A**. Figures 4.15 **B** and **C** are HR-TEM images of

the nanoparticles. These particles are seen to be single crystals. Figure 4.15 **D** shows particle size distribution histogram and average particle size is 2.36 nm with a standard deviation of 0.44 nm.

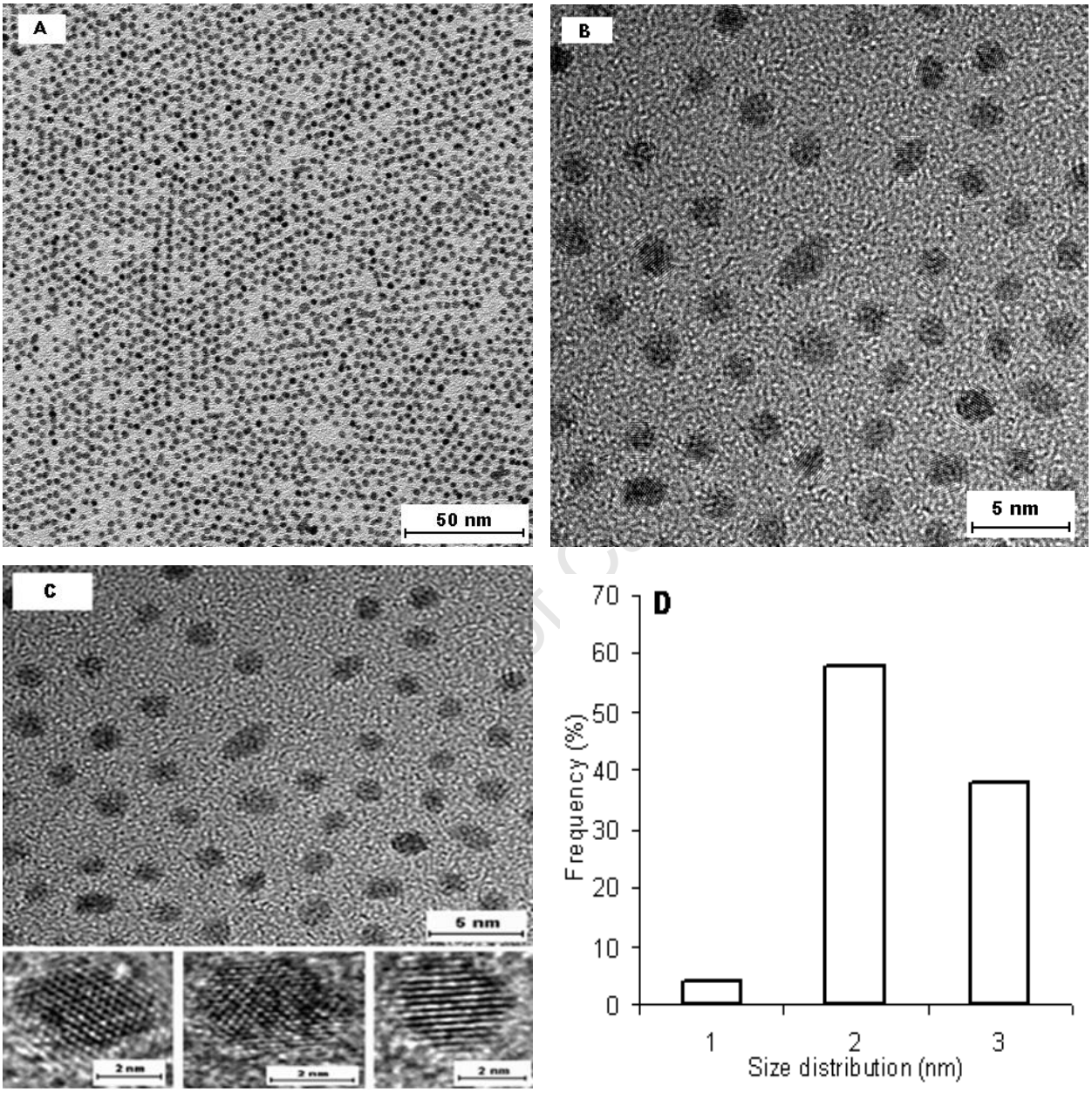

Figure 4.15: Bright-field TEM image (**A**), HR-TEM image (**B**) and (**C**), and particle size distribution histogram (**D**) of cubic, cuboctahedral and irregular Pt nanoparticles.

4.2 VANADIUM METAL AND VANADIUM OXIDE NANOPARTICLES

Vanadium has a high affinity for oxygen and oxidises very easily. The reduction and decomposition of vanadium precursor salts to vanadium metal in the presence of water is therefore almost impossible. Furthermore, vanadium has a low reduction potential. There is no preparative route reported in the literature to synthesize vanadium nanoparticles with good size distribution and dispersity. The preparation of high quality and good monodispersity vanadium nanoparticles of different morphologies in water-free environments thus remains a challenge.

In the synthesis strategy developed in this present work: VCl_3 was reduced to zero-valent metal using thermal decomposition in high boiling point solvents such as BE and OE, in the presence of aliphatic amine groups as surface-active agents to coat and stabilize the nanoparticles at a particular size.

4.2.1 Synthesis of Vanadium Metal Nanoparticles

(a) Thermal Decomposition

The preparation of V nanoparticles from VCl_3 as the starting material in the presence of OAm (surfactant) and OE (solvent), produced particle monomers with narrow size distribution and good dispersion. The morphology, size and crystallinity of the as-prepared V nanoparticles were imaged using TEM as shown in Figures 4.16 **A** and **B**. The particle size distribution histogram is shown in Figure 16 **C,** giving an average diameter of 5.40 nm with a standard deviation of 0.89 nm.

The thermolysis of VCl_3 in BE using OAm as the solvent and surfactant, respectively, resulted in the formation of V nanoparticles with poor size distribution and crystallinity. The OAm-capped V nanocrystals nucleate and grow in size to diameters determined by the amount of precursor used, as shown in Figure 416 **D**. Figure 4.16 **E** shows an HR-TEM image of these particles which are seen to adopt a cubic morphology.

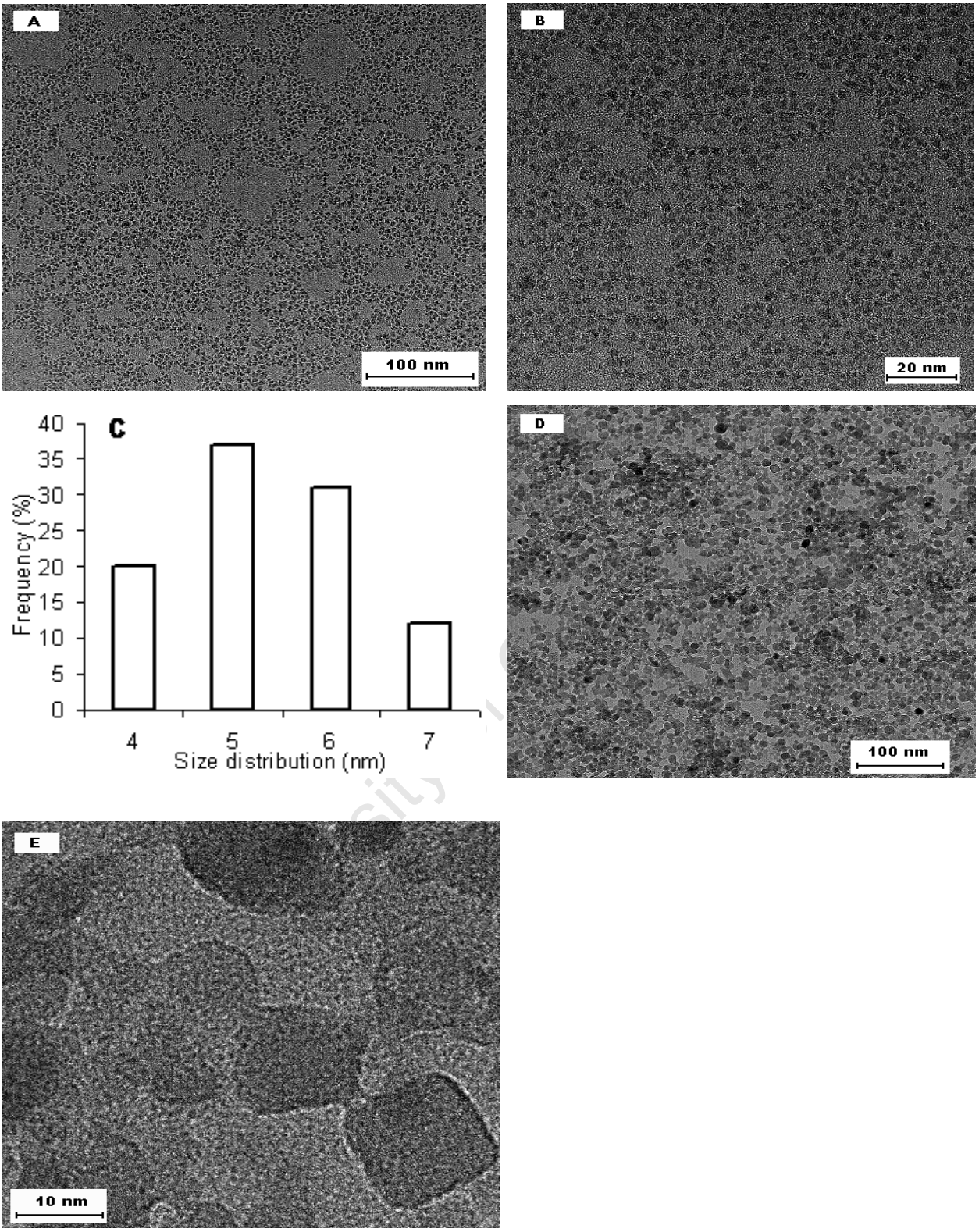

Figure 4.16: Bright-field TEM images (**A**), (**B**) and (**D**), particle size distribution histogram (**C**) and HR-TEM image (**E**) of V metal nanoparticles.

(b) Thermolysis of VCl_3 using OA and DOA as the Surfactants

Thermal decomposition of VCl_3 precursor to zero-valent V metal in the presence of high boiling-point solvent such as BE was carried out using both OA and DOA as the surfactants. This preparative route yielded high quality nanocrystals with good size distribution, dispersity and crystallinity. Figure 4.17 **A** and **C** show TEM images of these particles which adopt a cubic morphology. Figure 4.17 **B** shows the particle size distribution histogram. The diameters (and standard deviation) of the particles were calculated from randomly chosen areas, giving an average size of 11.15 nm with a standard deviation of 2.50 nm. Figure 4.17 **D** is a HR-TEM image of these particles showing good crystallinity.

Energy-dispersive X-ray spectroscopy (EDX) was used to determine the chemical composition of the V nanoparticles, as shown in Figure 4.18. In this EDX spectrum, excluding carbon and copper from the carbon-supported Cu grid, the peaks for V, O, Si and S are visible. The presence of oxygen suggests possible oxidation of nanoparticles either during their synthesis or the precipitation-redispersion process, whereas, Si and S came from the support.

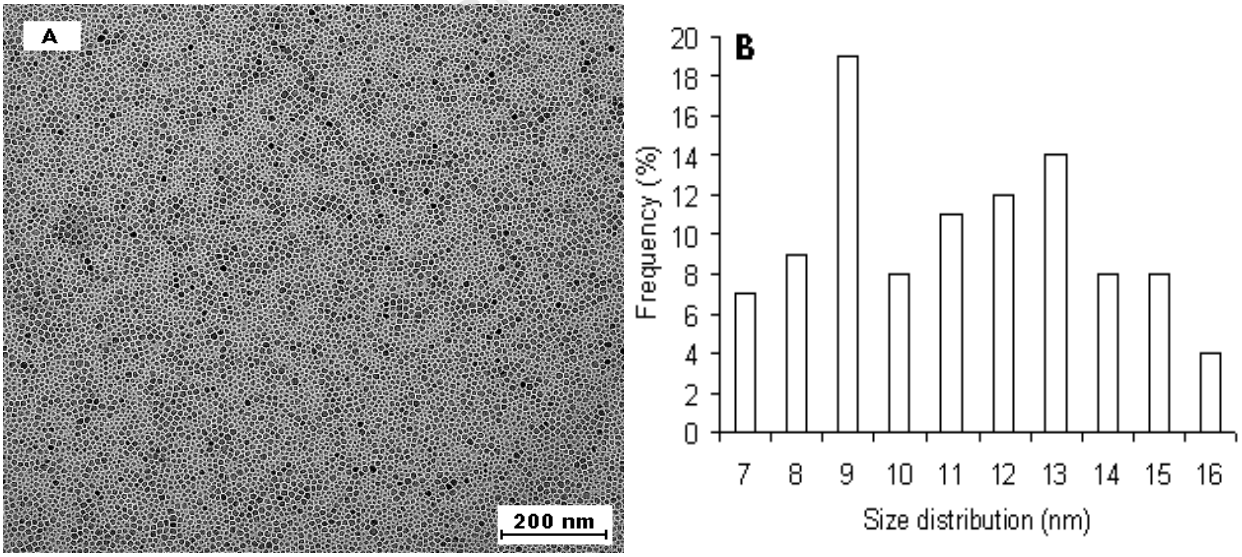

Figure 4.17: Bright-field TEM images (**A**) and particle size distribution histogram (**B**) of V metal nanoparticles.

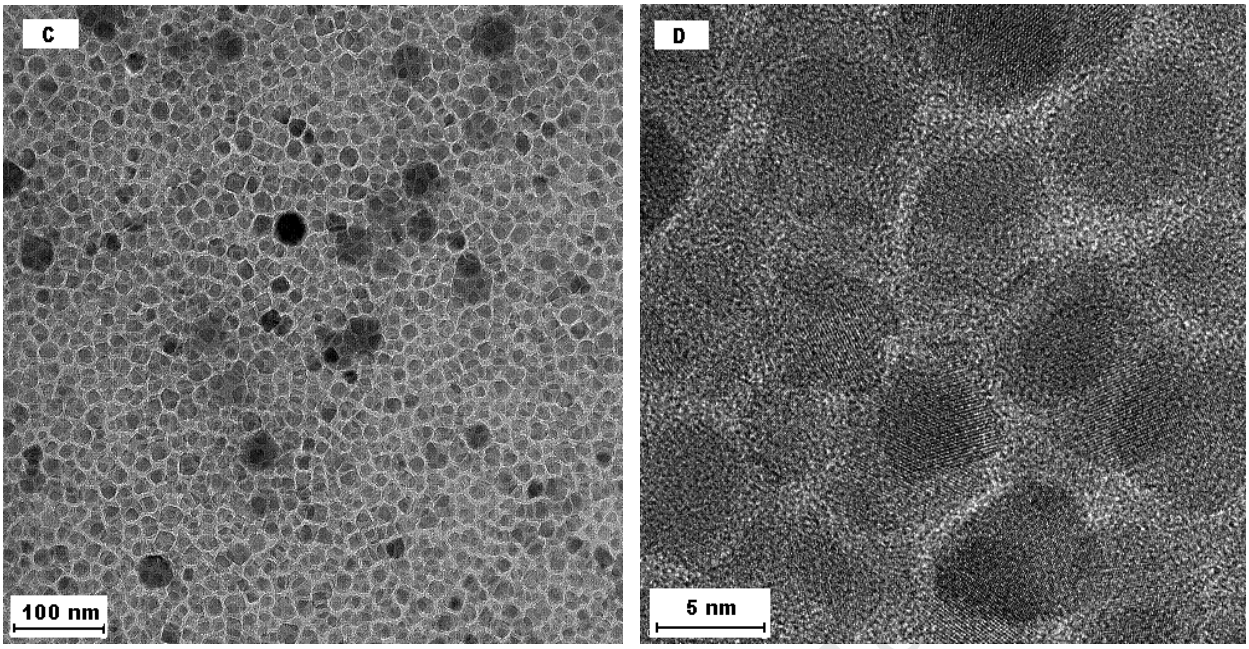

Figure 4.17: Bright-field TEM image (**C**) and HR-TEM image (**D**) of V metal nanoparticles.

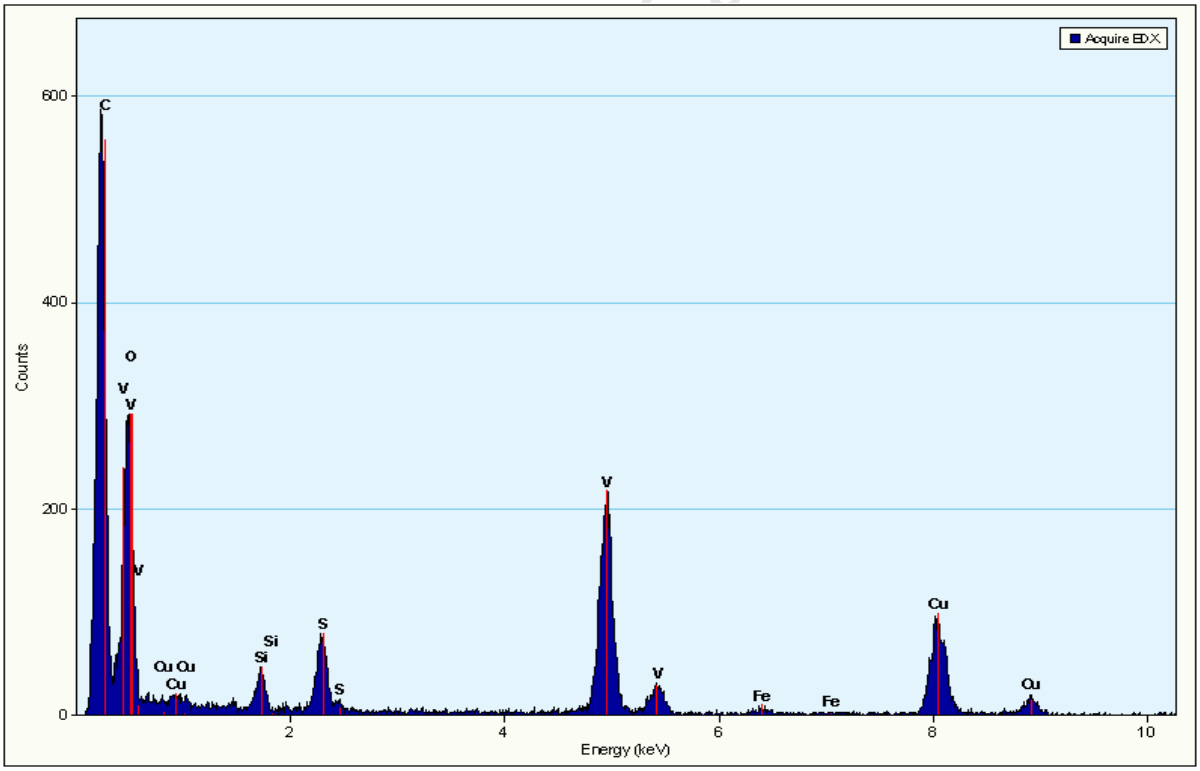

Figure 4.18: EDX spectrum of V metal nanoparticles.

4.2.2 Synthesis of Vanadium Oxide Nanoparticles

(a) Solvothermal Protocol

(i) OAm capped-vanadium oxide nanocrystals, prepared using a solvothermal protocol in the absence of water, yielded monodisperse vanadium oxide nanocrystals from a V_2O_5 precursor salt. In this synthesis route: the structure of V_2O_5 was first modified using TOABr to form V(V) diperoxo tetraoctylammonium complexes, $VO(O_2)_2$(TOA), and OAm was employed as the surface-active agent. Using EtOH as the solvent, cubic nanocrystals with narrow size distribution were obtained. TEM image of the as-prepared V oxide nanocrystals is shown in Figure 4.19 **A**. Figure 4.19 **B** shows the particle size distribution histogram and the diameters (and standard deviation) of the particles were calculated from arbitrarily chosen areas, giving an average size of 4.82 nm with a standard deviation of 1.20 nm.

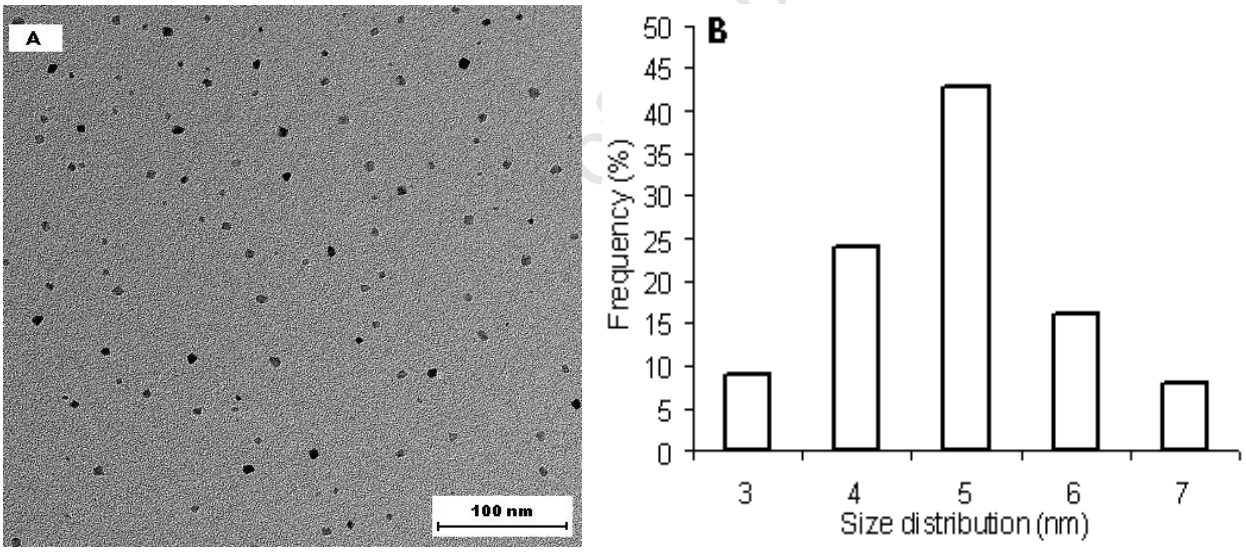

Figure 4.19: Bright-field TEM image (**A**) and particle size distribution histogram (**B**) of V oxide nanoparticles.

(ii) Vanadium oxide nanocrystals were synthesized within a short period of time using the present preparation route: the separated orange toluene phase was dissolved in BE and OAm was added as the surfactant. Heating the resultant solution above the boiling point of BE at 330 ºC, toluene (boiling point of 110.6 ºC) evaporated and the black

product of V oxide nanocrystals formed within 10 minutes.

Figure 4.20 **A** is a TEM image of the particles, showing irregular morphologies and broad size distribution; an HR-TEM image is shown in Figure 4.20 **B**. Figure 4.20 **C** shows the effect of increasing the amount of the surfactant on the diameter, distribution and morphology of the particles. Energy-dispersive X-ray spectroscopy (EDX) was used to determine the chemical composition of the V nanoparticles, as shown in Figure 4.21. In this EDX spectrum, excluding carbon and copper from the carbon-supported Cu grid, the peaks for V, O, Si, S and Fe are visible. The presence of oxygen indicates vanadium oxide nanoparticles whereas Si and S come from the support.

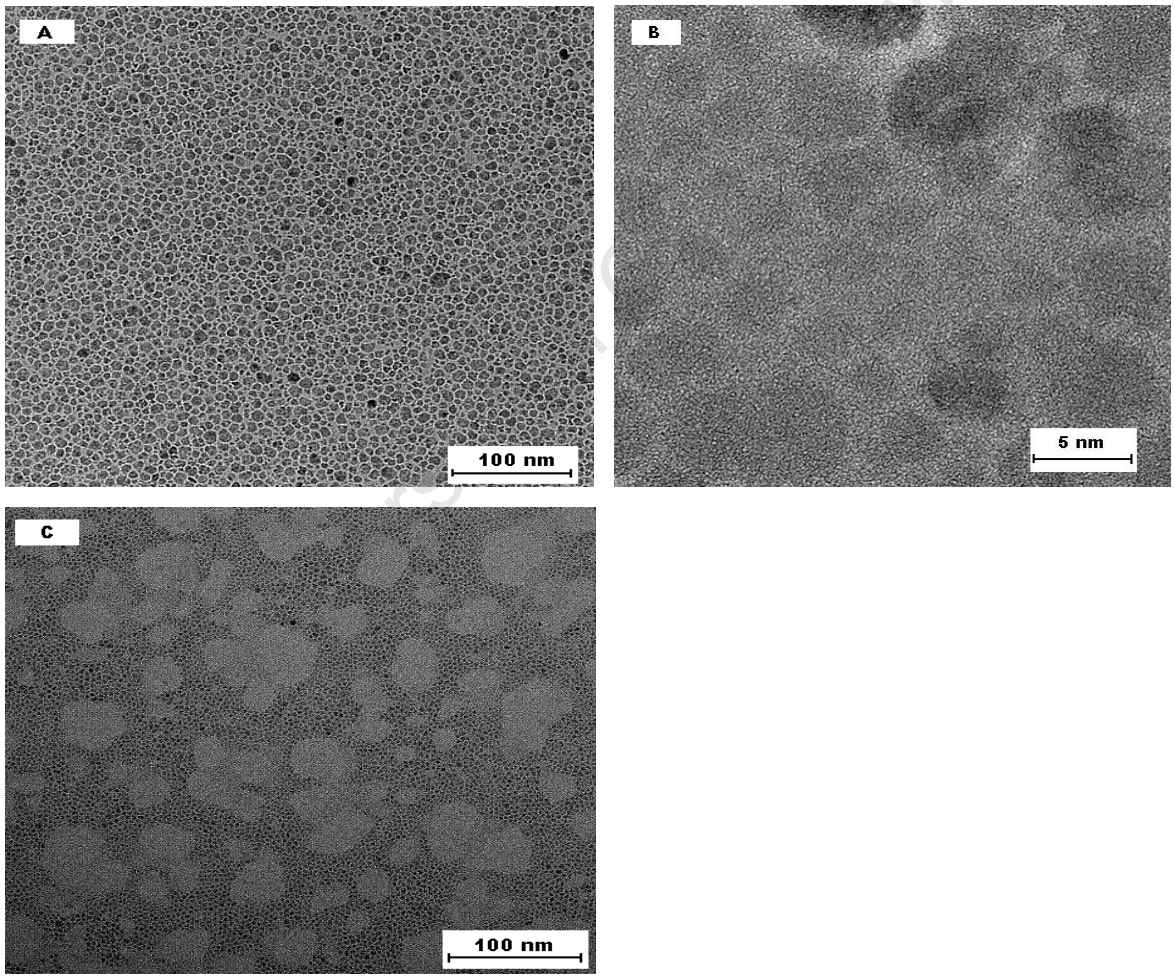

Figure 4.20: Bright-field TEM image (**A**), HR-TEM image (**B**) and bright-field TEM image (**C**) of V oxide nanoparticles obtained after increasing the amount of OAm.

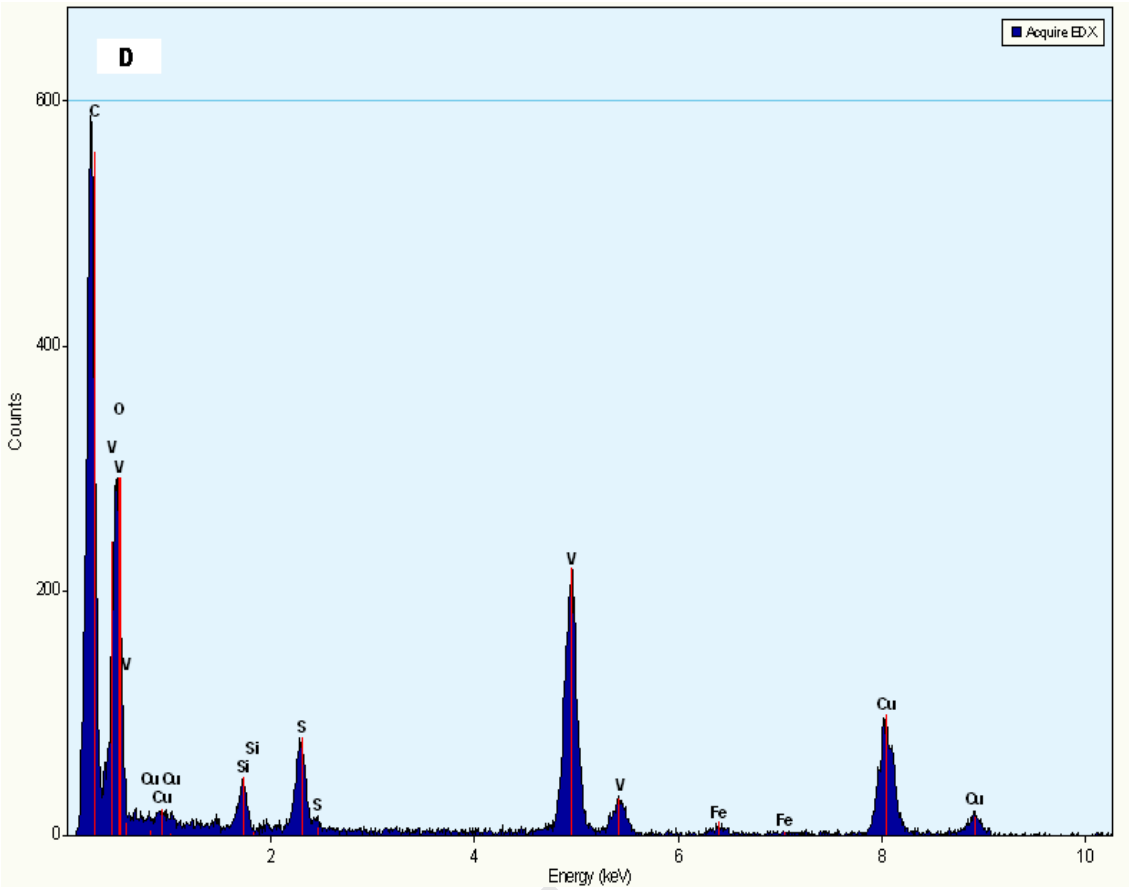

Figure 4.21: EDX spectrum of V oxide nanoparticles.

(iii) Vanadium oxide nanoparticles were synthesized by the thermal decomposition of V_2O_5 in the presence of surface-coating and stabilizing agents, OAm and OLEA. The thermolysis reaction was performed at 300 ºC for 60 minutes in high-boiling point organic solvent BE. TEM images of the as-prepared vanadium oxide nanoparticles, Figures 4.22 **A**, **B** and **C**, show the particles with poor crystallographic configuration. These nanoparticles exhibit a uniform size distribution and dispersity. Figure 4.22 **D** shows particle size distribution histogram. The mean nanoparticle size is 5.27 nm with a standard deviation of 0.97 nm.

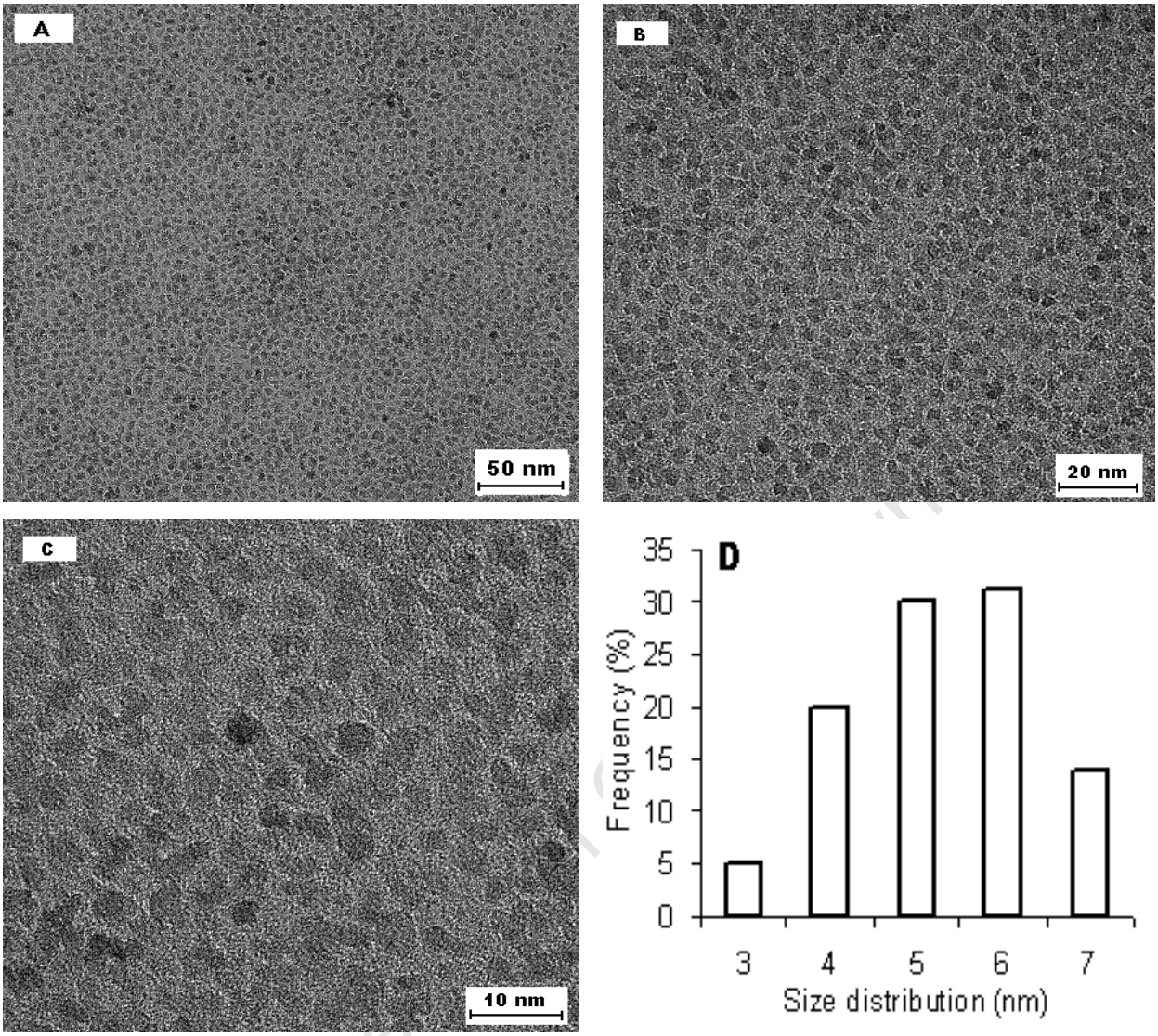

Figure 4.22: Bright-field TEM image (**A**), HR-TEM images (**B**) and (**C**), and particle size distribution histogram (**D**) of V oxide nanoparticles.

Table 4.1 summarizes the different synthesis approaches used to prepare nanoparticles of Pt, V and V oxide in colloidal solution, the solvents used to dissolve precursor salts, surfactants employed to stabilize nanoparticles as well as the reductants, additives and methods used to synthesize nanoparticles of different morphologies.

Table 4.1: The preparation methods and shapes of monodisperse Pt, V and V oxide nanocrystals.

Precursors	Surfactant(s)[a]	Reductant(s)[b]	Solvent(s)[c]	Additive[d]	Method[e]	Shape[f]
K_2PtCl_6	PVP	H_2	H_2O	HCl	R	T
K_2PtCl_4	PVP	EtOH	H_2O		R	T
$(NH4)_2PtCl_4$	PVP	Gly	Gly		R	S, WL
K_2PtCl_6	TBABr	AA	H_2O		R	P
K_2PtCl_4	OAm	FA	OAm		R	C
K_2PtCl_6	OAm	FA	OAm		R	CO
H_2PtCl_6	OAm	FA	OAm		R	C, IR, E
$(NH4)_2PtCl_4$	OAm	FA	OAm		R	IR
H_2PtCl_6	OAm	TBAB	OAm		R	TRI, IR
H_2PtCl_6	OAm	TBAB	OAm + BE		R	CO
H_2PtCl_6	OAm	$NaBH_4$	OAm		R	IR
VCl_3	OAm		OAm + OE		TR	IR
	OAm		OAm + BE		TR	C
	OA + DOA		OAm + DOA		TR	C
V_2O_5	OAm		EtOH		TR	C
	OAm		BE		TR	IR
	OLEA + OAm		OLEA		TR	C, IR, E

[a] PVP = poly(N-vinyl-2-pyrrolidone); CTAB = hexadecyltrimethyammonium bromide; OAm = oleylamine; TOAB = tetraoctylammonium bromide; OLEA = oleic acid; TBABr = tetrabutylammonium bromide; TOA = trioctylamine; OA = oleyl alcohol; DOA = dioctylamine: TTAB = tetradecyltrimethylammonium bromide;

[b] EtOH = ethanol; AA = ascorbic acid; FA = formic acid; TBAB = tetrabutylammonium borohydride; $NaBH_4$ = sodium borohydride; Gly = glycerol

[c] OAm = oleylamine; BE = benzyl ether; OE = octyl ether

[d] HCl = Hydrochloric acid

[e] R = Reduction; TR = thermal reduction

[f] T = tetrahedral; S = spherical; WL = worm-like; P = porous; C = cubic; CO = cuboctahedral; IR = irregular; E = elongated

4.2.3 VPt Nanoparticles

(a) In an attempt to synthesis VPt nanoparticles: VCl_3 precursor was dissolved in deionized water. THAB and TTAB were both used as surfactants, and Gly as the reductant. After twenty hours of reflux, a Pt precursor salt, K_2PtCl_4, was added and the resultant solution was refluxed for another four hours. The morphology of the particles is shown in Figures 4.23 (**A – D)**. Figures 4.23 **C** and **D** exhibit lattice fringes showing the orientation of crystal lattices of porous nanoclusters. According to the EDX spectrum shown in Figure 4.24, there is no visible peak for V. This indicates that VCl_3 was not reduced to V^0.

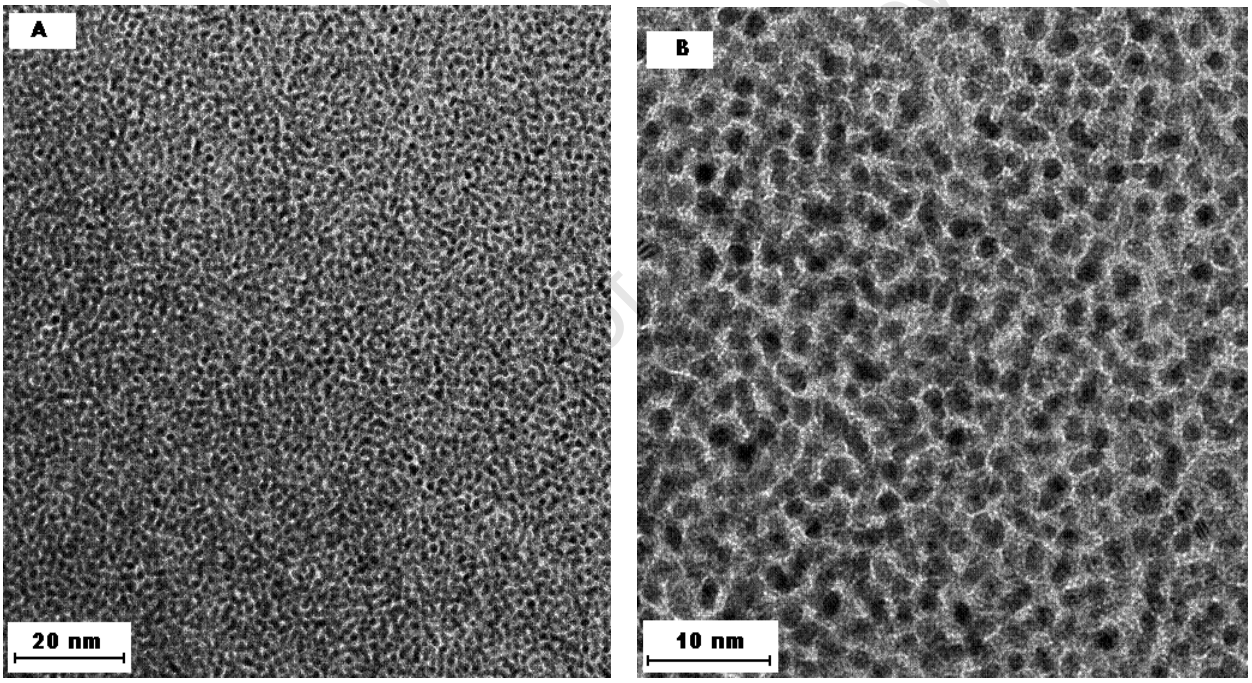

Figure 4.23: Bright-field TEM images (**A**) and (**B**) of VPt nanoparticles.

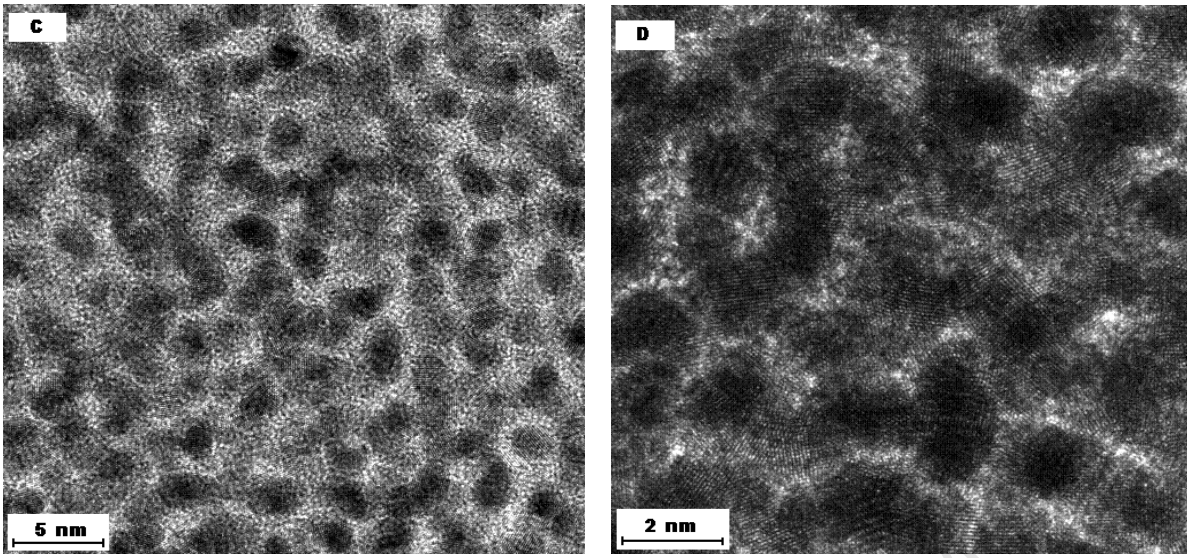

Figure 4.23: HR-TEM images (**C**) and (**D**) of VPt nanoparticles.

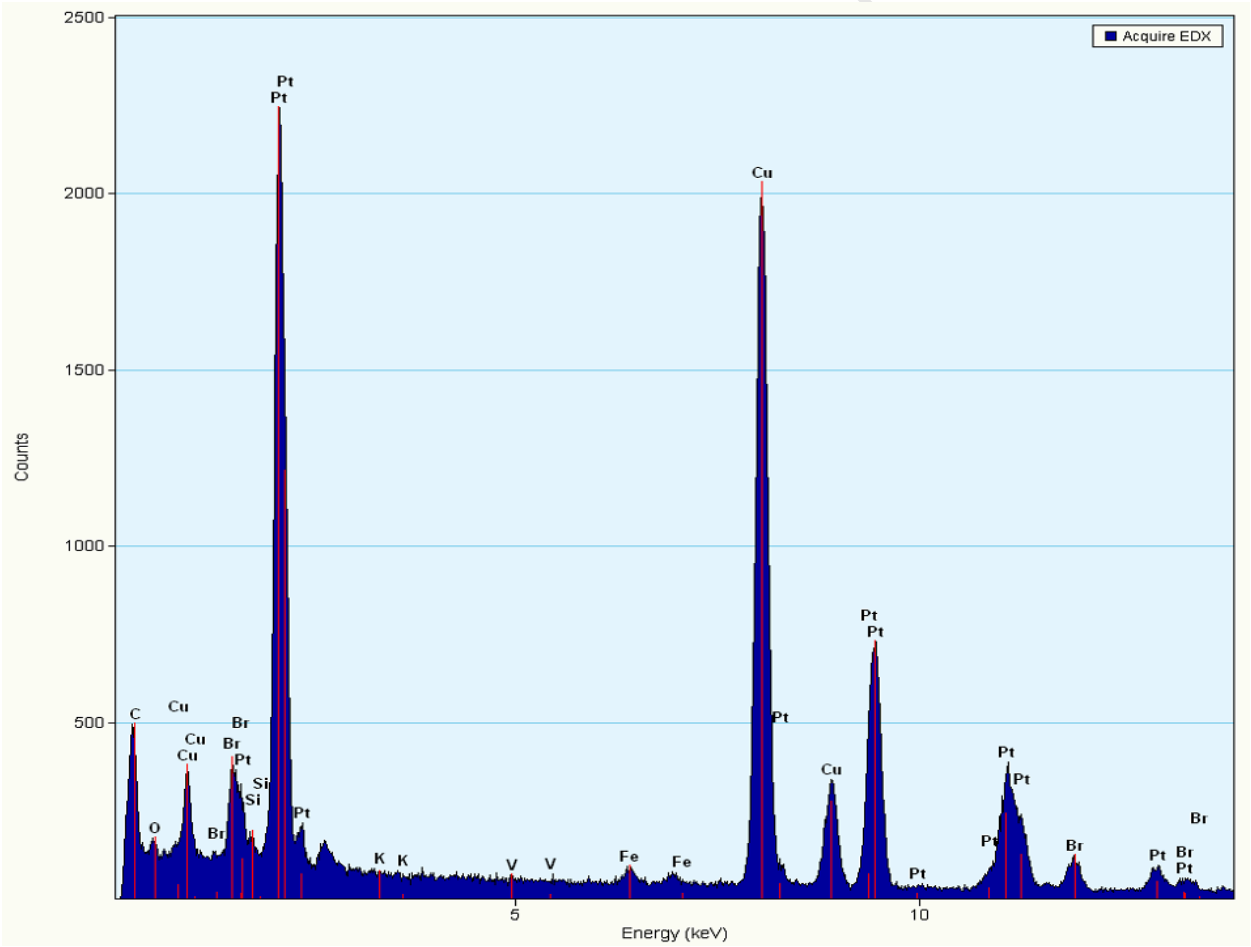

Figure 4.24: EDX spectrum of VPt nanoparticles.

(b) Both VCl_3 and K_2PtCl_4 precursor salts were dissolved in deionized water, CTAB was used as surfactant and FA as the reductant. The morphology of the particles is shown in Figure 4.25 (**A**, **C – F)**. Figure 4.25 **A** shows the monospersity of nanoparticles. Figure 4.25 **B** indicates a wide particle size distribution, calculated from a population of 150 particles in randomly chosen areas, yielding a mean of 17.33 nm with a standard of 4.78 nm. Figures 4.25 **C**, **D**, **E** and **F** are HR-TEM images indicating good crystallinity. The EDX spectrum however exhibits only Pt peaks and no indication of V features, as shown in Figure 4.26.

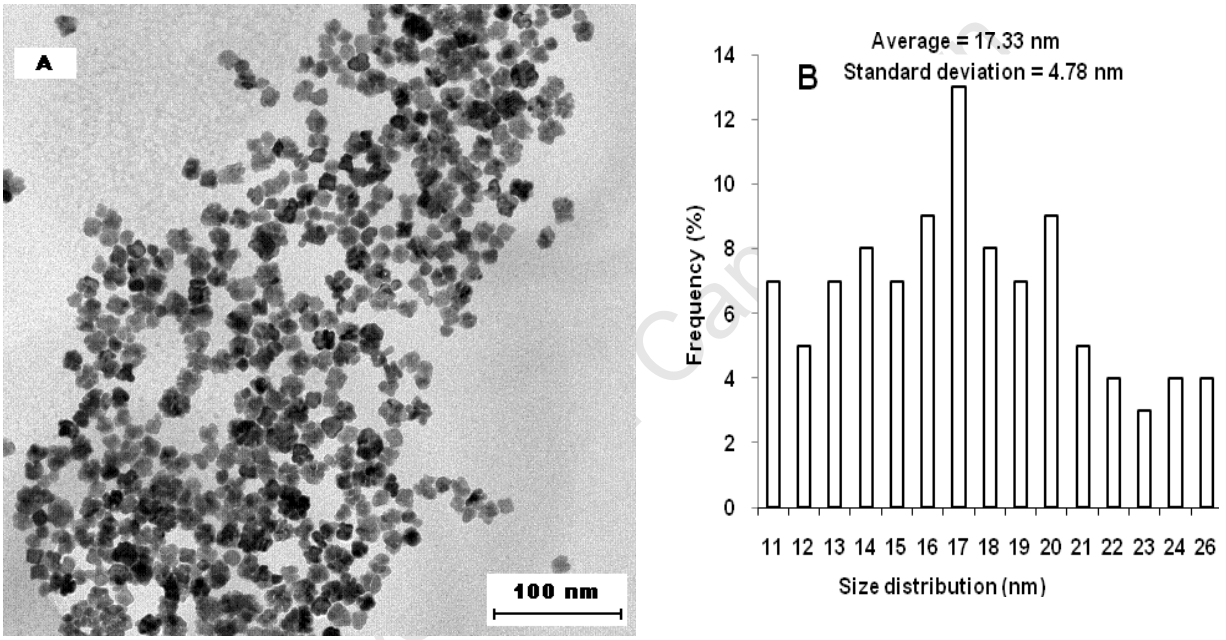

Figure 4.25: Bright-field HR-TEM images (**A**) and (**B**) particle size distribution histogram of irregular shapes of VPt nanoparticles.

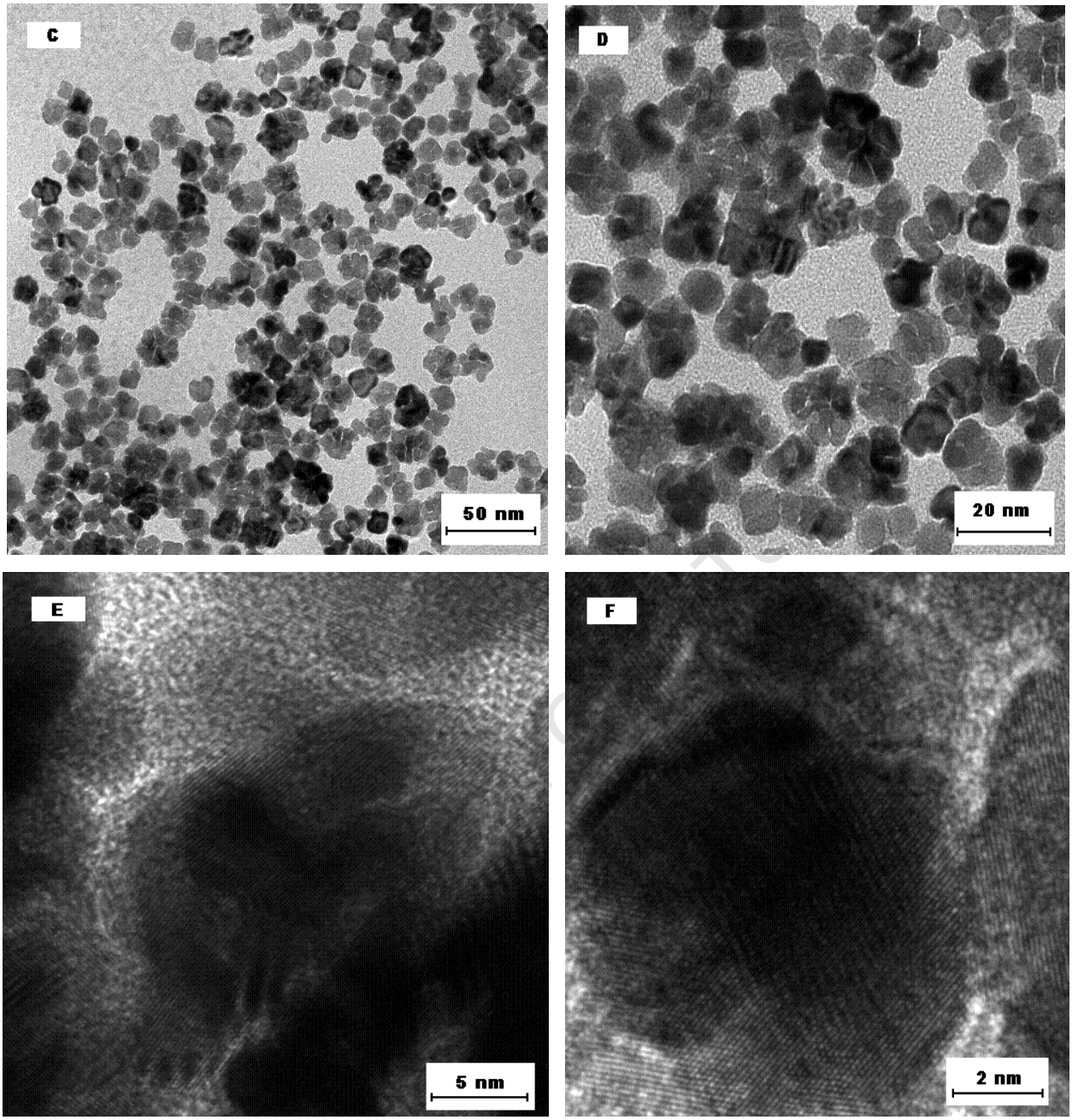

Figure 4.25: Bright-field TEM images (**C**) and (**D**), HR-TEM images (**E**) and (**F**) of irregular shapes of VPt nanoparticles.

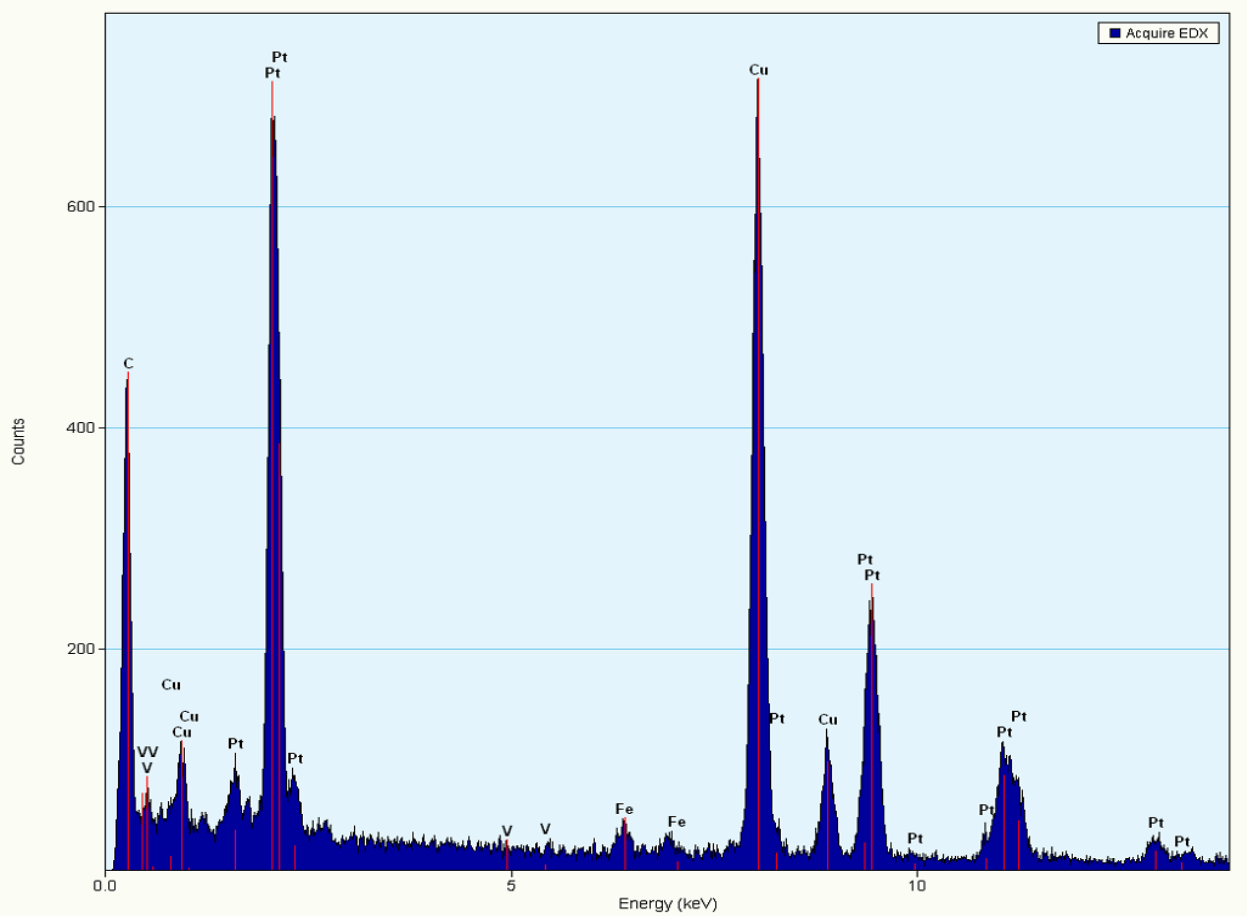

Figure 4.26: EDX spectrum of VPt nanoparticles.

(c) Bimetallic nanoparticles of VPt were synthesized by the thermal decomposition of VCl_3 and H_2PtCl_6 precursor salts in the presence of high boiling-point solvent BE using both SA and TOA as the surfactants. This preparative route yielded a continuous mixture of linked VPt nanoparticles of high quality and different edge shapes. HR-TEM images of these particles exhibiting good crystallinity are shown in Figures 4.27 **A**, **B**, **C** and **D**.

Energy-dispersive X-ray spectroscopy (EDX) was used to determine the chemical composition of the VPt nanoparticles, as shown in Figure 4.28. In this EDX spectrum, excluding carbon and copper from the carbon-supported Cu grid, the peaks for V, Pt, Si, S, Fe and O are visible. The presence of oxygen suggests possible oxidation of nanoparticles either during their synthesis or the precipitation-redispersion process,

whereas, Si, Fe and S came from the support. The EDX spectrum shows ~5% V and 95% Pt.

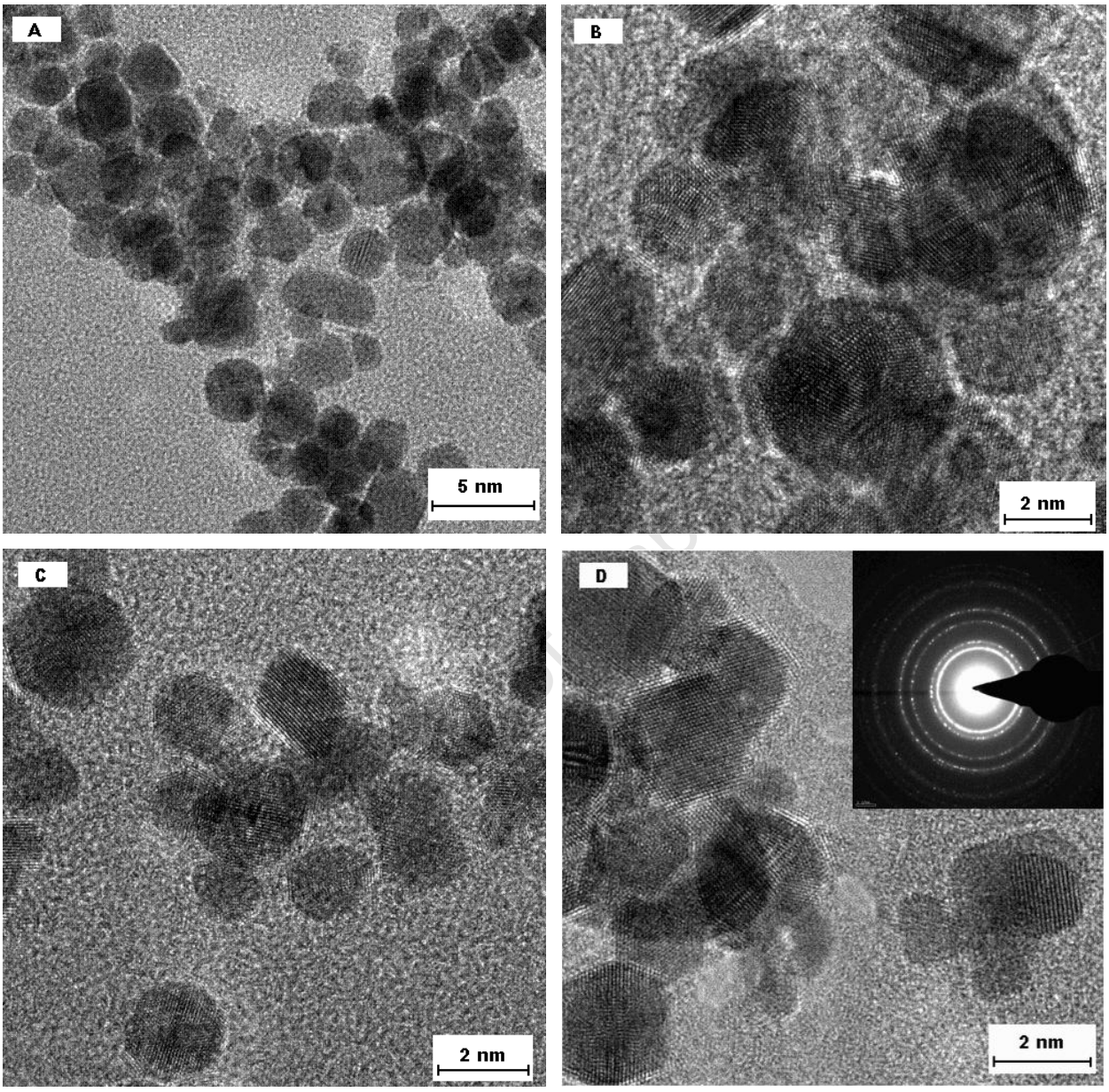

Figure 4.27: HR-TEM images (**A**) (**B**), (**C**) and (**B**) of VPt nanoparticles.

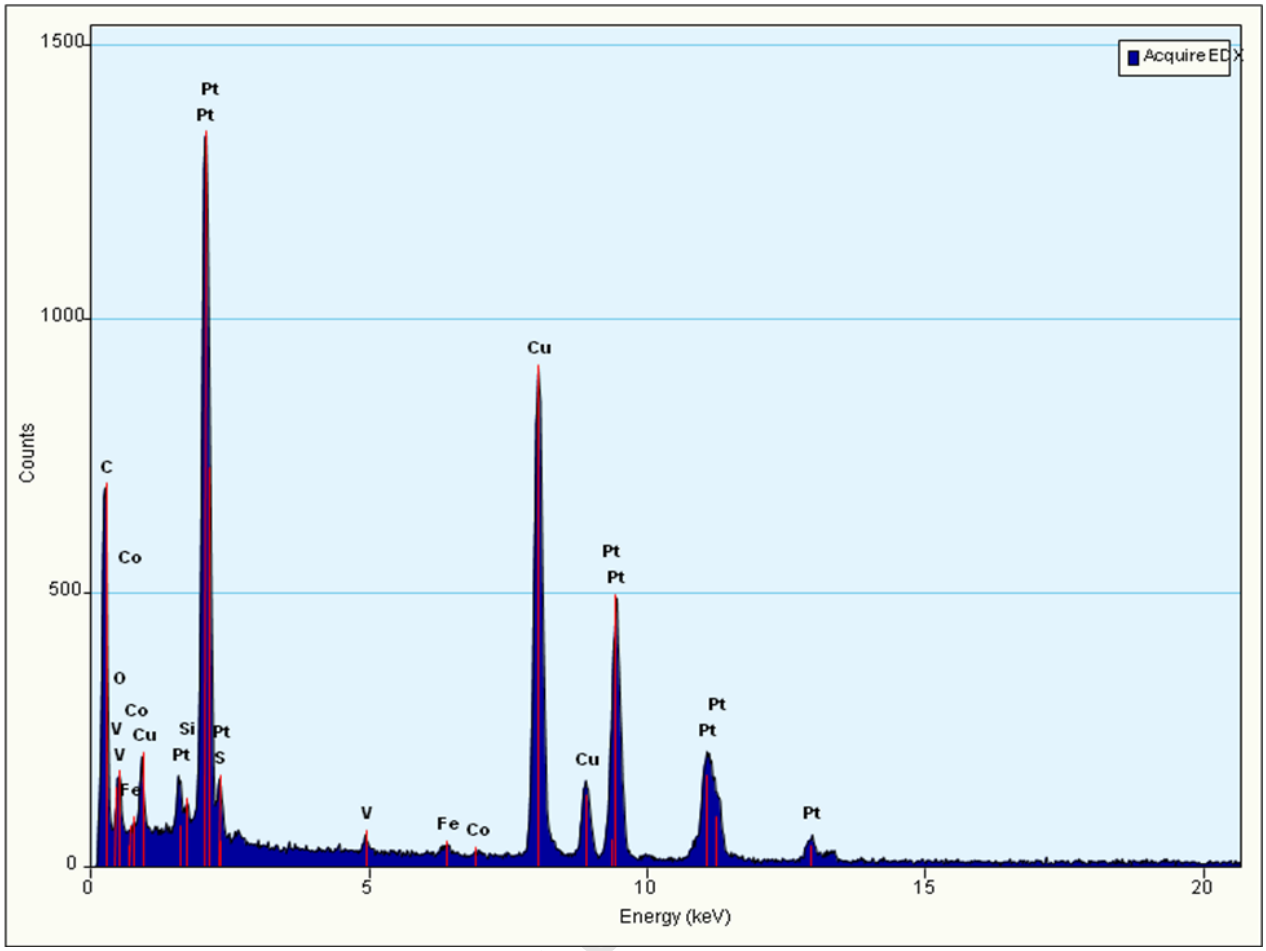

Figure 4.28: EDX spectrum of VPt nanoparticles.

(d) Bimetallic nanoparticles of VPt were synthesized by the thermolysis of VCl_3 and H_2PtCl_6 precursor salts in the presence of high boiling-point solvent BE using both OAm and TBA as the surfactants. This preparative route yielded a mixture of separate V and Pt nanoparticles of different shapes and high quality. Both V and Pt nanoparticles show good size distribution, dispersity and crystallinity. TEM images of these particles are shown in Figures 4.29 **A**, **B** and **C**. Figure 4.29 **D** is a HR-TEM image of the particles. Figures 4.29 **A** and **B** show two different morphologies of Pt nanoparticles with different dispersity and Figures 4.29 **C** and **D** show particles of separate Pt and V. The smaller particles are Pt and the larger particles are V.

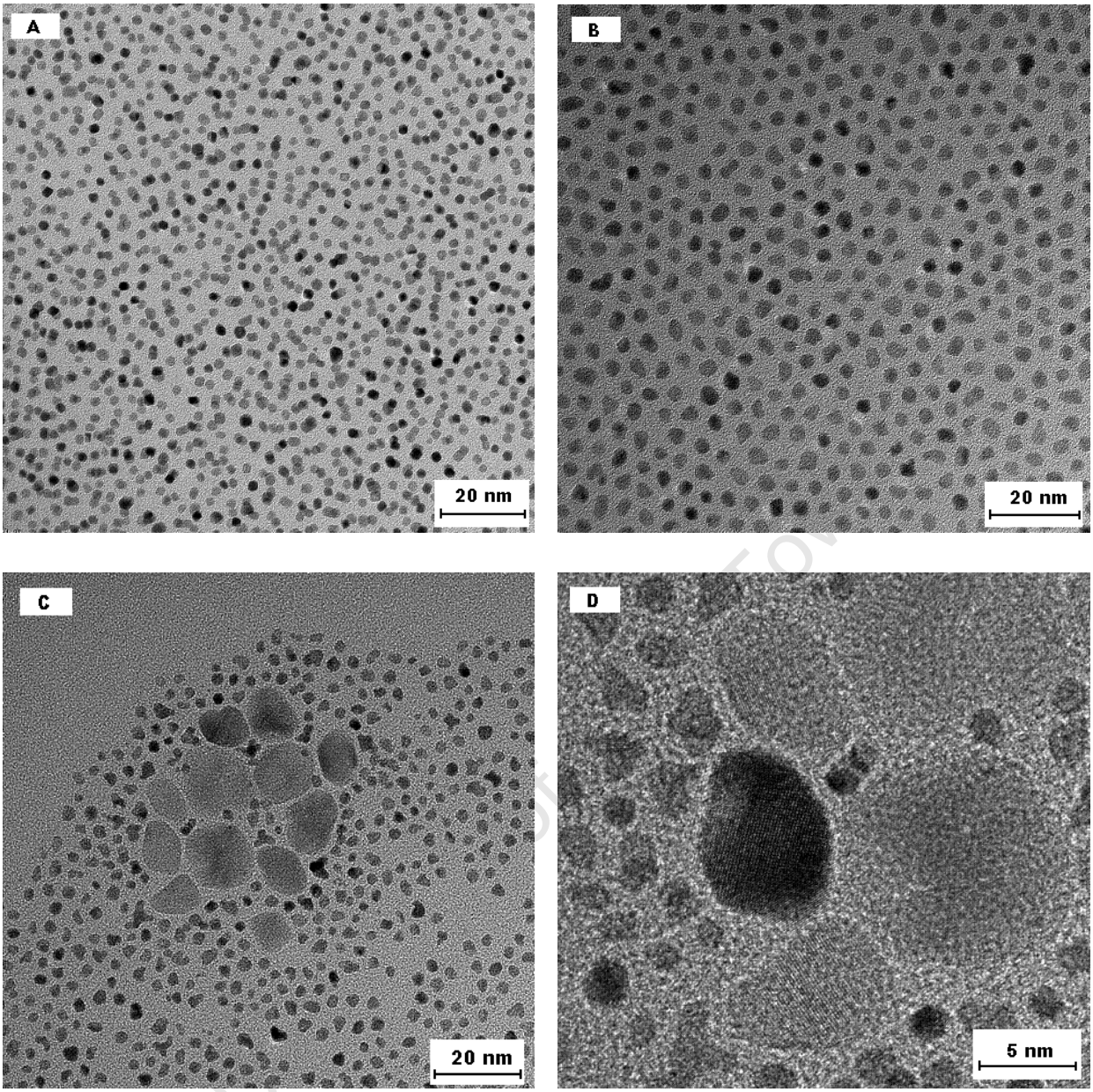

Figure 4.29: Bright-field TEM images (**A**) and (**B**) of Pt nanoparticles, bright-field TEM image of (**C**) and HR-TEM image (**D**) of separate V and Pt nanoparticles.

(e) In an attempt to synthesis core-shell V@Pt nanoparticles: VCl_3 was thermally decomposed to V^0, the particles were separated, purified and finally resuspended in toluene. TEM image of these particles is shown in Figure 4.30 **A**. Dried H_2PtCl_6 precursor salt was dissolved in the V nanoparticle suspension. Reducing this precursor salt around the preformed seeds of cubic V nanoparticles in the presence of OAm to

minimize agglomeration and using TBAB as the reductant resulted in the formation of VPt particle-on-particle. The morphology and size distribution of these particles are shown in Figures 4.30 **B** and **C**.

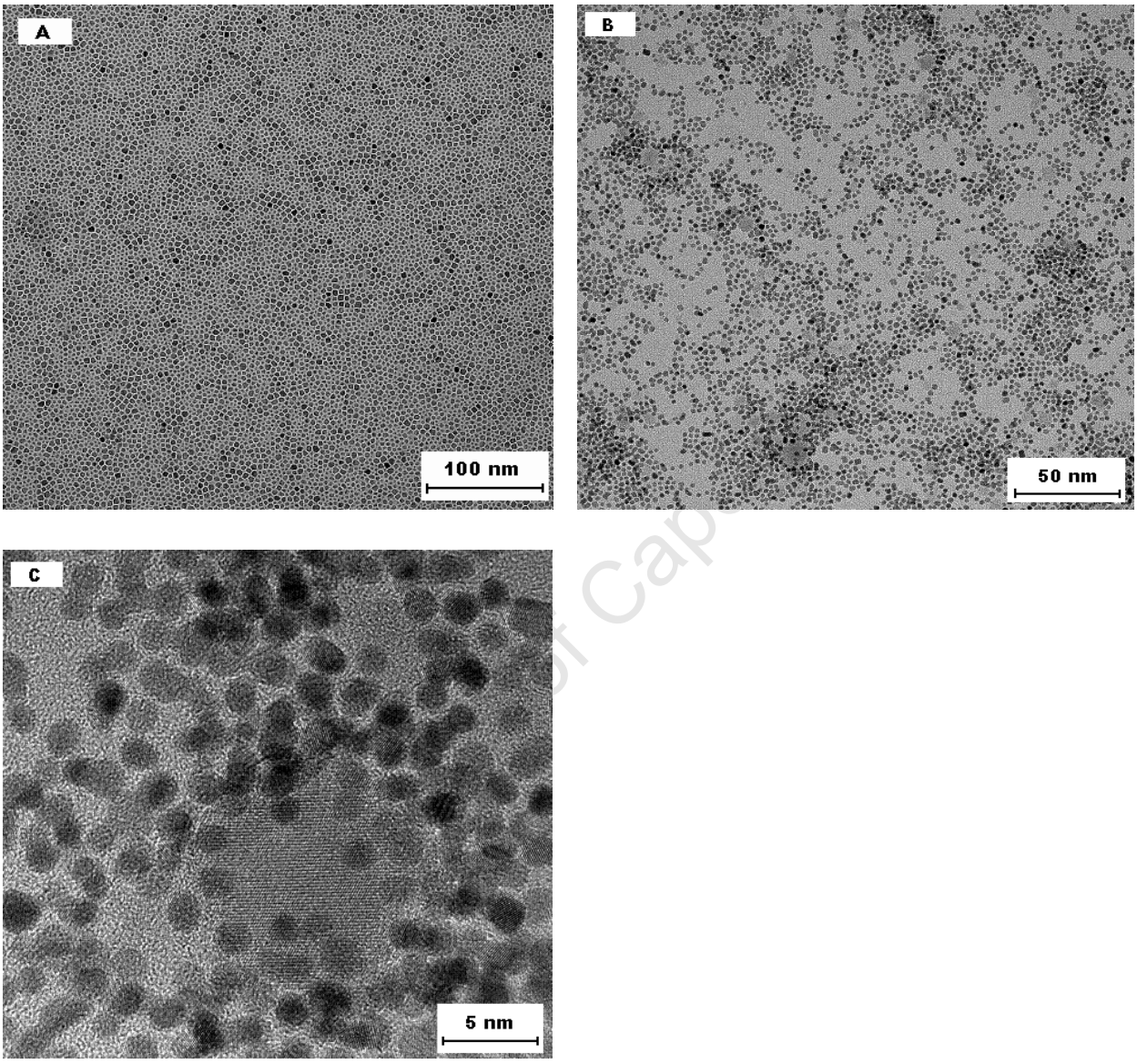

Figure 4.30: Bright-field TEM image (**A**) of V nanoparticles, (**B**) and HR-TEM image (**C**) of VPt nanoparticles.

(f) Separate bimetallic nanoparticles of VPt were synthesized by the thermolysis of VCl_3 for one hour in DOA and OA serving as both solvents and surfactants. The particles were separated, purified and redispersed in 20 ml of toluene. This preparative route

yielded V nanoparticles of high quality, good dispersity and different edge shapes. A dried H_2PtCl_6 precursor salt was dissolved in the OA and BE. The resulting solution was mixed with V nanoparticle suspension. Reducing this precursor salt around the preformed seeds of V nanoparticles using TBAB as the reductant resulted in the formation of separate V and Pt particles. The morphology and size distribution of these particles are shown in Figures 4.31 **A**. The smaller particles (< 5 nm) are Pt and the larger ones (> 10 nm) are V. Figure 4.31 **B** is a HR-TEM image of these particles with lattice fringes.

Energy-dispersive X-ray spectroscopy (EDX) was used to determine the chemical composition of the VPt nanoparticles, as shown in Figure 4.32, from two areas. Area 1 shows V features (grey) and the rest is Pt. In this EDX spectrum, excluding carbon and copper from the carbon-supported Cu grid, the peaks for V, Pt, Si, S and O are visible. The presence of oxygen suggests possible oxidation of nanoparticles either during their synthesis or the precipitation-redispersion process, whereas, Si and S came from the support.

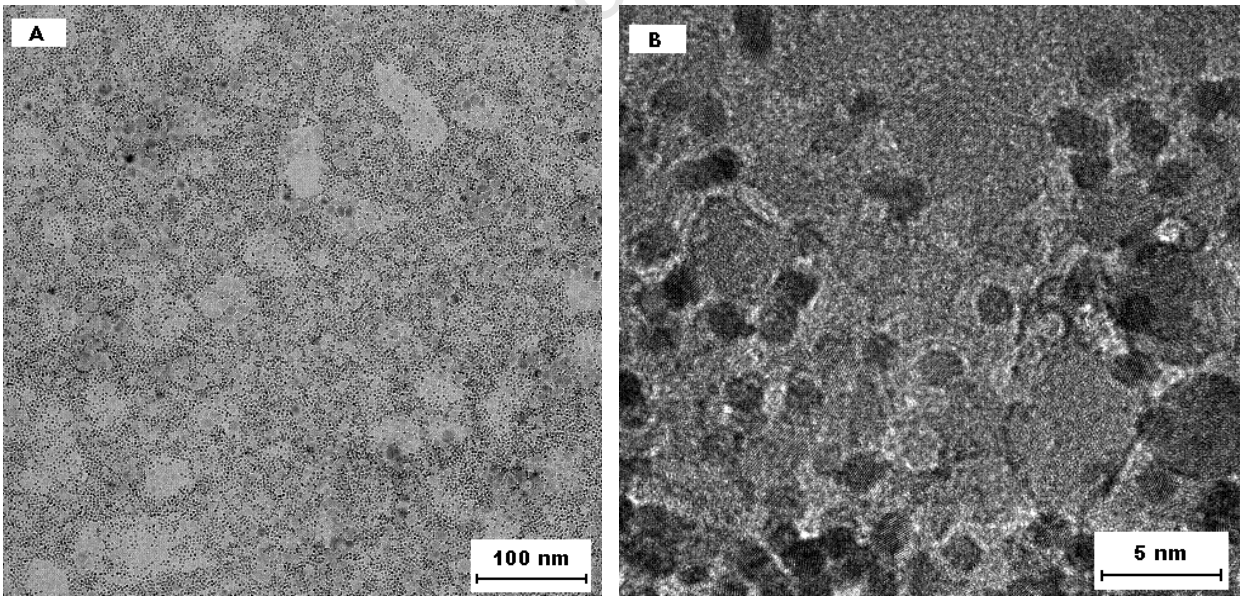

Figure 4.31: Bright-field TEM image (**A**) and HR-TEM image (**B**) of separate V and Pt bimetallic nanoparticles.

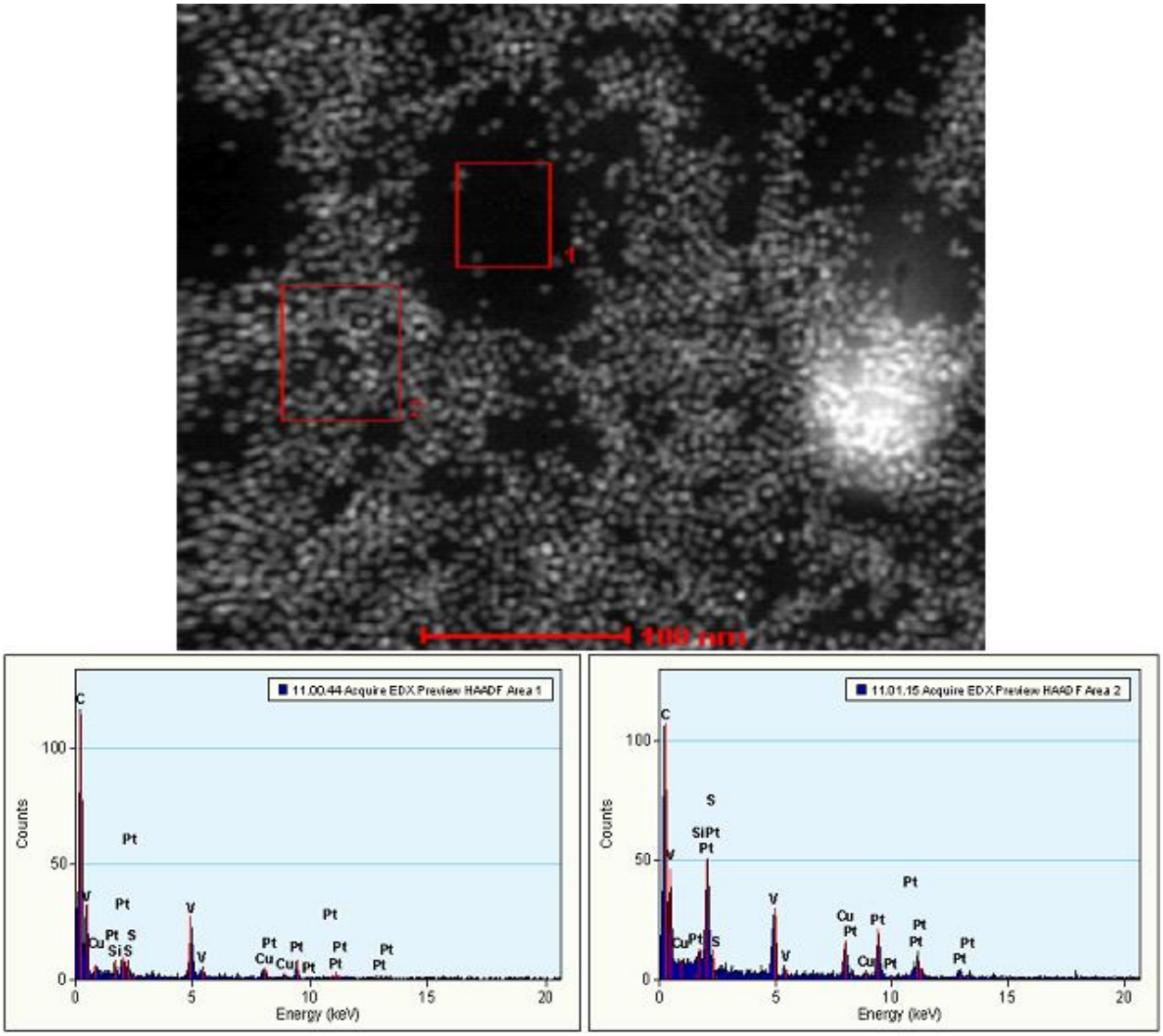

Figure 4.32: Dark-field image (top) and EDX spectrums (bottom) acquired from areas 1 and 2 of VPt nanoparticles.

5 DISCUSSION

The development of colloidal nanoparticles with uniform size and morphology from reproducible synthesis routes is particularly important for future studies, as the size and shape of nanoparticles determine their catalytic functionality in specific reactions. The experimental results in the present work show that various synthesis approaches can be employed to fabricate nanoparticles of Pt, V metal, V oxide and VPt. By varying reaction parameters such as the choice of precursor salts, solvents, surfactants, metal precursor-to-surfactant ratio, temperature, reaction time and reductants, the size, shape and quality of nanoparticles can be regulated.

5.1 EXPERIMENTAL PARAMETERS

(a) The Precursor Salts

Pt, V and V oxide precursor salts were chosen from potassium hexachloroplatinate (K_2PtCl_6), hexachloroplatinic acid (H_2PtCl_6), potassium tetrachloroplatinate (K_2PtCl_4), ammonium tetrachloroplatinate ($(NH_4)_2PtCl_4$), platinum acetylacetonate ($Pt(acac)_2$), vanadium trichloride (VCl_3) and vanadium pentoxide (V_2O_5) on the basis of their solubility in different solvents such as H_2O or organic liquids. Depending on the reduction potential of Pt and V, and their stability to oxidation, the decomposition and reduction of their metal ions to Pt^0 or V^0 (zero-valent metal) were performed under different reaction conditions. Unlike Pt, V has limited stability to oxidation and the reduction of its metal ion to metal V required dry environments under a flow of an inert gas.

Table 5.1 summarizes the solubility of different Pt, V and V oxide precursor salts in water and organic liquids.

Table 5.1: Solubility of Pt, V and V oxide precursor salts in water or organic liquids.

Precursor salt	Solubility in water or organic liquids
K_2PtCl_6	Water
H_2PtCl_6	Water
H_2PtCl_6 (dried)	Organic liquids
K_2PtCl_4	Water
$(NH_4)_2PtCl_4$	Water
$Pt(acac)_2$	Organic liquids
VCl_3	Water and organic liquids
V_2O_5	Water + H_2O_2
V_2O_5	Organic liquids + H_2O_2

(b) The Effect of Solvents

The choice of the solvent in which to dissolve the metal precursor is quite critical in order to obtain a homogeneous reaction solution prior to heating to the desired temperature. Some organic liquid surfactants can also serve as solvents. For instance, the precursor salts: VCl_3, Pt acetylacetonate and H_2PtCl_6 (dried) were chosen on the basis of their solubility in either high boiling point long chain surfactants (amines, dry alcohol and fatty acids) or solvents (BE and OE). The resultant solution was sonicated or heated at 100 – 150 ºC under vigorous stirring for 20 – 30 minutes. In this case, the colloidal nanoparticles of Pt, V and V oxide were directly synthesized by the thermal decomposition of their precursors in the presence of stabilizers (long-chain amines, alcohol and fatty acids) at temperatures determined by the boiling point of the solvent. This approach does not, therefore, require the employment of reductants.

The main challenge remained in the reduction of precursor salts of more reactive metals such as vanadium as a result of their limited stability to oxidation. The fabrication of nanoparticles of these reactive metal species requires careful control of the reaction conditions and nanoparticles are synthesized in dry environments and under a flow of inert gases. The most robust and successful synthetic protocol is thermolysis, which involves the use of high boiling point solvents to thermally decompose the metal

precursor-surfactant complexes and form nanoparticles. The boiling point of inert solvents such as benzyl ether (297 ºC) and octyl ether (287 ºC) determine the temperature of the reduction reaction. These solvents were used to prepare Pt, V metal and V oxide nanoparticles in the presence of long chain stabilizers. Heating the reaction solution to temperatures as high as 300 ºC for at least one hour resulted in the synthesis of nanoparticles with good crystallinity.

(c) The Effect of Surfactants

The aim here is the production of nanoparticles as stable colloids and this is attained by employing surfactants. In general, surfactants serve to regulate nanoparticle growth by adsorbing reversibly to the surfaces of nanoparticles to form a protective shell that mediates particle growth, stabilizes the particles and prevents the particles from oxidation after synthesis.

Surfactants not only serve to stabilize nanoparticles from agglomeration and oxidation but also act to regulate crystal growth and shape. The surfactants bind differently to different nanoparticle surfaces during growth and different morphologies of nanoparticles can therefore be produced depending on the nature of the surfactants and reductants used. In some cases, the surfactants can behave as both stabilizers and reductants. In order to achieve well-defined nanopartciles, it is important to choose a combination of precursor salts and surfactants which are highly soluble in the same solvent.

(d) The Effect of Precursor-to-Surfactant Ratio

The size of nanoparticles can be tuned by varying the precursor-to-surfactant ratio because in general, the lower the ratio of precursor-to-surfactant the smaller the nuclei; smaller nanoparticles are thus synthesized. Final particle size is however ultimately determined by the termination of particle growth (removing the solution from the heat source). Furthermore, during thermolysis, increasing of the heating rate of the reaction

mixtures leads to synthesis of nanoparticles with small dimensions due to high nuclei formation. The mean particle diameter can be increased with time as the concentration of the particles in the solution drops. The employment of the correct ratio of surfactant-to-precursor precludes the agglomeration of particles during synthesis and yields the desired nanoparticle size range. In addition to precursor-to-surfactant ratio, the size of the particles depends on factors such as the temperature and reductant.

(e) The Effect of Temperature

The synthesis of colloidal nanoparticles at room temperature requires the use of powerful reductants to reduce metal ions in the presence of surfactants. Increasing temperature has the beneficial effect of (a) ensuring the homogeneity of the chemical mixture, and (b) increasing the kinetics of the reduction reaction. Furthermore, the metal precursor-surfactant reaction solution must be heated only to temperatures high enough to improve the reduction kinetics, but not sufficiently high to induce reduction by the surfactants prior to the introduction of the selected reductant into the solution.

The synthesis of colloidal nanoparticles at elevated temperatures in the presence of a high molecular weight metal precursor-surfactant complex yields nanoparticles with large diameters, as shown in Figure 4.25. The size range can be optimized by the adjustment of the heating rate of the chemical reaction mixtures. Rapid heating of the chemical reaction solution induces fast decomposition of the metal precursor, resulting in a high concentration of nuclei in the solution. This is followed by fast growth which favours the creation of particles with small diameters. At low heating rate of the solution, nuclei formation occurs at low rates and remains relatively constant, leading to the creation of larger nanoparticles.

(f) The Effect of Reductants

Due to the high reduction potential of Pt, the formation of nanoparticles does not require rigorous control of the reaction conditions and nanoparticle synthesis occurs even at

very low temperatures. Depending on the nature and reducing strength of the reductant, the formation of nanoparticles may require refluxing of the solution until their growth to a particular size is attained. That is, poor reductants require prolonged reaction times to complete the reaction. For instance, the reduction of many metal ions by H_2 requires longer reaction time at room temperature and the strong reductants such $NaBH_4$ and TBAB are employed in such reactions. The use of powerful reductants such as borohydrides does not always require the heating of the solution and these are commonly used to reduce metal ions with highly negative reduction potential.

Furthermore, the proper choice of the kind and the amount of reductants to be used is critical in regulating the size of the particles because the reduction rate of different precursor salts to form metal nanoparticles is different and is influenced by the nature and concentration of reductants. Generally, the use of high concentrations of reductants results in the production of particles with small sizes due to the increased reduction rate of the metal ions. These kind of experimental approaches, however, work exceptionally well for most unreactive metals. A wide range of reductants used in this present work resulted in the formation of nanoparticles of different morphologies and sizes.

5.2 REDUCTION METHODS

(a) Pt Nanoparticles

The reduction of a second Pt precursor salt (K_2PtCl_4) around the pre-formed Pt nanoparticles made from a different Pt precursor salt (K_2PtCl_6) resulted in the formation of “multiarmed” nanocrystals. The evolution of such arms could be attributed to overgrowth at the sites of initially preformed nanoparticles, which acted as seeds for this overgrowth. These particles possess shorter and longer arms, which are influenced by the rate of coating and stabilizing at different facets on the particle by PVP. The number of arms on each particle depends on the precursor salt solution reduced around each preformed seed and the rate of passivating of the particle by the capping agent[145].

The as-synthesized porous nanoparticles using AA as the reductant were identified to be polycrystalline, even though the orientation of the lattice fringes is the same. These particles are made up of many single crystals with the lattice fringes aligned with respect to each other: thus, polycrystalline nanomaterials that are highly orientated. This was shown by taking diffraction patterns of both single crystals and nanoparticles. The diffraction pattern obtained from a single crystal in a nanoparticle formed discrete reflections, whereas when taken from a whole nanoparticle, diffraction rings of fcc Pt were observed.

The reduction of different Pt precursor salts to form Pt nanoparticles using FA as the reductant in the presence of OAm as the surfactant was demonstrated to be a novel, effective and reproducible route to synthesize monodisperse Pt nanoparticles exhibiting good crystallinity. The formation of Pt nanoparticles occurred at low operating temperatures and resulted in the formation of particles showing good size distribution and particle dispersion. In all cases, the particles adopted mostly cubic or cuboctahedral morphologies even though a few particles were elongated and irregular in shapes.

The use of a strong reducing agent, TBAB, in a high boiling-point BE resulted in the formation of particles with good size distribution and dispersion. Growth control of nanoparticles is obtainable by selecting an appropriate operating temperature of decomposition and the optimal ratio of surfactant and reductant. By controlling the evaporation of the solvent used to resuspend the nanoparticles, 2D and 3D superlattice structures with hexagonal close-packing of particles were achieved[136]. This hexagonal close-packed arrangement of colloidal crystals usually arises due to the slow evaporation of the solvent and the particles self-assemble through van der Waals forces of attraction and surface tension between the particles[139],[140]. Furthermore, close-packing of nanoparticles requires good control over the size and shapes. That is, nanoparticles with uniform size and shape tend to self-assemble.

5.3 THERMAL DECOMPOSITION

(a) V Metal Nanoparticles

Vanadium metal nanoparticles were synthesized using a novel preparative technique. In the preparation of V^0, VCl_3 was reduced by employing thermal decomposition in the presence of a high boiling point solvent BE, and using OAm as the surfactant. This new route resulted in the formation of V metal nanoparticles with poor size distribution and crystallinity. The poor particle distribution is probably due to the insufficient use of the surfactant which hinders their agglomeration and settling during synthesis. The oleylamine-capped V nanocrystals nucleate and grow in size to diameters determined by the ratio of precursor-to-surfactant.

The more effective, economical and novel synthesis approach developed in this present work showed that the employment of surface-active agents, OA and DOA, provides a powerful reducing and capping environment via the thermal decomposition of VCl_3 precursor to zero-valent V metal in the presence of high boiling-point solvent such as BE. This preparative route yielded high quality nanocrystals with good size distribution, dispersity and crystallinity. The nanoparticles are of various sizes and can be separated through a size selective precipitation process.

(b) V Oxide Nanoparticles

V Oxide Nanoparticles synthesized in BE as the solvent and OAm as the surfactant, after evaporating toluene, showed a broad particle distribution and good dispersion. However, the particles did not exhibit good crystallinity. This synthesis protocol was effective, economical and required no prolonged reaction time to complete the reaction. The formation of V oxide nanoparticles in high boiling-point solvent BE is an easy, quick and new approach. This route does not involve the modification of V_2O_5 structure with ammonium bromides such as TOABr to form V(V) diperoxo tetraoctylammonium complexes, $VO(O_2)_2(TOA)$. V_2O_5 was dissolved in a solution of BE and H_2O_2 in absolute

EtOH by sonication. Thermal decomposition was performed after the addition of surfactants, OAm and OLEA, in different ratios. Depending on the boiling point of the solvent, vanadium oxide nanocrystals were synthesized within a short period of time. Nanoparticles synthesized by using this technique showed a narrow size distribution and good dispersity but poor crystallinity.

5.4 THERMAL DECOMPOSITION AND REDUCTION METHODS

(a) Bimetallic VPt Nanoparticles

In a mixture of V and Pt precursor salts: the use of reductants such as AA and FA resulted in the formation of only Pt nanoparticles, suggesting the impossible reduction of V ions to V metal nanoparticles in the presence of water as the solvent. This can be attributed to its highly negative reduction potential and instability to oxidation. Size- and shape-controlled design of bimetallic VPt nanoparticles required the preparative routes that use dry and high boiling point solvents. In this regard, thermolysis was used to ensure the reduction of both V and Pt ions to metal nanoparticles in BE and OE as solvents, and in the presence of different surfactants. This novel design of preparative approach produced bimetallic nanoparticles of VPt of different sizes, size distribution and morphologies exhibiting high crystallinity. In some cases, reductants such as TBAB were used to facilitate the reduction of Pt ions.

Different morphologies of possible bimetallic nanoparticles have been reported in the literature as shown in Figure 5.1 and depend entirely on synthesis approaches[115]. In the present work investigated: bimetallic VPt alloy particles, particle-on-particle and separate particles were synthesized. The challenge remains in the fabrication of core-shell and super core-shell nanoparticles. For the synthesis of core-shell nanoparticles, the core metal requires the use surfactants to preclude agglomeration and obtain particles with good size distribution and dispersity. Prior to the reduction of a second metal ion around the pre-formed nanoaprticles, the particles must be separated and purified to eliminate excess surfactants and the shell is created from a highly

catalytically active metal, thus anticipated to play a great role during catalysis[71].

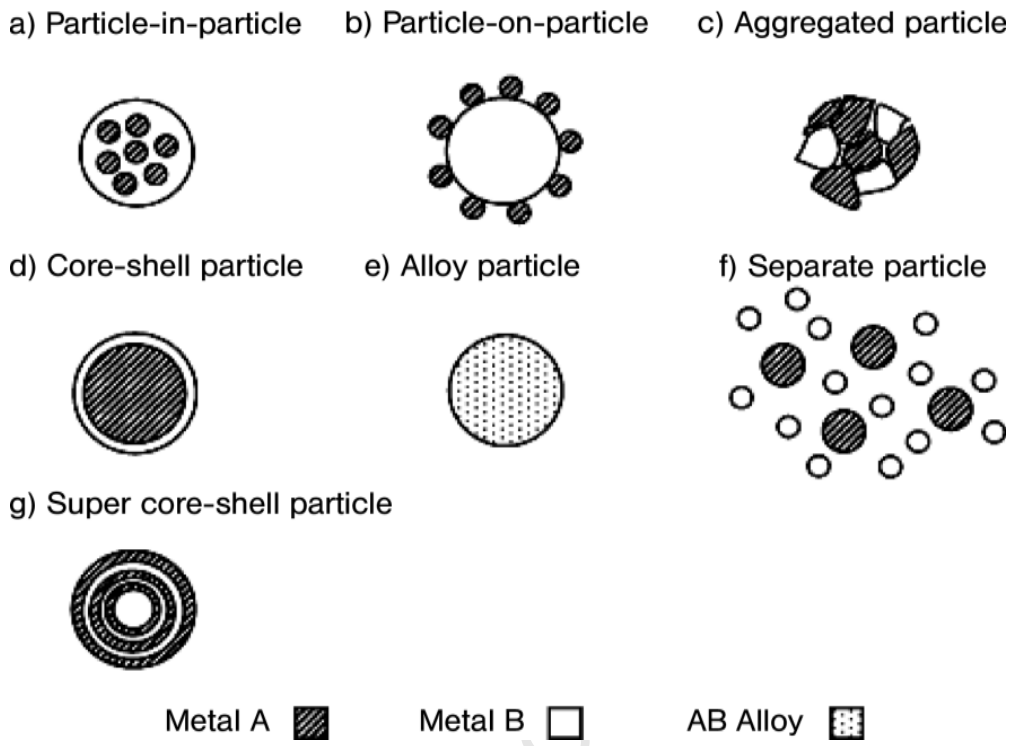

Figure 5.1: Schematic illustration of possible morphologies of bimetallic nanocrystals (after He *et al.*[115]).

5.5 OPTIMAL PROCESSING ROUTES

The optimization of size, shape and particle distribution of nanoparticles requires a solid knowledge and understanding of the effect of experimental parameters such as a choice of solvents, precursor salts, metal precursor-to-surfactant ratio, temperature, reaction time and surfactants during their preparation as stable colloids. Most importantly, the size and shape of nanoparticles are potential building blocks for catalysis and for the development of other materials. Thus, good control of these two unique structural properties of nanoparticles that determine the catalyst activity, establishes a platform for their design and engineering for use in specific industrial applications.

Size- and shape-evolution of Pt, V metal, V oxide and VPt nanoparticles depended entirely on optimal processing approaches which involved the employment of high boiling point solvents to thermally decompose the metal precursor-surfactant complexes. The boiling point of such inert solvents determined the temperature of the reduction reaction. High boiling point solvents such as BE (297 ºC) and OE (287 ºC) provided a versatile dry environment for the synthesis of Pt, V metal, V oxide and VPt nanoparticles of different morphologies in the presence of long chain stabilizers.

Heating the reaction mixture to temperatures just above the boiling points of these solvents, for at least 30 – 60 minutes, produced nanoparticles of uniform size, shape, with good size distribution, dispersity and crystallinity. Thermolysis served as the most robust and successful synthetic protocol deployed in this present work. Furthermore, the use of some reductants such as FA, $NaBH_4$ and TBAB to decompose and reduce Pt ions to Pt^0 (zero-valent metal) using OAm as surfactant provided another reduction pathway for the successful size- and shape-control synthesis of Pt, (not V and V oxide) nanoparticles. The particles prepared using these reductants are less than 10 nm in size, and hold promise as useful catalysts in a variety of chemical processes.

6 CONCLUSIONS AND RECOMMENDATIONS

The design and synthesis of platinum (Pt), vanadium (V) and vanadium oxide nanoparticles with an extremely high surface area was achieved by the employment of various solution-based synthesis approaches which include reduction, nonhydrolytic sol-gel and thermal decomposition. The size, shape, morphology and quality of nanoparticles can be controlled by adjusting the reaction parameters such as the choice of precursor salts, solvents, surfactants, metal precursor-to-surfactant ratio, temperature, reaction time and reductants.

The precursor salts and surfactants were selected on the basis of their solubility in different solvents such as water or organic liquids. The ratio of precursor-to-surfactant influenced the final size of the particles. Different morphologies of nanoparticles were obtained by using different precursor salts, surfactants and reductants in different solvents. Pt ions were easily reduced to Pt metal nanoparticles using both mild and strong reductants due to its high reduction potential. The formation of V metal and V oxide nanoparticles of uniform size and shape in the presence of water was limited due to their instability to oxidation. Furthermore, V ions have highly negative reduction potential and the formation of nanoparticles required the use of elevated temperatures to thermally decompose the metal ions.

The novel design of synthesis approaches for the development of VPt nanoparticles in the same reaction medium was achieved by the employment of high boiling point solvents. The temperature for the reduction reaction is determined by the boiling point of such solvents. This high temperature chemical solution-based method is robust and reproducible, resulting in uniform size, size distribution, shape, high yield and quality nanoparticles. About 90 – 95% of the particles synthesized in this present field using different preparative techniques are < 10 nm and did not require any size selective process.

The results presented in this dissertation show the optimal synthesis routes to be as follows:

- Pt nanoparticles: The reduction of metal ions using various reductants either in water or organic liquids.

- V metal and V oxide nanoparticles: Thermolysis was the successful technique used in the preparation of V and V oxide nanoparticles, in dry and inert environments.

- VPt nanoparticles: Thermolysis served as the powerful reducing approach for the synthesis of both Pt and V nanoparticles in the same reaction solution.

REFERENCES

1. Zhong, C., Luo, J., Njoki, N. P., Mott, D., Wanjala, B., Loukrakpam, R., Lim, S., Wang, L., Fang, B., Xu, Z., Energy Environ. Sci. (2008) **1**: p. 454.
2. Lin, Y., Huber, W. G., Energy Environ. Sci., (2009) **2**: p. 71.
3. Ferrando, R., Jellinek, J., Johnston, L. R., Chem. Rev., (2008) **108**: p. 845.
4. Meunier, C.F., ^{ACS}NANO (2008) **2**: p. 2441.
5. Somorjai, A.G., Tao, F., Park, Y. J., Top Catal (2008) **47**: p. 1.
6. Somorjai, A.G., Tao, F., Park, Y. J., Angew. Chem. Int. Ed. (2008) **47**: p. 9212.
7. Astruc, D., 2008(Wiley-VCH, Weinheim).
8. Greeley, J., Mavrikakis, M., Nature (2004) **3**: p. 810.
9. Greeley, J., Mavrikakis, M., Catalysis Today (2006) **111**: p. 52.
10. Ross, B.R., 4th Ed., 1992 (London, Chapman and Hall): p. 269.
11. Savitsky, E., Polyakova, V., Gorina, N., Roshina, N., (1978) (Mir Publishers, Moscow): p. 23.
12. Berger, J.D., Science (1999) **286**: p. 49.
13. Keyser, A.C., 1959. **2nd Ed** (Eaglewood Cliffs, Prentice-Hall): p. 344.
14. Savitskii, M.Y., 1989 (New York, Hemisphere Pub. Corp): p. 465
15. Merker, J., Lupton, D., Topfer, M., Knake, H., Platinum Metals Rev. (2001) **45**: p. 74.
16. Fischer, B., Behrends. A., Freund, D., Lupton, F. D., Merker. J., Platinum Metals Rev. (1999) **43**: p. 18.
17. Waterstrat, R.W., Met. Trans. (1973) **4**: p. 1585.
18. Weckhuysen, M.B., Keller, E. D., Catalysis Today (2003) **78**: p. 25.
19. Guo, Q., Kleppa, O. J., J. Alloys. Compd. (1994) **205**: p. 63.
20. Poole Jr, C.P., Owens, F. J., 2003 (Hoboken, NJ, J. Wiley).
21. Somorjai, A.G., Nature (2004) **430**: p. 730.
22. Haber, J., Pure and Appl. Chem., (1994) **66**: p. 1598.
23. Somorjai, A.G., Tao, F., Park, Y. J., Top Catal (2008) **47**: p. 1.

24. Schwarz, A.J., Chem. Rev. (1995). **95**: p. 477.
25. Libuda, J., Freund, -J. H., Surf. Sci. Rep. (2005) **57**: p. 157.
26. Sinfelt, H.J., Rev. Mod. Phys. (1979) **51**: p. 569.
27. Boudart, M., Chem. Rev. (1995) **95**: p. 661.
28. Nilsson, A., Pettersson, M. G. L., Hammer, B., Bligaard, T., Christensen, H. C., Norskov, K. J., Catal. Lett. (2005) **100**: p. 111.
29. Xia, Y., Xiong, Y., Lim, B., Skrabalak, E. S., Angew. Chem. Int. Ed. (2009) **48**: p. 60.
30. Lin, Y., Huber, W. G., Energy Environ. Sci. (2009) **2**: p. 71.
31. Nur, H., Akta Kimindo, (2006) **3**: p. 1.
32. Somorjai, A.G., Contreras, M. A., Montano, M., Rioux, M. R., Clusters, surfaces, and catalysis (2006) **103** p: 10577.
33. Lin, Y., Huber, W. G., Energy Environ. Sci. (2009) **2**: p. 71.
34. Corma, A., Garcia, H., Top Catal (2008) **48**: p. 8.
35. Nur, H., Akta Kimindo (2007) **3**: p. 1.
36. Somorjai, A.G., Chem. Rev. (1996) **96**: p. 1224.
37. Somorjai, A.G., Langmuir (1991) **7**: p. 3177.
38. Coughlin, W.R., Ind. Eng. Chem. (1967) **59**: p. 45 .
39. Ruban, A., Hammer, B., Stoltze, P., Skriver, L. H., NΦrskov, K. J., J. Mol. Catal. Chem. **A** (1997) **115**: p. 421.
40. Zaera, F., Chem. Rec. (2005) **5**: p. 133
41. Bonnemann, H., Nagabhushana, S. K., J. New. Mat. Electrochem. Systems (2004) **7**: p. 93
42. Gopalakrishnan, J., Chem. Mater. (1995) **7**: p. 1265.
43. Narayanan, R., El-Sayed, A. M., J. Phys. Chem. B (2004) **108**: p. 5726.
44. Ahmadi, S.T., Wang, L. Z., Green, C. T., Henglein, A., El-Sayed, A. M., Science (1996) **272**: p. 1924.
45. Henglein, A., J. Phys. Chem. B (2000) **104**: p. 2201.
46. Yu, W., Liu, H., Chem. Mater. (1998) **10**: p. 1205.

47. Teranishi, T., Hosoe, M., Tanaka, T., Miyake, M., J. Phys. Chem. B (1999) **103**: p. 3819.
48. Yu, Y.-T., Xu, B-Q., Appl. Organometal. Chem. (2006) **20**: p. 639.
49. Tang, Z., Geng, D., Lu, G., Mater. Lett. (2005) **59**: p. 1567.
50. Mahmoud, A.M., Tabor, E. C., El-Sayed, A. T., Ding, Y., Wang, L. Z., J. Am. Chem. Soc. (2008) **130**: p. 4590.
51. Li, Y., Hong, M. H., Collard, MM. D., El-Sayed, A. M., Org. Lett. (2000) **2**: p. 2385.
52. Liang, H.-P., Zhang, H-M., Hu, J-S., Guo, Y-G., Bai, C-L., Angew. Chem. Int. Ed. (2004) **43**: p. 1542.
53. Wang, L., Guo, Shaojun, S., Zhai, J., Dong, S., J. Phys. Chem. C (2008) **112**: p. 13373.
54. Lee, H., Habas, E. S., Kweskin, S., Butcher, D., Sormjai, A. G., Yang, P., Angew. Chem. Int. Ed. (2006) **45**: p. 7824
55. Wang, L., Yamauchi, Y., J. Am. Chem. Soc. (2009) **131**: p. 9152.
56. Xiong, Y., McLellan, M. J., Chen, J., Yin, Y., Li, Z-Y., Xia, Y., J. Am. Chem. Soc. (2005). **127**: p. 17119.
57. Herricks, T., Chen, J., Xia, Y., Nano Lett. (2004) **4**: p. 2368.
58. Tsung, C.-K., Kuhn, N. J., Huang, W., Aliaga, C., Hung, L-I., Somorjai, A. G., Yang, P. , J. Am. Chem. Soc. (2009) **131**: p. 5817.
59. Wiley, B., Sun, Y., Mayers, B., Xia, Y., Chem. Eur. J. (2005) **11**: p. 454.
60. Furlong, N.D., Launnikonis, A., Sasse, F. H. W., Sanders, V. J., J. Chem. Soc. Faraday Trans. (1984) **80**: p. 571.
61. Harriman, A., Thomas, M. J., Millward, R. G., New J. Chem. (1987) **11**: p. 757.
62. Wu, H.S., Chen, H. D. , Chem. Lett. (2004) **33**: p. 406.
63. Zhang, X., Chang, Y. K., Chem. Mat. (2003) **15**: p. 451.
64. Zhong, X., Feng, Y., Lieberwirth, I., Knoll, W., Chem. Mater. (2006) **18**: p. 2469.
65. Xu, Z., Shen, C., Hou, Y., Gao, H., Sun, S., Chem. Mater. (2009) **21**: p. 1778.
66. Yin, Y., Alivisatos, P. A., Nature (2005) **437**: p. 665.
67. El-Sayed, A.M., Acc. Chem. Res. (2004) **37**: p. 326.

68. Cushing, L.B., Kolesnichenko, L. V., O'Connor, J. C., Chem. Rev. (2004) **104**: p. 3893.
69. Xia, Y., Xiong, Y., Lim, B., Skrabalak, E. S., Angew. Chem. Int. Ed. (2009) **48**: p. 60.
70. Bonnemann, H., Nagabhushana, S. K., Chem. Ind. (2004) **58**: p. 271.
71. Roduner, E., 2006 (RSC Publishing, Stuttgart).
72. Burda, C., Chen, X., Narayanan, R., El-Sayed, A. M., Chem. Rev. (2005) **105**: p. 1025.
73. Murray, B.C., Kagan, R. C., Bawendi, G. M., Annu. Rev. Mater. Sci. (2000) **30**: p. 545.
74. Finney, E.E., Finke, G. R., J. Colloid. Inter. Sci. (2008) **317**: p. 351.
75. Skrabalak, E.S., Xia, Y., ^{ACS}NANO (2009) **3**: p. 11.
76. Tao, R.A., Habas, S., Yang, P., Small (2008) **4**: p. 310.
77. Murphy, J.C., Jana, R. N., Adv. Mater. (2002) **14**: p. 80.
78. Wang, L.Z., Ahmad, S.T., El-Sayed, A. M., Surf. Sci. (1997) **380**: p. 302.
79. Lar Mer, K.V., Dinegar, H. R., J. Am. Chem. Soc. (1950) **72**: p. 4847
80. Murray, B.C., Norris, J. D., Bawendi, G. M., J. Am. Chem. Soc. (1993) **115**: p. 8706
81. Evans, L.M.R., Fairhurst, J. D., Poon, K. C. W., Phys. Rev. Lett. (1998) **81**: p. 1326.
82. Chemseddine, A., Weller, H., Ber. Bunsen-Ges, Phys. Chem. (1993) **97**: p. 636
83. Yamaka, M., Higo, J., Nagayama, K., Langmuir (1995). **11**: p. 2975
84. Ohara, C.P., Leff, V. D., Heath, R. J., Gelbart, M. W., Phys. Rev. Lett. (1995) **75**: p. 3466.
85. Doome, J.R., Fonseca, A., Richter, H., Nagy, B. J., Thiry, A. P., Lucas, A. A., J. Phys. Chem. Soc. (1997) **58**: p. 1839.
86. Ullah, H.M., Chung, W-S, Kim, I., Ha, C-S., Small (2006) **2**: p. 872.
87. Bond, C.G., Platinum Metals Rev., (1975) **19**: p. 126.
88. Xiong, Y., Wiley, J. B., Xia, Y., Angew. Chem. Int. Ed. (2007) **46**: p. 7157.
89. Guczi, L., Peto, G., Beck, A., Paszti, Z., Topics in Catalysis (2004) **29**: p. 129.

90. de Heer, A.W., Rev. Mod. Phys. (1993) **65**: p. 611.
91. Somorjai, A.G., Chem. Rev. (1996) **96**: p. 1223.
92. Narayanan, R., El-Sayed, A. M., J. Phys. Chem. B (2003) **107**: p. 12416.
93. Wang, L.Z., 2000 (Wiley-VCH, Weinheim).
94. Narayanan, R., El-Sayed, A. M., J. Phys. Chem. B (2005) **109**: p. 12663.
95. Narayanan, R., Tabor, C., El-Sayed, A. M., Top. Catal. (2008) **48**: p. 60.
96. Bell, T.A., The Impact of Nanoscience on Heterogeneous Catalysis (2003) **299**: p. 1688.
97. Komanicky, V., Iddir, H., Chang, K., Menzel, A., Karapetrov, G., Hennessy, D., Zapol, P., You, H. , J. Am. Chem. Soc. (2009) **131**: p. 5732.
98. Chen, C., Tano, D., Akashi, M., J. Colloid and Interface Science (2000) **225**: p. 349.
99. Bratlie, M.K., Lee, H., Komvopoulos, K., Yang, P., Somorjai, A. G., Nano Lett. (2007) **7**: p. 3097.
100. El-Sayed, A.M., Acc. Chem. Res. (2001) **34**.
101. Alivisatos, A.P., Semiconductor Clusters, Nanocrystals, and Quantum Dots. Science (1996) **271**: p. 933.
102. Rao, R.N.C., Kulkarni, U. G., Thomas, J. P., Edwards, W., Chem. Eur. J. (2002) **8**: p. 29.
103. Jena, P., Castleman, Jr. W. A., Clusters: A bridge across the disciplines of physics and chemistry (2006).**103**: p. 10560.
104. Brust, M., Kiely, C. J., Some Recent Advances in Nanostructure Preparation from Gold and Silver: A Short Topical Review. Colloids Surf. A: Physiochem. Eng. Asp. (2002) **202**: p. 175.
105. Daniel, M., Astruc, D., Chem. Rev. (2004) **104**: p. 293.
106. Schmid, G., Chem. Rev. (1992) **92**: p. 1709.
107. Wen, Y., Fang, H., Zhu, Z., Sun, S., Phys. Lett. A (2009) **373**: p. 272.
108. Wang, W., Chen, X., Cai, Q., Mo, G., Jiang, S. L., Zhang, K., Chen, J. Z., Wu, H. Z., Pan, W., Eur. Phys. J. B. (2008) **65**: p. 57.
109. Burton, J.J., Cat. Rev. (1973) **3**: p. 209.

110. Tian, N., Zhou, Z., Sun, S., J. Phys. Chem. C (2008) **112**: p. 19801.
111. Xiong, Y., Wiley, J. B., Xia, Y., Angew. Chem. Int. Ed. (2007) **46**: p. 7157.
112. Wang, L.Z., J. Phys. Chem. B (2000) **104**: p. 1153.
113. Tian, N., Zhou, Z., Huang, Z., Chen, D., Sun, S., Faraday Discuss. (2008) **140**: p. 1.
114. Blakely, W.D., Somorjai, A. G., Surf. Sci. (1977) **65**: p. 419.
115. He, -.H.J., Ichinose, Kunitake, T., Nakao, A., Shiraishi, Y., Toshima, N., J. Am. Chem. Soc. (2003) **125**: p. 11034.
116. Van Santen, A.R., Acc. Chem. Res. (2009) **42**: p. 57.
117. Rioux, S., H., Hoefelmeyer, D. J., Yang, P., Sormorjai, A. G., J. Phys. Chem. B (2005) **109**: p. 2192.
118. Yang, C., Kalwei, M., Schuth, F., Chao, K., Appl. Catal. A: Gen. (2003) **254**: p. 289.
119. Yoo, W.J., Hathcock, J. D., El-Sayed, A. M., J. Catal. (2003) **214**: p. 1.
120. Balint, I., Miyakazi, A., Aika, K., Chem. Comm. (2002) **10**: p. 1044.
121. Liu, Z., Lee, Y. J., Chen, W., Han, M., Gan, M. L., Langmuir (2004) **20**: p. 181.
122. Bulushev, A.D., Yuranov, I., Suvorona, I. E., Buffat, A. P., Kiwi-Minsker, L., J. Catal. (2004) **224**: p. 8.
123. Takasu, Y., Itaya, H., Kawaguchi, T., Sugimoto, W., Murakami, Y., Stud. Surf. Sci. Catal. (2003) **145**: p. 279.
124. Wu, Z.C., Wang, P., Yao, X., Liu, C., Chen, M. D., Lu, Q. G., Cheng, M. H., J. Alloys. Compd. (2006) **420**: p. 278.
125. Lopez, N., Jassens, W. V. T, Clausen, S. B., Xu, Y., Mavrikakis, M., Bligaard, T., Norskov, K. J., J. Catal. (2004) **223**: p. 232.
126. Liu, Z., Ling, Y. Z., Lee, Y. J., Su, X., Gan, M. L., J. Mat. Chem. (2003) **13**: p. 3049.
127. Moshfegh, A.Z., J. Phys. D: Appl. Phys. (2009) **42**: p. 1
128. McCathy, J.T., Marques, P. M. C., Trevino, H., Sachtler, H. M. W., Catal. Lett. (1997) **43**: p. 11.

129. Guczi, L., Konya, Z., Koppany, Z., Stefler, G., Kirisci, I., Catal. Lett. (1997) **44**: p. 7.
130. Vaarkamp, M., Miller, T. J., Modica, S. F., Koningsberger, C. D., J. Catal. (1996) **163**: p. 294.
131. Menacherry, V.P., Fernandez-Garcia, M., Haller, L. G., J. Catal. (1997) **166**: p. 75.
132. Bentzon, D.M., Wonterghem, V. J., Morup, S., Thoelen, A., Koch, W. J. C. , Philos. Mag. B (1989) **60**: p. 169.
133. Murray, B.C., Sun, S., Gaschler, W., Doyle, H., Bentley, A. T., Kagan, R. C. , IBM J. Res. and Dev. (2001) **45**: p. 45.
134. Puntes, F.V., Krishnan, M. K., Alivisatos, P. A., Science (2001) **291**: p. 2115.
135. Whitesides, M.G., Grzybowski, B., Science (2002) **295**: p. 2418.
136. Pileni, P.M., Acc. Chem. Res. (2007) **40**: p. 685.
137. Murray, B.C., Kagan, R. C., Bawendi, G. M., Science (1995) **270**: p. 1335.
138. Shevchenko, V.E., Talapin, D., Kornowski, A., Wiekhorst, F., Kotzler, J., Haase, M., Rogach, L. A., Weller, H., Adv. Mater. (2002) **14**: p. 287.
139. Shevchenko, V.E., Talapin, V. D., Kotov, A. N., O'Brien, S., Murray, B. C. , Nature (2006) **439**: p. 55.
140. Talapin, V.D., Shevchenko, V. E., Bodnarchuk, I. M., Ye, X., Murray, B. C., Nature (2009) **461**: p. 964.
141. Rogach, L.A., Talapin, V. D., Shevchenko, V. E., Kornowski, A., Haase, M., Weller, H. , Adv. Funct. Mater. (2002) **12**: p. 653.
142. Harfenist, A.S., Wang, L. Z., Alvarez, M. M., Vezmar, I., Whetten, L. R., J. Phys. Chem. B (1996) **100**: p. 13904.
143. Motte, L., Billoudet, F., Lacaze, E., Douin, J., Pileni, P. M., J. Phys. Chem. B (1997) **101**: p. 138.
144. Pileni, P.M., Appl. Surf. Sci. (2001) **171**: p. 1.
145. Mahmoud, A.M., Tabor, E. C., El-Sayed, A. M., Ding, Y., Wang, L. Z., J. Am. Chem. Soc. (2008) **130**: p. 4590.
146. Nguyen, T.-D., Do, T-O., Langmuir (2009) **25**: p. 5322.

147. http://rsbweb.nih.gov/ij/.